國 立 交 通 大 學

電控工程研究所

碩士論文

應用可變結構控制技術於反戰術彈道飛彈

具有側向力與氣動力之複合控制技術之研究

Application of Variable Structure Schemes to the Control of

Anti-Tactical Ballistic Missile Having Lateral Thrust and

Aerodynamic Forces

研 究 生：康詠鈞

指導教授：梁耀文　博士

中 華 民 國 一 百 零 二 年 七 月

應用可變結構控制技術於反戰術彈道飛彈具有側向力與氣動力之複合控制技術之研究

Application of Variable Structure Schemes to the Control of Anti-Tactical Ballistic Missile Having Lateral Thrust and Aerodynamic Forces

研 究 生：康詠鈞　　Student： Yung-Chun Kang

指導教授：梁耀文 博士　　Advisor： Dr. Yew-Wen Liang

國立交通大學電控工程研究所

碩士論文

A Thesis

Submitted to Institute of Electrical Control Engineering
College of Electrical Engineering and Computer Science
National Chiao Tung University
in Partial Fulfillment of the Requirements
for the Degree of Master
in
Electrical and Control Engineering
July 2013
Hsinchu, Taiwan, Republic of China

中 華 民 國 一 百 零 二 年 七 月

應用可變結構控制技術於反戰術彈道飛彈具有側向力與氣動力之複合控制技術之研究

研究生：康詠鈞　　指導教授：梁耀文 博士

國立交通大學電控工程研究所

摘 要

本論文的主要目的在探討具有氣動力和側向力的反戰術彈道飛彈之複合控制技術。由於科技的不斷發展，目標飛彈的機動性不斷提升，為了在攔截末段實現直接碰撞高機動性目標飛彈的攔截任務，複合式控制的概念油然而生，取代傳統僅依賴氣動力控制的飛彈。相對於純尾翼控制，複合控制具有如下之特點：1) 系統時間響應速度快；2) 側向力不受海拔高度影響；3) 複合控制能降低側向力的能量消耗並且提升系統的追蹤性能表現。本論文首先建立複合式的反戰術彈道飛彈六自由度數學模型，並探討應用三種可變結構控制技術：1) 傳統順滑模控制(conventional sliding mode control)技術、2) 終端順滑模控制(terminal sliding mode control)技術與3) 非奇異終端順滑模控制(nonsingular terminal sliding mode control)技術在氣動力與側向力的複合控制之性能比較。由模擬結果顯示，除驗證了本文所設計之控制器的性能表現外，也展示了複合式飛彈的系統響應速度的確比傳統只使用氣動力的飛彈快，這些模擬具體地說明了複合式飛彈未來發展的潛力。

Application of Variable Structure Schemes to the Control of Anti-Tactical Ballistic Missile Having Lateral Thrust and Aerodynamic Forces

Student: Yung-Chun Kang Advisor: Dr. Yew-Wen Liang

Institute of Electrical Control Engineering

National Chiao Tung University

ABSTRACT

This thesis studies the control of anti-tactical ballistic missiles (ATBM) having lateral thrust and aerodynamic forces, called blended control. With increasing technological sophistication, the maneuverability of tactical ballistic missiles is improving. Compared with tail control, the blended control possesses the following three features: 1) timing response is faster; 2) lateral thrust is independent of altitude; and 3) tracking performance is promoted. In this thesis, we first build the mathematical model of ATBM and then import the following three variable structure schemes (VSS): 1) conventional sliding mode, 2) terminal sliding mode and 3) nonsingular terminal sliding mode to the blended control design task. Simulation results clearly demonstrate the performances of the presented three SMC schemes and confirm that the performance by blended control is superior to that by the tail control only.

誌　　謝

本篇論文的完成，實在要感謝許多人的關心與協助，沒有你們恐怕無法有所精進，希望日後能繼續給與指教與鼓勵，必銘記在心。

首先特別要感謝指導教授梁耀文博士，感謝老師兩年來細心與耐心的指導及孜孜不倦的教誨，除了讓我對於控制理論的懵懂漸漸有了體悟與想法，且在人生中待人處事有許多的不一樣的思維，其中一句：「作而無作，無作而作。」更是深得我心。同時也要感謝口試委員廖德誠博士、鄭治中博士和徐勝均博士給予建設性的建議與指導，使得本論文更臻完備。

感謝實驗室的同學們，徐勝均博士、林立岡學長、陳智強學長、馮仰靚學長、陳弘儒學長及呂鈞鈞學姐，感謝他們在我研究上或學業上有問題時，可以即刻的幫助我，或是提供我意見。感謝同窗的實驗室同學陳俊宇、陳逸庭與王國欽，感謝他們在一起修課時互相幫忙，以即互相鼓勵督促。感謝學弟張修維、朱韋銘、吳竣民與洪靜怡，在我需要幫忙時，適時的給予幫助。感謝我的好友在人生不如意時聽述說痛苦。若無他們的幫助，我無法完成今天的碩論。

感謝我的女朋友乃慈，在我忙碌時默默地在背後支持我、幫助我、體諒我，使我能更能專心在學業上衝刺。最後感謝我的家人，由於你們的大力支持與鼓勵，使我在求學過程中無後顧之憂，如果沒有他們，就沒有今天的我，也就無法完成今天的論文。

康詠鈞 于新竹交大

102 年 7 月

TABLE OF CONTENT

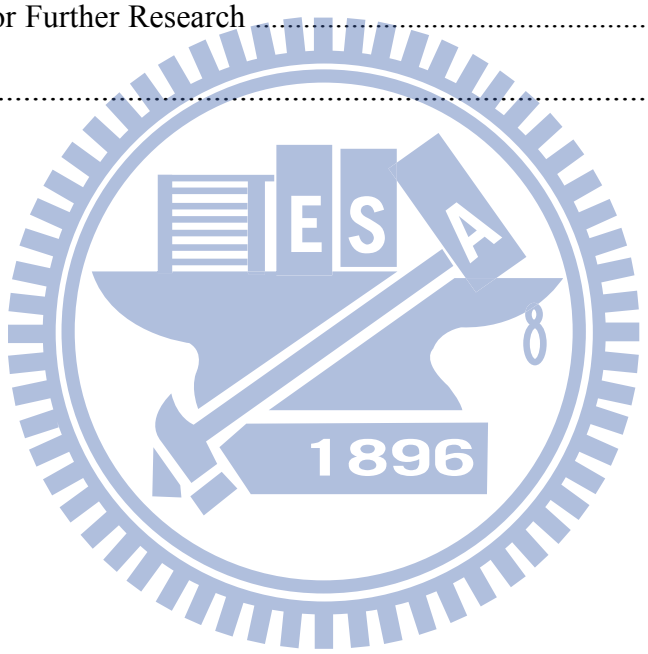

LIST OF FIGURES

LIST OF TABLES

NOMENCLATURE

ω_{xb}, ω_{yb}, ω_{zb} : Body-axis roll rate, yaw rate, and pitch rate relative to the inertial frame, respectively;

I_{xx}, I_{yy}, I_{zz} : The components of the centroidal mass moment of inertia corresponding to the body axes;

m : Missile mass;

V : Missile velocity;

S : Reference wing area;

g : Acceleration due to gravity;

d : Reference Diameter;

ρ : Atmospheric density;

q : Dynamic pressure;

f_{rd} : Radians to degrees;

x, y, z : the position vector of center of mass of the missile transformed corresponding to the inertial frame, respectively;

F_{pbx} : Propulsion of the missile corresponding to the body axes;

F_{tbyc}, F_{tbzc} : Lateral thrust in the direction of pitch and azimuth corresponding to the body axes, respectively;

X, Y, Z : Drag (axial) force, lift (normal) force, and side force corresponding to the wind axes, respectively;

γ, ϑ, ψ : Body-axis bank angle, pitch angle, and yaw angle relative to the inertial frame, respectively;

α, β : Angle of attack and sideslip angle relative to the wind axes, respectively;

γ_v : Velocity bank angle relative to the ballistic axes.

θ, ψ_v : Fight path angle and ground tracking angle relative to the inertial frame, respectively;

δ_x, δ_y, δ_z : Aileron deflection angle, rudder deflection angle, and elevator deflection angle, respectively;

c_{x0} : Total drag coefficient evaluated at $\alpha = 0$;

c_x^i : Total drag coefficient variation with $i = \alpha$, β, $\alpha\beta$ and δ_x;

$c_y^{\delta_y}$, $c_z^{\delta_z}$: Total drag coefficient variation with δ_y and δ_z;

c_y^{α}, c_y^{β}, $c_y^{\delta_z}$: Total lift coefficient variation with α, β, and δ_z;

c_z^{α}, c_z^{β}, $c_z^{\delta_y}$: Total side force coefficient variation with α, β, and δ_z;

m_x^{α}, m_x^{β}, $m_x^{\delta_x}$: Rolling moment coefficient variation with α, β, δ_x;

m_y^{β}, $m_y^{\delta_y}$: Yawing moment coefficient variation with β, δ_y;

m_z^{α}, $m_z^{\delta_z}$: Pitching moment coefficient variation with α, δ_z;

CHAPTER ONE
INTRODUCTION

1.1 Motivation

In the 1990s, the science and technology of tactical ballistic missile (TBM) developed rapidly. The features of the TBM included: I) The maximum range is more than 1000 (km). II) The maximum speed is 2 to 3 (km/s) in the attack region of the air defense missile (or anti-tactical ballistic missile, ATBM). III) The maximum overloading is approximate 10 (g). IV) The hitting precision is high. And, VI) The destructive power is strong. Consequently, progressing the ATBM to defend has become a primary mission [1]. Moreover, in the First Gulf War (2 August 1990 - 28 February 1991), the U.S. Patriot missile was used in combat for the first time. The U.S. military claimed a high effectiveness against Iraq's Scuds at the time, but later the Patriot Program Office reported to high-ranking Administration officials and Members of Congress that a total of 158 Patriot missiles were fired during the war, while only 86 Patriots had intercepted at Scud targets (89 percent of the Iraqi Scuds launched against Saudi Arabia and 44 percent of the Scud warheads directed against Israel). In other words, almost half were fired at false targets and debris (15 percent at false targets, 30 percent at Scud debris) [2]. This result shows that the magnitude of miss distance (MD) is a factor to judge whether the missile intercepts the target successfully. The magnitude of MD is related to the missile's overloading and the time response of the attitude stability system. In short, developing the hit-to-kill (HTK) technique is necessary in no time. The U.S.A. had made a rocket sled test which proved that the HTK technique can provide enough energy and penetrating force to destroy the target carrying mass destruction warhead successfully [3]. In view of the change of TBM's characteristics and attacking ways and the great progress of the

relevant scientific and technological field, the flight control system of the ATBM has a fundamental revolution in the following aspects [1]:

I) Reducing warhead's weight greatly. ATBM is equipped with modern high-accuracy microelectronic devices extensively such that its size and weight lessens extremely. In theory, the overload can reach above 40 (g). This guarantees the ATBM's requirement for high maneuverability.

II) Equipped with active radar homing in the warhead and a inertial navigation system. The ground guidance radar just informs ATBM of the present position of a target and the predictive impact point, while the other guidance information is from ATBM itself. As a result of a computer embedded in a ATBM, the operation of control problem can directly calculate in a ATBM instead of ground guidance radar indirectly. This can not only improve the guidance precision but also reduce the time response of the guidance loop. The method is helpful to increase the capability of HTK.

III) Adopting the blended control with aerodynamic force and reaction-jet control system (RCS) [4]-[9] in the terminal phase of interception, the RCS can make ATBM's maneuverability promote strongly. Compared to traditional aerodynamic control, it can decrease about 1/10 (sec) of the time response and improve agility about 10 to 20 times in the high altitude. Thus, this equipment has capability to achieve HTK.

IV) Benefiting from the advanced computer technology, new control theory and control system design method applied to the blended control system, it has succeeded in solving the contradiction between operational requirements and control system under the traditional aerodynamic control (conventional control or tail control). Besides, this result increases controlling precision and robustness of the ATBM. Generally speaking, the developing trends of the air defense missile control will be faster time response, higher control precision, and more powerful maneuvering performance.

Tails or air rudders are the control mechanisms for the traditional aerodynamic control. According to the command from guidance and control regulation, turning the control

surface yields moment to change the missile's attitude and then produces the lateral overloading. It may be inferred that the relation between the performance of the attitude stability system and intercepting precision in terminal phase is closely related. Taking the traditional aerodynamic control into account, it can be guaranteed to predict successfully near the impact point in the midcourse phase. On the contrary, in order to realize HTK in the terminal phase, just using tails is not enough because the aerodynamic force has two defects as follows [1], [10], [11]:

I) The overload is insufficient in the high altitude. It assures that maneuverability of the ATBM must be at least three times larger than one of the TBM. The efficiency of aerodynamic force decreases at above 10 (km) altitude during the terminal phase since aerodynamic force is directly proportional to air density and missile velocity. Hence, the low air density at high altitude cause insufficient overloads.

II) The time response of the attitude stability system is long. Time is short in the terminal phase. Depending on manufacturing technique of aerodynamic mechanisms, the time delay of these mechanisms is around 0.1 to 0.5 (sec), whereas the standard for the air defense missile is around 0.1 (sec).

In consideration of physical constraints of purely aerodynamic control, the concept of the blended control with aerodynamic force and RCS for the air defense missile came up. There are three types of the RCS according to their positions [12]: 1) attitude type, which means the location of the RCS is between center of gravity and the missile's top and produces moment to change the missile's attitude, e.g. PAC-3 shown in Fig. 1.1; 2) orbit type, which means the location of the RCS is around center of gravity and makes missile produce linear motion, e.g. S-400, Aster-15, and Aster-30; 3) attitude-orbit type, which means it combines above two types, e.g. TLVS (Taktisches Luft Verteidigungs Systems). The features of RCS are listed roughly below [1], [5], [8], [13], [14]:

I) Advantages

i) The time response of the attitude stability system is short. The time response the RCS is about 5 (msec) to 10 (msec) which is much faster than the one of

purely aerodynamic control.

ii) The maneuverability of the RCS is regardless of the altitude. This characteristic is suitable in the terminal phase as it can warrant that the ATBM has enough agility during the guidance process.

II) Disadvantages

i) There is a limitation of the fuel consumption. After exhausting the foil, the thruster cannot use continuously.

ii) The fuel consumption can make the missile's center of gravity drift.

iii) The jet interaction effect is complicated such that the actual thrust does not meet the theoretical one.

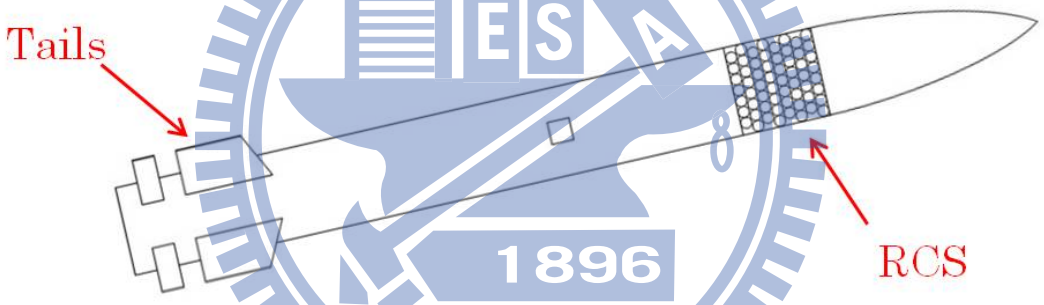

Fig. 1.1. The locations of the tails and the RCS of the PAC-3

Thus, using blended control can diminish the energy consumption compared with only using RCS and compensate the uncertainties of RCS. In short, the goal of using blended control is to reduce the MD and to achieve HTK.

In existing results, some papers have dealt with the control design of missile with RCS. Chadwick [7] proposed the blended control to improve the guidance performance of missiles against weaving targets in high altitude and analyzed the influence of the location of RCS. Wise [15] proposed the autopilot for aero-fin controlled missile with the RCS using linear quadratic regulator technique. Menon [16], Schroeder [17] and [18] proposed adaptive techniques for multiple actuator blending using fuzzy control. Yin [13] proposed blended control via inverse dynamics technique and used extended states observer

to improve the estimation precision of system states. Bi [19] proposed blended control via model predictive technique and used active disturbance rejection control to resist the model uncertainties and external disturbances. In addition, Weil [5] and Innocenti [8] proposed the blended missile autopilot formulating via the variable structure schemes (VSS) or sliding mode control (SMC) techniques.

In the recent years, the research of SMC of nonlinear systems have attracted much attention. It is known that SMC have the advantages of fast response and small sensitivity to system uncertainties and disturbances [20], [21]. Hence, the SMC approach has been widely applied to a variety of control problems [20], [22], [23], especially in spacecraft attitude control [24]-[27] and robotic control [28]-[32].

Although those two papers [5] and [8] had used SMC techniques to synthesize the control laws, the former one [5] imposes an assumption that the RCS is continuous and both papers only consider a linear model. On the other hand, in this thesis, we consider a more practical nonlinear model with the pulse-like (or constant during a short time period once the RCS was triggered) RCS. Moreover, we will organize blended control laws via the following three SMC techniques: 1) conventional sliding mode control (CSMC) scheme, 2) terminal sliding mode control (TSMC) scheme and 3) nonsingular terminal sliding mode control (NTSMC) scheme for the control of missile, and compare the performances under the three SMC schemes.

1.2 Outline

The organization of the work is as follows. Chapter 1 includes the motivation and objective of this thesis, as well as the survey of relative works. Chapter 2 reviews the basic concept of SMC theories. The mathematical model of the PAC-3 missile is given in Chapter 3. The problem formulation and controller design via the CSMC, TSMC and NTSMC schemes are illustrated in Chapter 4. Then, in Chapter 5, the analytic results are applied to a simplified model to demonstrate the performances of the three SMC schemes. Finally, the conclusions and suggestions for further research are made in Chapter 6.

CHAPTER TWO
PRELIMINARIES

2.1 Conventional Sliding Mode Control (CSMC)

The history of CSMC up until the early 70's has been described in [33]. By 1980, the main part of CSMC theory had been finished [34] and later reported by Russian Prof. Utkin's monograph in 1981 [35]. The main advantages of CSMC were the following [36]: 1) exact compensation (insensitivity) with respect to bounded matched uncertainties; 2) reduced order of sliding equations; 3) finite-time convergence to the sliding surface.

Consider a nth-order single-input system

$$x^{(n)} = f(\mathbf{x}) + g(\mathbf{x})u + d(\mathbf{x}) \tag{2.1}$$

where $\mathbf{x} = [x\ \dot{x}\ \cdots\ x^{(n-1)}]^T$ denotes the state vector and u is control input. In system (2.1), the functions $f(\mathbf{x})$ and $g(\mathbf{x})$ (in general, nonlinear) are not exactly known, but the extent of the imprecision on $f(\mathbf{x})$ is upper bounded by a known continuous function of x, and control gain $g(\mathbf{x})$ is of known sign and bounded by a known continuous function of x, respectively. And $d(\mathbf{x})$ is set to combine the model uncertainties of $f(\mathbf{x})$ and $g(\mathbf{x})$ and external disturbances. The control problem is to get the state $\mathbf{x}$ to track a specific time-varying state $\mathbf{x}_d = [x_d\ \dot{x}_d\ \cdots\ {x_d}^{(n-1)}]^T$ in the presence of $d(\mathbf{x})$. In order to achieve the tracking task by using a finite control u, the initial desired state $\mathbf{x}_d(0)$ must be such that:

$$\mathbf{x}_d(0) = \mathbf{x}(0). \tag{2.2}$$

Then, defining the tracking error

$$\mathbf{e} = \mathbf{x} - \mathbf{x}_d \tag{2.3}$$

where the error vector composed of derivatives of error between output and desired output is denoted by

$$\mathbf{e} = [e \ \dot{e} \ \cdots \ e^{(r-1)}]^T \tag{2.4}$$

In a second-order system, for example, position or velocity can not "jump", so that any desire trajectory feasible from t=0 necessarily starts with the same position and velocity as those of the plant. Otherwise, tracking can only be achieved after a transient.

According to [37], the two-step procedure for sliding mode control design was clearly stated: 1) Sliding surface design. When the trajectory of closed-loop system is fixed in the sliding surface, it will be asymptotically stable. And, 2) Discontinuous controllers ensuring the sliding modes. The control law can let the trajectory of the closed-loop system reach the desired sliding surface in a finite time and stick on the the desired sliding surface. A typical phase portrait is illustrated in Fig. 2.1.

In first step, defining $s(\mathbf{x})$ is a smooth scalar constraint function: $\mathbb{R}^n \rightarrow \mathbb{R}$, we select

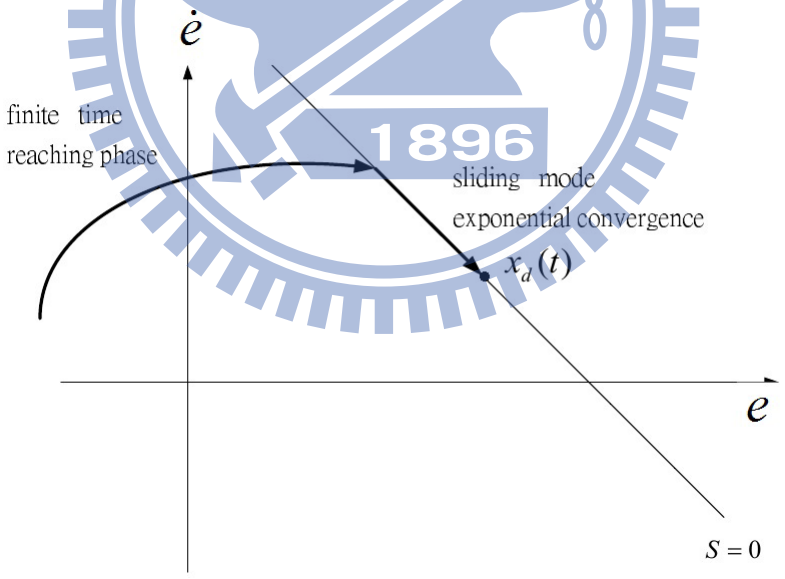

Fig. 2.1. A typical phase portrait under sliding mode control

time-varying sliding surface to be $s = 0$ with

$$s = a^T \mathbf{e} \tag{2.5}$$

where the constant coefficient vector $a^T = [a_1 \ \cdots \ a_r]$. Here, a_i for i=1,$\cdots$, $r-1$ are selected constants and $a_r = 1$ is chosen such that

$$\lambda^{r-1} + a_{r-1}\lambda^{r-2} + \cdots + a_2\lambda + a_1 \tag{2.6}$$

are Hurwitz polynomials. As the states trajectory remain on the sliding surface, i.e., $s = 0$, we can know Eq. (2.5) will be asymptotically stable, which means the error approaches zero as the time approaches infinity.

Second, designing the control law u, consisting of two parts

$$u = u^{eq} + u^{re} \tag{2.7}$$

where u^{eq} is continuous called a feedback control law and u^{re} is discontinuous or switched. As designing the u^{eq}, there exists a condition which it must let the sliding surface $s = 0$ be invariant set relatively to the closed-loop system for unpresence of uncertainties or external disturbances of the matched type system [37]. That is $s(\mathbf{x}(\mathbf{t_0})) = 0$ and $s(\mathbf{x}(\mathbf{t})) = 0$, $\forall\ t \geq t_0$. Moreover, the time derivative of s is given by

$$\dot{s} = a^T \dot{\mathbf{e}} \tag{2.8}$$

where

$$\dot{\mathbf{e}} = [\dot{e} \ \cdots \ e^{(r)}]^T \tag{2.9}$$

Expanding Eq. (2.8), the sliding variable dynamics as follows

$$\begin{aligned} \dot{s} &= f(\mathbf{x}) + g(\mathbf{x})u + d(\mathbf{x}) - x_d^{(r)} \\ &\quad + a_{r-1}e^{(r-1)} + \cdots + a_2\ddot{e} + a_1\dot{e} \end{aligned} \tag{2.10}$$

Herein, it is regardless of d and u^{re} such that $u = u^{eq}$ can verify sliding condition. The equilibrium point of Eq. (2.10) will be $s = 0$. u^{eq} is designed as

$$u^{eq} = -\frac{1}{g(\mathbf{x})}\left[f(\mathbf{x}) - x_d^{(r)} + a_{r-1}e^{(r-1)} + \cdots + a_2\ddot{e} + a_1\dot{e}\right] \tag{2.11}$$

The effect of u^{eq} is to eliminate the known form of Eq. (2.10). Substituting designed u^{eq} into Eq. (2.10), we get

$$\dot{s} = g(\mathbf{x})u^{re} + d(\mathbf{x}) \tag{2.12}$$

Obviously, if we do not consider the disturbance term d and just use the feedback controller $u = u^{eq}$, Eq. (2.12) exists a equilibrium point at $s = 0$. Next, we consider Eq. (2.12) and assume $s(\mathbf{e}(t_0)) \neq 0$ to design u^{re}. The action of u^{re} is to make sliding variable s be zero in a finite time. That is the trajectory of the closed-loop system will achieve the sliding surface in limited time. To guarantee the reaching condition, we impose a assumption:

Assumption 2.1 There exists a nonnegative number $\rho(\mathbf{x})$ such that

$$|d(\mathbf{x})| \leq \rho(\mathbf{x}) \tag{2.13}$$

From Eq. (2.12), we obtain the other controller u^{re} designed as

$$u^{re} = -\frac{1}{g(\mathbf{x})}\left[\rho + \eta\right] \mathrm{sgn}(s) \tag{2.14}$$

where

$$\mathrm{sgn}(s) := \begin{cases} 1 & \text{if } s > 0 \\ 0 & \text{if } s = 0 \\ -1 & \text{if } s < 0 \end{cases} \text{ is the sign function} \tag{2.15}$$

and $\eta > 0$ is selected positive constant. Then, we substitute Eq. (2.14) into Eq. (2.12), the sliding variable dynamics becomes

$$\dot{s} = -\left[\rho + \eta\right] \mathrm{sgn}(s) + d(\mathbf{x}) \tag{2.16}$$

In order to prove the feasibility of Eq. (2.14), with $V = 1/2s^2$ as a Lyapunov function candidate for Eq. (2.16), we have

$$\dot{V} = s\dot{s} = -\left[\rho + \eta\right] s \cdot \mathrm{sgn}(s) + s \cdot d(\mathbf{x}) \tag{2.17}$$

Using the relation of $s \cdot \mathrm{sgn}(s) = |s|$ and Cauchy-Schwarz inequality to get $s \cdot d(\mathbf{x}) \leq |d(\mathbf{x})||s|$ and Assumption 2.1, the time derivative of Lyapunov function candidate becomes

$$\begin{aligned} \dot{V} &= -\left[\rho + \eta\right] s \cdot \mathrm{sgn}(s) + s \cdot d(\mathbf{x}) \\ &\leq -\left[\rho + \eta\right] |s| + |d(\mathbf{x})||s| \\ &\leq -\left[\rho + \eta\right] |s| + \rho|s| \\ &\leq -\eta|s| \end{aligned} \tag{2.18}$$

According to (2.18), we have known that the Lyapunov function converges. The result explains that the Eq. (2.16) is asymptotically stable, i.e., $s \to 0$ as $t \to \infty$. In other words, focusing on Eq. (2.12), u^{re} will make s approach the sliding surface in limited time when the sliding variable is not zero. Now, we discuss when the sliding variable reach the sliding surface. Actually, there is another form of the time derivative of Lyapunov function presented as

$$\dot{V} = \frac{d}{dt}V = \frac{1}{2}\frac{d}{dt}|s|^2 = |s|\frac{d}{dt}|s| \tag{2.19}$$

As a result of Ieq. (2.18) and Eq. (2.19), we obtain

$$|s|\frac{d}{dt}|s| \leq -\eta|s| \tag{2.20}$$

That is

$$\frac{d}{dt}|s| \leq -\eta \tag{2.21}$$

It implies that $|s|$ converges along with its slope less than or equal to $-\eta$. Integrating Ieq. (2.21) with t on $[0, t_r]$, we get

$$\int_0^{t_r} \frac{d|s(\mathbf{x}(t))|}{dt} dt \leq -\int_0^{t_r} \eta dt \tag{2.22}$$

According to the second fundamental theorem of calculus [38], Eq. (2.22) equals

$$|s(\mathbf{x}(t))| - |s(\mathbf{x}(0))| \leq -\eta t \tag{2.23}$$

or

$$0 \leq |s(\mathbf{x}(t))| \leq |s(\mathbf{x}(0))| - \eta t \tag{2.24}$$

The above inequality shows that $|s(\mathbf{x}(t))|$ must converge before $t = |s(\mathbf{x}(0))|/\eta$, which is illustrated in Fig. 2.2.

However, in order to account for the presence of modelling uncertainties and disturbances, the control law has to be discontinuous across $s(t)$. Since the implementation of the associate control switchings is necessarily imperfect (for example, in practice switching is not instantaneous, and the value s is not known with infinite precision), this leads to

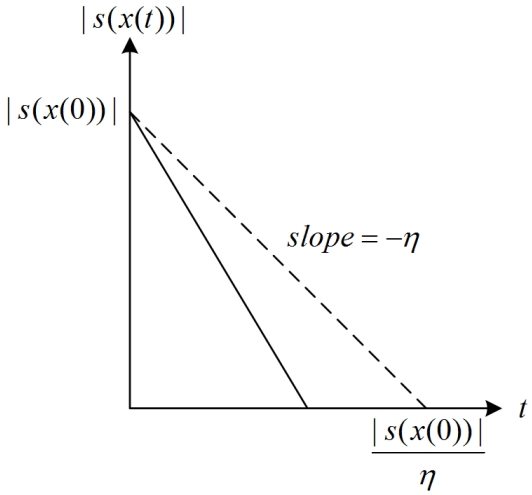

Fig. 2.2. Sliding condition

chattering which is shown as Fig. 2.3. Now, chattering is undesirable in practice, since it involves high control activity and further may excite high-frequency dynamics neglected in the course of modelling such as unmodeled structure modes, neglected time-delays, and so on. Thus, in a second part, the discontinuous control law u^{re} is suitably smoothed to achieve an optimal trade-off between control bandwidth and tracking precision: while the first part accounts for parametric uncertainty, the second part achieves robustness to high-frequency unmodeled dynamics [20].

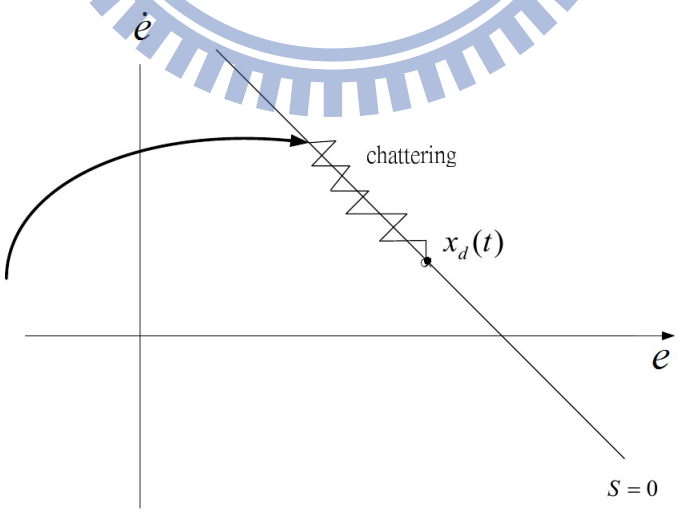

Fig. 2.3. Chattering as result of imperfect control switchings

2.2 Terminal Sliding Mode Control (TSMC)

Although the CSMC has received much attention as an efficient control technique for handling systems with large uncertainties, nonlinearities, and bounded external disturbances and can guarantee finite-time convergence to the sliding surface, the closed-loop system states may only be guaranteed within infinite time. Thus, the terminal sliding mode control (TSMC) was evolved by Zak in the Jet Propulsion Laboratory (JPL) in 1988 [39]. The main idea of TSMC is the concept of terminal attractors which guarantee finite time convergence of the states. The TSMC was first introduced to the control of the dynamic systems based on second-order differential equations. After that, Yu and Man [40], [41] extended it to high-order system (2.1). The problem formulation is the same as Section 2.1. Defining $s(\mathbf{x})_i$ for i=1, $\cdots$, $r-1$ is a smooth scalar constraint function: $\mathbb{R}^n \rightarrow \mathbb{R}$, the hierarchical terminal sliding mode structure is

$$s_1 = \dot{s}_0 + b_1 s_0^{q_1/p_1} \tag{2.25}$$

$$s_2 = \dot{s}_1 + b_2 s_1^{q_2/p_2} \tag{2.26}$$

$$\vdots$$

$$s_{r-1} = \dot{s}_{r-2} + b_{r-1} s_{r-2}^{q_{r-1}/p_{r-1}} \tag{2.27}$$

where $s_0 = e$, $b_i > 0$, $p_i > q_i$ and p_i, q_i are positive odd integers This assumption allows us to achieve high-order continuous differentiation. For instance, the geometry plot for third-order system is shown in Fig. 2.4.

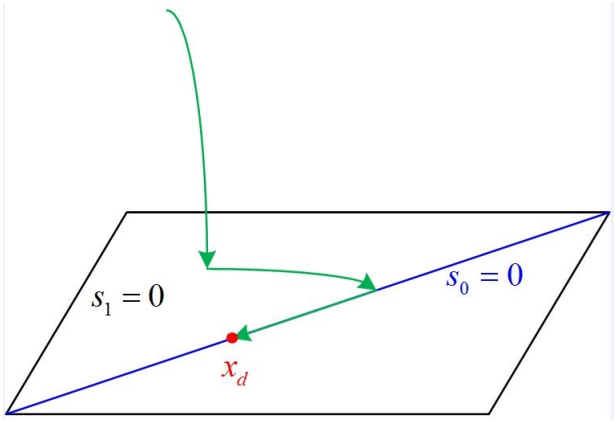

Fig. 2.4. The sliding mode of the third-order system

The control is divided into

$$u = u^{eq} + u^{re} \tag{2.28}$$

where u^{eq} is the equivalent control for system (2.1) without model uncertainties and external disturbances, such that $s_{r-1} = 0$ and $\dot{s} = 0$ and u^{re} is to compensate the internal parameter variations and turbulence. Furthermore, the time derivative of s_{r-1} is given by

$$\frac{d}{dt}s_{r-1} = \frac{d^2}{dt^2}s_{r-2} + b_{r-1}\frac{d}{dt}s_{r-2}^{q_{r-1}/p_{r-1}} \tag{2.29}$$

Besides, it can be easily calculated that

$$\frac{d^2}{dt^2}s_{r-2} = \frac{d^3}{dt^3}s_{r-3} + b_{r-2}\frac{d^2}{dt^2}s_{r-3}^{q_{r-2}/p_{r-2}} \tag{2.30}$$

$$\frac{d^3}{dt^3}s_{r-3} = \frac{d^4}{dt^4}s_{r-4} + b_{r-3}\frac{d^3}{dt^3}s_{r-4}^{q_{r-3}/p_{r-3}} \tag{2.31}$$

$$\vdots \tag{2.32}$$

$$\frac{d^{(r-2)}}{dt^{(r-2)}}s_2 = \frac{d^{(r-1)}}{dt^{(r-1)}}s_1 + b_2\frac{d^{(r-2)}}{dt^{(r-2)}}s_1^{q_2/p_2} \tag{2.33}$$

$$\frac{d^{(r-1)}}{dt^{(r-1)}}s_1 = \frac{d^{(r)}}{dt^{(r)}}s_0 + b_1\frac{d^{(r-1)}}{dt^{(r-1)}}s_0^{q_1/p_1} \tag{2.34}$$

Substituting Eqs. (2.52)-(2.34) into Eq. (2.29), we obtain

$$\frac{d}{dt}s_{r-1} = \frac{d^{(r)}}{dt^{(r)}}s_0 + \sum_{k=0}^{r-2} b_{k+1}\frac{d^{(r-1-k)}}{dt^{(r-1-k)}}s_k^{q_{k+1}/p_{k+1}} \tag{2.35}$$

Importing Eq. (3.4), the time derivative of s_{r-1} will be

$$\begin{aligned}\dot{s}_{r-1} &= f(\mathbf{x}) + g(\mathbf{x})u + d(\mathbf{x}) - x_d^r \\ &\quad + \sum_{k=0}^{r-2} b_{k+1}\frac{d^{(r-1-k)}}{dt^{(r-1-k)}}s_k^{q_{k+1}/p_{k+1}}\end{aligned} \tag{2.36}$$

Thus, the controller u is designed as follows:

$$u^{eq} = -\frac{1}{g(\mathbf{x})}\left[f(\mathbf{x}) - x_d^r + \sum_{k=0}^{r-2} b_{k+1}\frac{d^{(r-1-k)}}{dt^{(r-1-k)}}s_k^{q_{k+1}/p_{k+1}}\right] \tag{2.37}$$

and

$$u^{re} = -\frac{1}{g(\mathbf{x})}\left[\rho + \eta\right]\mathrm{sgn}(s) \tag{2.38}$$

Since $|d| \leq \rho$, $s \cdot \text{sgn}(s) = |s|$, Cauchy-Schwarz inequality $s \cdot d(\mathbf{x}) \leq |d(\mathbf{x})||s|$, and selected positive constant η which have been accounted for in Section 2.1., the resulting expression is substituted into Eq. (2.37) and Eq. (2.38) and multiplied by s_{r-1} as

$$\begin{aligned} s_{r-1}\dot{s}_{r-1} &= -\left[\rho+\eta\right] s \cdot \text{sgn}(s) + s \cdot d(\mathbf{x}) \\ &\leq -\left[\rho+\eta\right]|s| + |s||d(\mathbf{x})| \\ &\leq -\left[\rho+\eta\right]|s| + \rho|s| \\ &\leq -\eta|s| \end{aligned} \tag{2.39}$$

which means that the sliding mode $s_{r-1} = 0$ will be reached in finite time along with its slope less than or equal to $-\eta$ proved in Section 2.1. The finite time is directly proportional to the initial norm of s_{r-1} and the selected positive constant η expressing as $t_r \leq |s(\mathbf{x}(0))/\eta|$. However, the magnitude of the designed controller will become infinity if $s_i = 0$ when $\dot{s}_i \neq 0$. That is, it is the singularity problem. For example, the controller of second-order system is described

$$u = -\frac{1}{g(\mathbf{x})}\left[f(\mathbf{x}) - x_d^2 + b_1\left(q_1/p_1\right)e^{(q_1/p_1)-1}\dot{e} + \left(\rho+\eta\right)\text{sgn}(s)\right] \tag{2.40}$$

The term $b_1\left(q_1/p_1\right)e^{(q_1/p_1)-1}\dot{e}$ will occur singularity phenomenon since $e^{(q_1/p_1)-1} = 1/e^{((p_1-q_1)/p_1}$ where $(q_1/p_1) - 1 = (q_1 - p_1)/p_1$ is negative constant causes $1/e^{(p_1-q_1)/p_1} \to \infty$ as $e \to 0$. In this situation, if $\dot{e} = 0$, the designed controller diverges. The problem is unexpected and will be solved in later Section.

Next, we will discuss whether or not the closed-loop system states can converge within finite time when sliding condition is exactly verified. First, importing the second-order differential equations [42], basically a nonlinear switch line,

$$s = \dot{e} + be^{q/p} \tag{2.41}$$

where $e = x - x_d$, $b > 0$, p, q are positive odd integers and $p > q$. Similar to the conventional sliding mode control technique, if the controller is designed such that s converges to zero, then we say that the switching variable s reaches the terminal sliding mode

$$\dot{e} + be^{q/p} = 0 \tag{2.42}$$

It has been shown in Zak [39] that $e = 0$ is the terminal attractor of dynamics (2.42). For a error $e(t_r)$ at $t = t_r$ when $s = 0$, then we integrate the time derivative of $\dot{e} = -be^{q/p}$ to predict the convergence time t_s at the sliding regime. That is

$$\int_{t_r}^{t_s+t_r} -\frac{1}{b}e^{-q/p}de = \int_{t_r}^{t_s+t_r} dt \tag{2.43}$$

Then, we have

$$\frac{-p}{b(p-q)}e(t_r+t_s)^{1-\frac{q}{p}} + \frac{p}{b(p-q)}e(t_r)^{1-\frac{q}{p}} = t_s \tag{2.44}$$

According to the conditions: 1) p, q are positive odd integers; and 2) $p > q$, we multiply $-b(p-q)/p$ into Eq. (2.44) and move the second term of left to the right

$$0 \leq |e(t_r+t_s)|^{1-\frac{q}{p}} = -\frac{b(p-q)}{p}t_s + |e(t_r)|^{1-\frac{q}{p}} \tag{2.45}$$

Obviously, as

$$t_s = \frac{p}{b(p-q)}|e(t_r)|^{1-\frac{q}{p}} \tag{2.46}$$

we can verify

$$0 \leq |e(t_r+t_s)|^{1-\frac{q}{p}} \leq 0 \tag{2.47}$$

The expression (2.46) means that in terminal sliding mode (2.42) the state error e converges to zero in finite time, the same for $\dot{e}$. The total time reaching $e = 0$ is $t = t_r + t_s$. Then, expanding to high-order continuous differentiation. With the structure (2.26)-(2.27), if $s_{r-1} = 0$ is reached, the stability and finite-time reachability of system equilibrium will be guaranteed because it is a concatenation of r dynamics of Eq. (2.41) type. If $s_{r-1} = 0$ is reached at $t = t_r = t_{s0}$, then s_{r-2} will reach $s_{r-2} = 0$ at

$$t_{s1} = t_r + \frac{p_{r-1}}{b_{r-1}(p_{r-1}-q_{r-1})}|s_{r-2}(t_r)|^{1-\frac{q_{r-1}}{p_{r-1}}} \tag{2.48}$$

The general form of the convergent time t_{si} for s_{r-1-i} will reach $s_{r-1-i} = 0$ for i=1,$\cdots$, $(r-1)$ is described by

$$t_{s0} = t_r \tag{2.49}$$

$$\text{and } t_{si} = t_{s(i-1)} + \frac{p_{r-i}}{b_{r-i}(p_{r-i}-q_{r-i})}\left|s_{r-1-i}(t_{s(i-1)})\right|^{1-\frac{q_{r-1}}{p_{r-1}}} \tag{2.50}$$

The total time reaching $e = 0$ is

$$t = t_{s0} + \sum_{i=1}^{r-1} \frac{p_{r-i}}{b_{r-i}(p_{r-i} - q_{r-i})} \left| s_{r-1-i}(t_{s(i-1)}) \right|^{1-\frac{q_{r-1}}{p_{r-1}}} \tag{2.51}$$

TSMC adds nonlinear functions into the design of the sliding upper plane. A terminal sliding surface is constructed and the tracking errors on the sliding surface converge to zero in a finite time. Thus, the TSMC can guarantee that the system will achieve the desired output in finite time if the controller is designed by Eqs. (2.37) and (2.38).

2.3 Nonsingular Terminal Sliding Mode Control (NTSMC)

The TSMC is characterized, like the CSMC, by strong robustness to uncertainties and disturbances and guaranteed to achieve the desired state in finite time, yet it exists a singular problem for control law, for instance in second-order system, if $\dot{e} \neq 0$ when $e = 0$; that is, $u \to \pm\infty$ if $\dot{e} \neq 0$ as $e = 0$. In order to overcome the singularity problem in the conventional TSMC systems, several methods have been proposed. For instance, one approach is to switch the sliding mode between terminal sliding mode and linear hyperplane based sliding mode [43]. Another approach is to transfer the trajectory to a pre-specified open region where TSMC is not singular [41]. These methods are adopting indirect approaches to avoid the singularity. Thus, in 2001, Feng [44] proposed a novel TSMC for second-order system, called nonsingular terminal sliding mode control (NTSMC) to overcome the singularity problem. The time taken to reach the manifold from any initial state and the time taken to reach the equilibrium point in the sliding mode can be guaranteed to be finite time. However, the NTSMC is just adapted to the second-order system. In other words, selecting $n = 2$ for system (2.1). Choosing the sliding surface of the second-order NTSMC:

$$s = e + \frac{1}{c}\dot{e}^{p_1/q_1} \tag{2.52}$$

where $c = b_1^{p_1/q_1}$, and p_1, q_1 are positive odd integers under the constraint $1 < (p_1/q_1) < 2$. One can easily see that when s = 0, Eq. (2.52) is equivalent to Eq. (2.26) for $n = 2$ so that the time of convergence is the same as TSMC for $n = 2$ when $s = 0$. For convenience, we simplify p_1, q_1 as p, q, respectively. The finite time is taken to to travel from $e(t_r) \neq 0$

at $t = t_r$ to $e(t_r + t_s)$ is given by

$$t_s = \frac{p}{b(p-q)} |e(t_r)|^{1-\frac{q}{p}} \tag{2.53}$$

Note that in using Eq. (2.52) the derivative of s along the system dynamics does not result in terms with negative powers, but the parameters p and q must satisfy the constraint $1 < p/q < 2$ in addition. Next, we will account for the derivation process of the NTSMC controller. The controller is chosen

$$u = u^{eq} + u^{re} \tag{2.54}$$

where u^{eq} is the feedback control for system (2.1) for $n = 2$ without model uncertainties and external disturbances, such that $s = 0$ and $\dot{s} = 0$ and u^{re} is to compensate the internal parameter variations and turbulence. Furthermore, the time derivative of s is given by

$$\dot{s} = \dot{e} + \frac{1}{c}\left(\frac{p}{q}\right) \dot{e}^{\frac{p}{q}-1} \ddot{e} \tag{2.55}$$

Hence, the controller u can be designed as follows:

$$u^{eq} = -\frac{1}{g(\mathbf{x})}\left[f(\mathbf{x}) - x_d^2 + c\left(\frac{q}{p}\right) \dot{e}^{2-\frac{p}{q}}\right] \tag{2.56}$$

and

$$u^{re} = -\frac{1}{g(\mathbf{x})}\left[\rho + \eta\right] \mathrm{sgn}(s) \tag{2.57}$$

Since $|d(\mathbf{x})| \leq \rho$, $s \cdot \mathrm{sgn}(s) = |s|$, Cauchy-Schwarz inequality $s \cdot d(\mathbf{x}) \leq |d(\mathbf{x})||s|$, and selected positive constant η which have been accounted for in Section 2.1, the resulting expression of Eq. (2.55) is substituted into Eq. (2.56) and Eq. (2.57) and multiplied by s as

$$\begin{aligned} s\dot{s} &= s \cdot \left\{\frac{1}{c}\left(\frac{p}{q}\right) \dot{e}^{(p/q)-1} \left[(\rho+\eta)\,\mathrm{sgn}(s) + d(\mathbf{x})\right]\right\} \cdot \\ &\leq \frac{1}{c}\left(\frac{p}{q}\right) \dot{e}^{(p/q)-1} \left[-(\rho+\eta)|s| + |d(\mathbf{x})||s|\right] \\ &\leq \frac{1}{c}\left(\frac{p}{q}\right) \dot{e}^{(p/q)-1} \left[-(\rho+\eta)|s| + \rho|s|\right] \\ &\leq -\frac{1}{c}\left(\frac{p}{q}\right) \dot{e}^{(p/q)-1} \eta|s| \end{aligned} \tag{2.58}$$

Because p and q are positive odd integers and $1 < p/q < 2$, there is $\dot{e}^{(p/q)-1} > 0$ for $\dot{e} \neq 0$. Let $R(\dot{e}) = \frac{1}{c}\left(\frac{p}{q}\right)\dot{e}^{(p/q)-1}\eta$. As a result, we know $R(\dot{e}) > 0$ for $\dot{e} \neq 0$. Eq. (2.58) can be modified as

$$s\dot{s} \leq -R(\dot{e})|s| \text{ for } \dot{e} \neq 0 \tag{2.59}$$

will the NTSMC $s = 0$ be reached within finite time? The answer is yes [45]. The condition for Lyapunov stability is satisfied for the case $\dot{e} \neq 0$. According to Eq. (2.59), it implies that the slope of sliding variable is always negative expect for $\dot{e} = 0$. In addition, for the case $\dot{e} = 0$, substituting the control (2.56) and (2.57) into the second equation of (2.1) yields

$$\ddot{e} = -c\frac{q}{p}\dot{e}^{2-\frac{p}{q}} + d(\mathbf{x}) - (\rho+\eta)\,\mathrm{sgn}(s) \tag{2.60}$$

It can be easily seen that if $\dot{e} = 0$, then Eq. (2.60) becomes

$$\ddot{e} = d(\mathbf{x}) - (\rho+\eta)\,\mathrm{sgn}(s) \tag{2.61}$$

which suggests that $\dot{e} = 0$ while $e \neq 0$ is not an attractor. For the cases of $s > 0$ and $s < 0$, we can obtain $\ddot{e} \leq -\eta$ and $\ddot{e} \geq \eta$, respectively. In detail, there exists a vicinity $|\dot{e}| \leq \delta_{\dot{e}}$ for a small

$$\delta_{\dot{e}} = \left(\frac{\eta}{2}\frac{p}{cq}\right)^{\frac{q}{2q-p}} \tag{2.62}$$

For $s > 0$ and $\dot{e} > 0$, when $\dot{e}(t)$ reaches $\delta_{\dot{e}}$ from an initial state error rate $\dot{e}(0)$, we can obtain

$$\ddot{e} = -c\frac{q}{p}\dot{e}^{2-\frac{p}{q}} + d(\mathbf{x}) - (\rho+\eta) \leq -c\frac{q}{p}\dot{e}^{2-\frac{p}{q}} - \eta \leq -\frac{\eta}{2} \tag{2.63}$$

It means $\dot{e}(t)$ is monotonous decreasing and at least at the speed of $\frac{\eta}{2}$ cross the vicinity $\delta_{\dot{e}}$ within the finite time

$$t_{\delta_{\dot{e}}} \leq \frac{2\left(\dot{e}(0) - \dot{e}(t_{\delta_{\dot{e}}})\right)}{\eta} = \frac{4\delta_{\dot{e}}}{\eta} \tag{2.64}$$

In the same manner, for $s < 0$ and $\dot{e} < 0$, when $\dot{e}(t)$ reaches $\delta_{\dot{e}}$ from an initial state error rate $\dot{e}(0)$, we can obtain

$$\ddot{e} = -c\frac{q}{p}\dot{e}^{2-\frac{p}{q}} + d(\mathbf{x}) + (\rho+\eta) \geq -c\frac{q}{p}\dot{e}^{2-\frac{p}{q}} + \eta \geq \frac{\eta}{2} \tag{2.65}$$

It means $\dot{e}(t)$ is monotonous increasing and at least at the speed of $\frac{\eta}{2}$ cross the vicinity $\delta_{\dot{e}}$ within the finite time

$$t_{\delta_{\dot{e}}} \leq \frac{2\left(\dot{e}(t_{\delta_{\dot{e}}}) - \dot{e}(0)\right)}{\eta} = \frac{4\delta_{\dot{e}}}{\eta} \tag{2.66}$$

Therefore the crossing of trajectory from one boundary of the vicinity $\dot{e} = \delta_{\dot{e}}$ to the other boundary $\dot{e} = -\delta_{\dot{e}}$ for $s > 0$ and from $\dot{e} = -\delta_{\dot{e}}$ to $\dot{e} = \delta_{\dot{e}}$ for $s < 0$ is finite time. For the region outside the $|\dot{e}| < \delta_{\dot{e}}$, the time to reach the boundaries of the vicinity is finite. Indeed, we can easily show that

$$s\dot{s} \leq -\delta R(\dot{e})|s| \tag{2.67}$$

meaning the finite time reachability of the boundaries. The phase plane plot of the second-order system is presented in Fig. 2.5 as below:

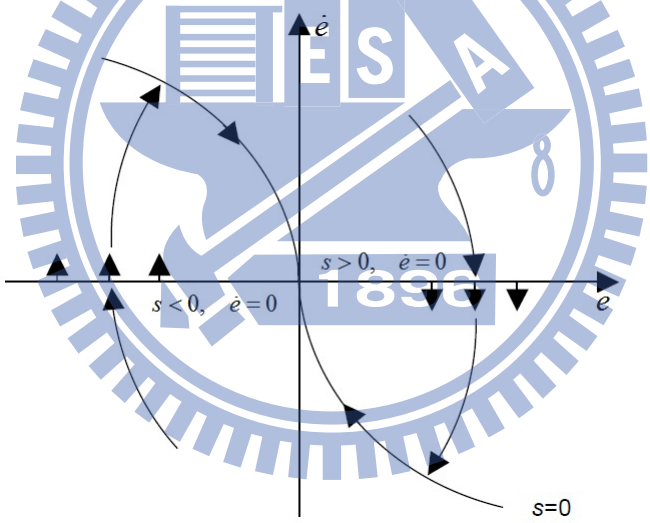

Fig. 2.5. The phase plot of the second-order system

Therefore we can conclude that the switching line can be reached within finite time. Furthermore, the designed controller does not contain the singularity term to occur singularity phenomenon compared with TSMC because the term $c\,(q/p)\,\dot{e}^{2-(p/q)}$ of Eq. (2.56) does not yield singularity under the constraint $1 < (p/q) < 2$. Thus, a NTSMC use the other nonlinear functions into the design of the sliding upper plane to not only overcome the singularity problem of TSMC but also verify the convergence of tracking desired output in finite time.

2.4 Mathematical Models of the Missile

2.4.1 Coordinate Systems

I) Definitions of Coordinate Frames

Before proceeding with the derivation, it is necessary to assume that the earth is an inertial reference, and unless otherwise stated the atmosphere is fixed with respect to the earth [46]. In addition, the coordinate systems adopted in the present discussion are right-handed axis systems.

i) Earth (Inertial) coordinate frame ($Ox_gy_gz_g$)

The origin O_g is at the ground tracker. Ox_g-axis is taken as north. The positive Oy_g-axis points upward in the vertical plane including Ox_g-axis. The positive Oz_g-axis is the right direction or completes the right-handed coordinate system.

ii) Body coordinate frame ($Ox_by_bz_b$)

The origin O_b is at the center of gravity of the missile. The positive Ox_b-axis coincides with the center line (or longitudinal axis) of the missile or forward direction. The positive Oy_b-axis points upward in the vertical plane including Ox_b-axis. The Oz_b-axis completes the right-handed coordinate system.

iii) Ballistic coordinate frame ($Ox_ty_tz_t$)

The origin O_t is at the center of gravity of the missile. The positive Ox_t-axis coincides with the velocity of the missile. The positive Oy_t-axis points upward in the vertical plane including Ox_t-axis and perpendicular to the horizontal plane of the earth. The Oz_t-axis completes the right-handed coordinate system.

iv) Wind coordinate frame ($Ox_vy_vz_v$)

The origin O_v is at the center of gravity of the missile. The positive Ox_v-axis coincides with the velocity of the missile. The positive Oy_v-axis points upward in the vertical plane including Ox_v-axis. The Oz_v-axis completes the right-handed coordinate system. Note that if the wind coordinate frame is nonrotating with respect to Ox_v-axis and the initial definition of the Oy_v-axis is including the vertical plane of the inertial coordinate frame (or the direction

of Oy_v-axis is always the same as Oy_t-axis), it is equal to ballistic coordinate frame.

II) Definitions of Angles

Herein, in order to clearly understand the definitions of the angles, the plus or minus sign of each angle is according to a rule which the rotation axis directs to the reader.

i) Angles between wind frame and body frame

α: It is between O_{x_v}-axis and the plane composed of O_{x_b}-axis and O_{z_b}-axis and defined the sign is positive when O_{x_v}-axis is under that plane.

β: It is between O_{x_v}-axis and the plane composed of O_{x_b}-axis and O_{y_b}-axis and defined the sign is positive when O_{x_v}-axis is on the right of that plane.

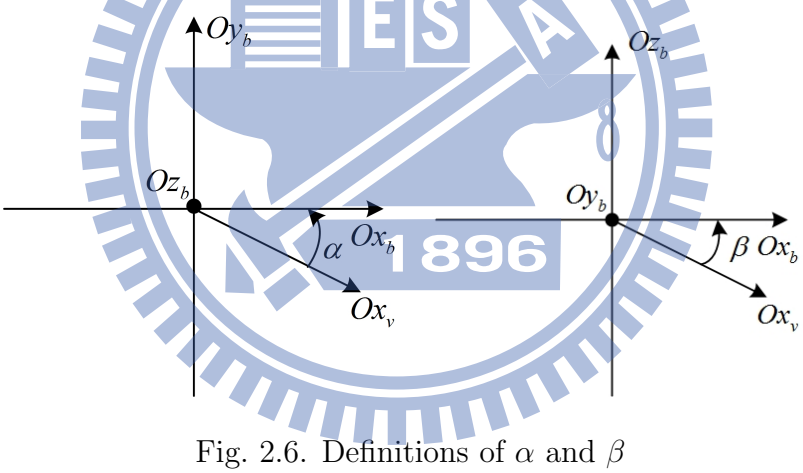

Fig. 2.6. Definitions of α and β

ii) Angles between ballistic frame and wind frame

γ_v: It is between O_{z_v}-axis and the plane composed of O_{x_t}-axis and O_{y_t}-axis and defined the sign is positive when O_{z_v}-axis is on the left of that plane.

iii) Angles between inertial frame and ballistic frame

θ: It is between O_{x_t}-axis and the plane composed of O_{x_g}-axis and O_{z_g}-axis and defined the sign is positive when O_{x_t}-axis is on the above of that plane.

ψ_v: It is between O_{x_t}-axis and the plane composed of O_{x_g}-axis and O_{y_g}-axis

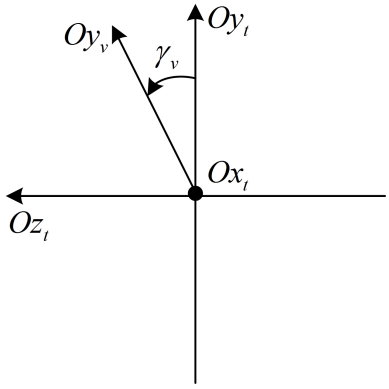

Fig. 2.7. Definition of γ_v

and defined the sign is positive when O_{x_t}-axis is on the left of that plane.

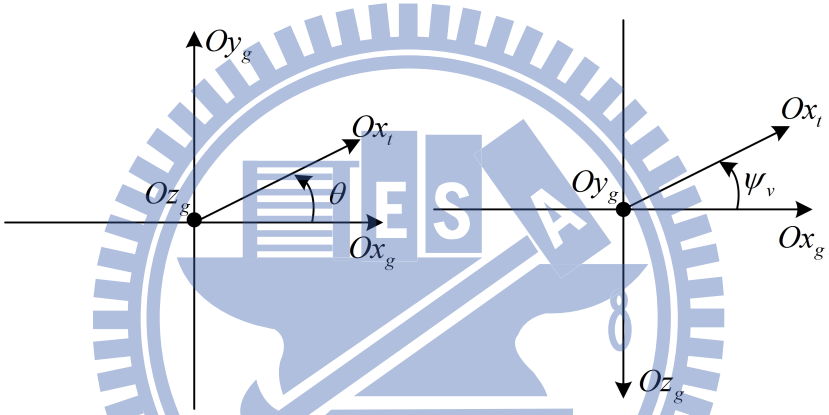

Fig. 2.8. Definitions of θ and ψ_v

iv) Angles between inertial frame and body frame

ϑ: It is between O_{x_b}-axis and the plane composed of O_{x_g}-axis and O_{y_g}-axis and defined the sign is positive when O_{x_b}-axis is on the above of that plane.

ψ: It is between O_{x_b}-axis and the plane composed of O_{x_g}-axis and O_{z_g}-axis and defined the sign is positive when O_{x_b}-axis is on the left of that plane.

γ: It is between O_{y_b}-axis and the plane composed of $O_{x'_g}$-axis and O_{y_g}-axis and defined the sign is positive when O_{y_b}-axis is on the left of that plane.

III) Coordinate Transformation

Define $M_k(\phi)$ to be the rotation by k axis with angle ϕ which any one frame is rotated counterclockwise away from other one with. and it is called direct cosine

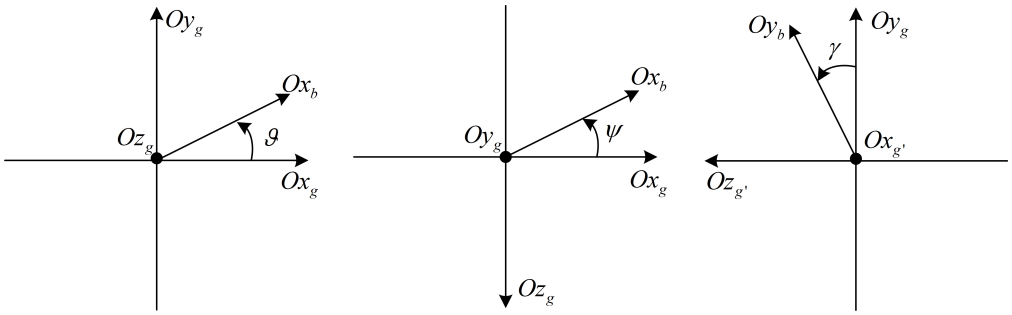

Fig. 2.9. Definitions of ϑ, ψ, and γ

matrix (DCM). So far as the surface-to-air missile is concerned, each one coordinate follows three rotated steps to other one: 1) yaw, 2) pitch, and 3) roll, and the derivation of the transformation only is established in the direction presented in Fig. 2.10. The DCM rotated by the axes y, z, and x will be:

$$M_y(\phi) = \begin{bmatrix} c_\phi & 0 & -s_\phi \\ 0 & 1 & 0 \\ s_\phi & 0 & c_\phi \end{bmatrix}$$
$$M_z(\phi) = \begin{bmatrix} c_\phi & s_\phi & 0 \\ -s_\phi & c_\phi & 0 \\ 0 & 0 & 1 \end{bmatrix} \tag{2.68}$$
$$M_x(\phi) = \begin{bmatrix} 1 & 0 & 0 \\ 0 & c_\phi & s_\phi \\ 0 & -s_\phi & c_\phi \end{bmatrix}$$

where c_ϕ and s_ϕ denote $\cos\phi$ and $\sin\phi$, respectively.

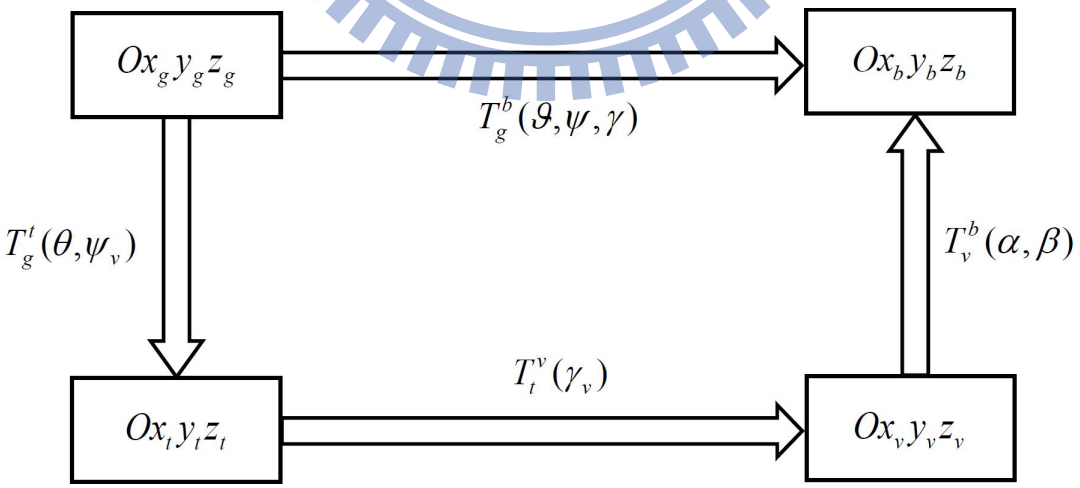

Fig. 2.10. The relationships among coordinates

And the each coordinate transformation is described separately as follows:

i) Wind frame transforms to body frame

$$\begin{aligned} T_v^b(\alpha,\beta) &= \begin{bmatrix} c_\alpha & s_\alpha & 0 \\ -s_\alpha & c_\alpha & 0 \\ 0 & 0 & 1 \end{bmatrix} \begin{bmatrix} c_\beta & 0 & -s_\beta \\ 0 & 1 & 0 \\ s_\beta & 0 & c_\beta \end{bmatrix} \\ &= \begin{bmatrix} c_\alpha c_\beta & s_\alpha & -c_\alpha s_\beta \\ -s_\alpha c_\beta & c_\alpha & s_\alpha s_\beta \\ s_\beta & 0 & c_\beta \end{bmatrix} \end{aligned} \tag{2.69}$$

ii) Ballistic frame transforms to wind frame

$$T_t^v(\gamma_v) = \begin{bmatrix} 1 & 0 & 0 \\ 0 & c_{\gamma_v} & s_{\gamma_v} \\ 0 & -s_{\gamma_v} & c_{\gamma_v} \end{bmatrix} \tag{2.70}$$

iii) Inertial frame transforms to ballistic frame

$$\begin{aligned} T_g^t(\theta,\psi_v) &= \begin{bmatrix} c_\theta & s_\theta & 0 \\ -s_\theta & c_\theta & 0 \\ 0 & 0 & 1 \end{bmatrix} \begin{bmatrix} c_{\psi_v} & 0 & -s_{\psi_v} \\ 0 & 1 & 0 \\ s_{\psi_v} & 0 & c_{\psi_v} \end{bmatrix} \\ &= \begin{bmatrix} c_\theta c_{\psi_v} & s_\theta & -c_\theta s_{\psi_v} \\ -s_\theta c_{\psi_v} & c_\theta & s_\theta s_{\psi_v} \\ s_{\psi_v} & 0 & c_{\psi_v} \end{bmatrix} \end{aligned} \tag{2.71}$$

iv) Inertial frame transforms to body frame

$$\begin{aligned} T_g^b(\gamma,\vartheta,\psi) &= \begin{bmatrix} 1 & 0 & 0 \\ 0 & c_\gamma & s_\gamma \\ 0 & -s_\gamma & c_\gamma \end{bmatrix} \begin{bmatrix} c_\vartheta & s_\vartheta & 0 \\ -s_\vartheta & c_\vartheta & 0 \\ 0 & 0 & 1 \end{bmatrix} \begin{bmatrix} c_\psi & 0 & -s_\psi \\ 0 & 1 & 0 \\ s_\psi & 0 & c_\psi \end{bmatrix} \\ &= \begin{bmatrix} c_\vartheta c_\psi & s_\vartheta & -c_\vartheta s_\psi \\ -s_\vartheta c_\psi c_\gamma + s_\psi s_\gamma & c_\vartheta c_\gamma & s_\vartheta s_\psi c_\gamma + c_\psi s_\gamma \\ s_\vartheta c_\psi s_\gamma + s_\psi c_\gamma & -c_\vartheta s_\gamma & -s_\vartheta s_\psi s_\gamma + c_\psi c_\gamma \end{bmatrix} \end{aligned} \tag{2.72}$$

2.4.2 Rigid-Body Equations of Motion

In this section we will consider a typical missile and derive the equations of motion according to Newton's laws. In deriving the rigid-body equations of motion, the following assumptions will be made [46], [47], [48]:

I) The missile is a rigid body, that is, the missile does not undergo any change in size and shape.

II) The missile is approximate a cylinder, that is, it is an axisymmetric or rotational symmetry missile.

III) The mass of the missile remains constant during any particular dynamic analysis.

IV) The aerodynamic forces and moments acting on the missile are invariant with the roll position of the missile relative to the free-stream velocity vector.

In addition, we note that in general, a vector $\mathbf{Q}$ can be transformed from a fixed frame $OXYZ$ to a rotating coordinate system $oxyz$ by the relation [49]

$$\dot{\mathbf{Q}}_{OXYZ} = \dot{\mathbf{Q}}_{Oxyz} + \boldsymbol{\omega}_{\boldsymbol{Q}} \times \mathbf{Q} \tag{2.73}$$

where $\boldsymbol{\omega}_{\boldsymbol{Q}}$ is the angular velocity of a rotating frame relatively to a fixed frame. Furthermore, if the rotating frame stops rotating, the two frames will has the same time rate of the change of state variables. Herein, the equations of motion are derived by the kinematics and dynamics. They will be presented in four formats: I) kinematics equations of translation about mass center, II) kinematics equations of rotation about mass center, III) dynamics equations of translation about mass center, and IV) dynamics equations of rotation about mass center, respectively [46], [47], [48].

I) Kinematics of Translation about Mass Center

In engineering practice, it is the simplest criterion for describing the missile translation in the ballistic frame. Denoting the angular velocity of ballistic frame relatively to inertial frame by $\boldsymbol{\Omega}$ and the missile velocity $\mathbf{V}$, the missile velocity expressed in the ballistic frame can be written in the form

$$m\frac{d\mathbf{V}}{dt} = m\left(\frac{\delta \mathbf{V}}{\delta t} + \boldsymbol{\Omega} \times \mathbf{V}\right) \tag{2.74}$$

Let us first resolve the vector $\boldsymbol{\Omega}$ and $\mathbf{V}$ into components Ω_{tx}, Ω_{ty}, Ω_{tz} and V_{tx}, V_{ty}, V_{tz}, respectively, along the axes of the ballistic frame. Denoting by $\mathbf{i_{tx}}$、$\mathbf{j_{ty}}$、$\mathbf{k_{tz}}$ the corresponding to unit vectors of the ballistic frame $(Ox_ty_tz_t)$, we write

$$\boldsymbol{\Omega} = \Omega_{tx}\mathbf{i_{tx}} + \Omega_{ty}\mathbf{j_{ty}} + \Omega_{tz}\mathbf{k_{tz}} \tag{2.75}$$

$$\mathbf{V} = V_{tx}\mathbf{i_{tx}} + V_{ty}\mathbf{j_{ty}} + V_{tz}\mathbf{k_{tz}} \tag{2.76}$$

$$\frac{\delta \mathbf{V}}{\delta t} = \frac{dV_{tx}}{dt}\mathbf{i_{tx}} + \frac{dV_{ty}}{dt}\mathbf{j_{ty}} + \frac{dV_{tz}}{dt}\mathbf{k_{tz}} \tag{2.77}$$

where

$$\begin{bmatrix} V_{tx} \\ V_{ty} \\ V_{tz} \end{bmatrix} = \begin{bmatrix} V \\ 0 \\ 0 \end{bmatrix} \tag{2.78}$$

Substituting from Eq. (2.78)into Eq. (2.76) ,

$$\frac{\delta \mathbf{V}}{\delta t} = \frac{dV}{dt}\mathbf{i_{tx}} \tag{2.79}$$

The Eq. (2.74) will be

$$\boldsymbol{\Omega} \times \mathbf{V} = \begin{vmatrix} \mathbf{i_{xt}} & \mathbf{j_{zt}} & \mathbf{k_{zt}} \\ \Omega_{xt} & \Omega_{yt} & \Omega_{zt} \\ V & 0 & 0 \end{vmatrix} = V\Omega_{zt}\mathbf{j_{ty}} - V\Omega_{yt}\mathbf{k_{tz}} \tag{2.80}$$

And, we have known that

$$\boldsymbol{\Omega} = \dot{\boldsymbol{\psi}}_{\boldsymbol{v}} + \dot{\boldsymbol{\theta}} \tag{2.81}$$

where $\dot{\boldsymbol{\psi}}_{\boldsymbol{v}}$ and $\dot{\boldsymbol{\theta}}$ are on the Oz_g-axis and Oy_t-axis, respectively. Eq. (2.81) can be modified as

$$\begin{aligned} \begin{bmatrix} \Omega_{xt} \\ \Omega_{yt} \\ \Omega_{zt} \end{bmatrix} &= \begin{bmatrix} c_\theta & s_\theta & 0 \\ -s_\theta & c_\theta & 0 \\ 0 & 0 & 1 \end{bmatrix} \begin{bmatrix} 0 \\ \dot{\psi}_v \\ 0 \end{bmatrix} + \begin{bmatrix} 0 \\ 0 \\ \dot{\theta} \end{bmatrix} \\ &= \begin{bmatrix} \dot{\psi}_v s_\theta \\ \dot{\psi}_v c_\theta \\ \dot{\theta} \end{bmatrix} \end{aligned} \tag{2.82}$$

Replacing Eq. (2.80) with Eq. (2.82), we have

$$\boldsymbol{\Omega} \times \mathbf{V} = \begin{bmatrix} 0 \\ V\dot{\theta} \\ -V\dot{\psi}_v \cos\theta \end{bmatrix} \tag{2.83}$$

Hence, substituting from Eqs. (2.77) and (2.79) into Eq. (2.74), we obtain

$$\begin{cases} F_{tx} = m\dot{V} \\ F_{ty} = mV\dot{\theta} \\ F_{tz} = -mV\dot{\psi}_v c_\theta \end{cases} \tag{2.84}$$

where F_{tx}, F_{ty}, F_{tz} are the components of net external force, which is formed by thrust, aerodynamic force, gravity, and lateral force, etc., with respect to the ballistic frame. Herein, we only analyze the first four sources of external force and the others are regarded as disturbances.

i) Thrust vector control (TVC)

The positive force of TVC $\mathbf{F}_{pb}$ is fixed in the direction of Ox_b-axis; that is,

$$\mathbf{F}_{pb} = \begin{bmatrix} F_p \\ 0 \\ 0 \end{bmatrix} \tag{2.85}$$

Using Eqs. (2.69) and (2.70), the force can be projected onto the ballistic frame and denoted as $\mathbf{F}_{pt}$.

$$\begin{aligned} \mathbf{F}_{pt} &= \left(T_t^v\right)^T \left(T_v^b\right)^T \mathbf{F}_{pb} \\ &= \begin{bmatrix} F_p c_\alpha c_\beta \\ F_p \left(s_\alpha c_{\gamma_v} + c_\alpha s_\beta s_{\gamma_v}\right) \\ F_p \left(s_\alpha s_{\gamma_v} - c_\alpha s_\beta c_{\gamma_v}\right) \end{bmatrix} \end{aligned} \tag{2.86}$$

ii) Aerodynamic force

The components of the force are defined as the positive drag force X along negative Ox_v-axis, the lift force Y positive to the Oy_b-axis, and the side force positive to the Oz_b-axis in the wind frame. Using Eq. (2.70), we can project it onto the ballistic frame.

$$\begin{aligned} \begin{bmatrix} F_{atx} \\ F_{aty} \\ F_{atz} \end{bmatrix} &= \left[T_t^v\right]^T \begin{bmatrix} -X \\ Y \\ Z \end{bmatrix} \\ &= \begin{bmatrix} -X \\ Yc_{\gamma_v} - Zs_{\gamma_v} \\ Ys_{\gamma_v} + Zc_{\gamma_v} \end{bmatrix} \end{aligned} \tag{2.87}$$

iii) Lateral thrust force

The components of the force are in the directions of Oy_b-axis and Oz_b-axis in the body frame, respectively. In the same manner as thrust vector force, we have

$$\begin{bmatrix} F_{tty} \\ F_{ttz} \end{bmatrix} = \begin{bmatrix} F_{tby}\left(c_\alpha c_{\gamma_v} - s_\alpha s_\beta s_{\gamma_v}\right) - F_{tbz}\left(c_\beta s_{\gamma_v}\right) \\ F_{tby}\left(c_\alpha s_{\gamma_v} + s_\alpha s_\beta c_{\gamma_v}\right) + F_{tbz}\left(c_\beta c_{\gamma_v}\right) \end{bmatrix} \tag{2.88}$$

iv) Gravity force

The negative force is in the direction of Oy_g-axis. Using Eq. (2.71), the force can be projected onto the ballistic frame.

$$\begin{aligned} \begin{bmatrix} mg_{tx} \\ mg_{ty} \\ mg_{tz} \end{bmatrix} &= \left(T_g^t\right) \begin{bmatrix} 0 \\ -mg \\ 0 \end{bmatrix} \\ &= \begin{bmatrix} -mgs_\theta \\ -mgc_\theta \\ 0 \end{bmatrix} \end{aligned} \tag{2.89}$$

Substituting Eqs. (2.86)-(2.89) into Eq. (2.84), the kinematics equations of translation about mass center are

$$\begin{cases} \dot{V} = \dfrac{1}{m}\left(F_{ptx} + F_{atx} + mg_{tx}\right) \\ \dot{\theta} = \dfrac{1}{mV}\left(F_{pty} + F_{aty} + F_{ltty} + mg_{ty}\right) \\ \dot{\psi}_v = \dfrac{-1}{mVc_\theta}\left(F_{ptz} + F_{atz} + F_{lttz} + mg_{tz}\right) \end{cases} \tag{2.90}$$

II) Kinematics of Rotation about Mass Center

In engineering practice, it is the simplest criterion for describing the missile rotation in body frame. Denoting the angular velocity of body frame corresponding to inertial frame by ω and the angular momentum $\mathbf{H}$, the kinematics equations of rotation about mass center has the form [49]

$$\frac{d\mathbf{H}}{dt} = \frac{\delta\mathbf{H}}{\delta t} + \boldsymbol{\omega} \times \mathbf{H} \tag{2.91}$$

The vectors $\boldsymbol{\omega}$ and $\mathbf{H}$ are divided into components ω_{bx}, ω_{by}, ω_{bz} and H_{bx}, H_{by}, H_{bz},respectively, along the axes of the body frame. Denoting by $\mathbf{i_{bx}}$, $\mathbf{j_{by}}$, $\mathbf{k_{bz}}$ the corresponding to unit vectors of the body frame, we write

$$\boldsymbol{\omega} = \omega_{bx}\mathbf{i_{bx}} + \omega_{by}\mathbf{j_{by}} + \omega_{bz}\mathbf{k_{bz}} \tag{2.92}$$

$$\mathbf{H} = H_{bx}\mathbf{i_{bx}} + H_{by}\mathbf{j_{by}} + H_{bz}\mathbf{k_{bz}} \tag{2.93}$$

The first term of the right side in Eq. (2.91) will be

$$\frac{\delta\mathbf{H}}{\delta t} = \frac{dH_{bx}}{dt}\mathbf{i_{bx}} + \frac{dH_{by}}{dt}\mathbf{j_{by}} + \frac{dH_{bz}}{dt}\mathbf{k_{bz}} \tag{2.94}$$

Besides, we have known that

$$\mathbf{H} = \mathbf{I} \cdot \boldsymbol{\omega} \tag{2.95}$$

where $\mathbf{I}$ is inertia tensor, including moments and products of inertia. According to the assumption 2, the products of inertia are zero in the body frame and Eq. (2.95) can be simplified as follows

$$\begin{bmatrix} H_{bx} \\ H_{by} \\ H_{bz} \end{bmatrix} = \begin{bmatrix} I_{xx}\omega_{bx} \\ I_{yy}\omega_{by} \\ I_{zz}\omega_{bz} \end{bmatrix} \tag{2.96}$$

Replacing the second term of the right side in Eq. (2.91) with Eq. (2.92) and Eq. (2.96), we can obtain

$$\boldsymbol{\omega} \times \mathbf{H} = \begin{vmatrix} \mathbf{i_{bx}} & \mathbf{j_{by}} & \mathbf{k_{bz}} \\ \omega_{bx} & \omega_{by} & \omega_{bz} \\ I_{xx}\omega_{bx} & I_{yy}\omega_{by} & I_{zz}\omega_{bz} \end{vmatrix} = \begin{bmatrix} (I_{zz} - I_{yy})\omega_{by}\omega_{bz} \\ (I_{xx} - I_{zz})\omega_{bx}\omega_{bz} \\ (I_{yy} - I_{xx})\omega_{bx}\omega_{by} \end{bmatrix} \tag{2.97}$$

Substituting Eqs. (2.94) and (2.97) into Eq. (2.91), we write

$$\begin{cases} M_{bx} = I_{xx}\dfrac{\omega_{bx}}{dt} + (I_{zz} - I_{yy})\omega_{by}\omega_{bz} \\ M_{by} = I_{yy}\dfrac{\omega_{by}}{dt} + (I_{xx} - I_{zz})\omega_{bx}\omega_{bz} \\ M_{bz} = I_{zz}\dfrac{\omega_{bz}}{dt} + (I_{yy} - I_{xx})\omega_{bx}\omega_{by} \end{cases} \tag{2.98}$$

where M_{bx}, M_{by}, M_{bz}, which are the rolling, yawing, and pitching moments, respectively, are the components of net external moment produced mainly by aerodynamic and lateral moments with respect to the body frame. Finally, we adjust Eq. (2.98), the kinematics equations of rotation about mass center are

$$\begin{cases} \dot{\omega}_{bx} = \dfrac{1}{I_{xx}}\left[M_{bx} + (I_{yy} - I_{zz})\omega_{by}\omega_{bz}\right] \\ \dot{\omega}_{by} = \dfrac{1}{I_{yy}}\left[M_{by} + (I_{zz} - I_{xx})\omega_{bx}\omega_{bz}\right] \\ \dot{\omega}_{bz} = \dfrac{1}{I_{zz}}\left[M_{bz} + (I_{xx} - I_{yy})\omega_{bx}\omega_{by}\right] \end{cases} \tag{2.99}$$

III) Dynamics of Translation about Mass Center

These equations are defined in the inertial frame such that we will understand the trajectory of the missile clearly. Furthermore, we must consider the altitude of the missile when calculating air density, dynamic pressure, and aerodynamic force. Hence, it is necessary to build these equations. In order to get these vectors, we must use Eqs. (2.69) and (2.72) to let Eq. (2.78) project into the inertial frame. The procedure is

$$\begin{bmatrix} \dot{x} \\ \dot{y} \\ \dot{z} \end{bmatrix} = \left(T_g^b\right)^T \left(T_v^b\right) \begin{bmatrix} V \\ 0 \\ 0 \end{bmatrix} \tag{2.100}$$

Expanding the above equation, we have dynamics equations of translation about mass center as follows:

$$\begin{cases} \dot{x} = V\left[c_\alpha c_\beta c_\vartheta c_\psi + s_\alpha c_\beta(s_\vartheta c_\psi c_\gamma - s_\psi s_\gamma) + s_\beta s_\vartheta c_\psi s_\gamma + s_\psi c_\gamma)\right] \\ \dot{y} = V\left(c_\alpha c_\beta s_\vartheta - s_\alpha c_\beta c_\vartheta c_\gamma - s_\beta c_\vartheta s_\gamma\right) \\ \dot{z} = -V\left[c_\alpha c_\beta c_\vartheta s_\psi + s_\alpha c_\beta(s_\vartheta s_\psi c_\gamma + c_\psi s_\gamma) + s_\beta(s_\vartheta s_\psi s_\gamma - c_\psi c_\gamma)\right] \end{cases} \tag{2.101}$$

IV) Dynamics of Rotation about Mass Center

For the purpose of describing the attitude of the missile in the inertial frame, it is indispensable to construct these equations. According to the relationship between body frame and inertial frame, we have known

$$\boldsymbol{\omega} = \dot{\boldsymbol{\psi}} + \dot{\boldsymbol{\vartheta}} + \dot{\boldsymbol{\gamma}} \tag{2.102}$$

where $\dot{\boldsymbol{\psi}}$, $\dot{\boldsymbol{\vartheta}}$, and $\dot{\boldsymbol{\gamma}}$ are in the direction of Oy_g-axis, Oz_g'-axis, and Ox_b-axis. We can modify Eq. (2.102)on the basis of the regulation of coordinate transformation in this thesis.

$$\begin{aligned} \begin{bmatrix} \omega_{bx} \\ \omega_{by} \\ \omega_{bz} \end{bmatrix} &= \begin{bmatrix} 1 & 0 & 0 \\ 0 & c_\gamma & s_\gamma \\ 0 & -s_\gamma & c_\gamma \end{bmatrix} \begin{bmatrix} c_\vartheta & s_\vartheta & 0 \\ -s_\vartheta & c_\vartheta & 0 \\ 0 & 0 & 1 \end{bmatrix} \begin{bmatrix} 0 \\ \dot{\psi} \\ 0 \end{bmatrix} \\ &+ \begin{bmatrix} 1 & 0 & 0 \\ 0 & c_\gamma & s_\gamma \\ 0 & -s_\gamma & c_\gamma \end{bmatrix} \begin{bmatrix} 0 \\ 0 \\ \dot{\vartheta} \end{bmatrix} + \begin{bmatrix} \dot{\gamma} \\ 0 \\ 0 \end{bmatrix} \\ &= \begin{bmatrix} 1 & s_\vartheta & 0 \\ 0 & c_\vartheta c_\gamma & s_\gamma \\ 0 & -c_\vartheta s_\gamma & c_\gamma \end{bmatrix} \begin{bmatrix} \dot{\gamma} \\ \dot{\psi} \\ \dot{\vartheta} \end{bmatrix} \end{aligned} \tag{2.103}$$

Inversing the above matrix and expanding Eq. (2.103), the dynamics equations of rotation about mass center will be

$$\begin{cases} \dot{\gamma} = \omega_{bx} - \dfrac{s_\vartheta}{c_\vartheta}(\omega_{by} c_\gamma - \omega_{bz} s_\gamma) \\ \dot{\psi} = \omega_{by} c_\gamma \dfrac{1}{c_\vartheta} - \omega_{z_b} s_\gamma \dfrac{1}{c_\vartheta} \\ \dot{\vartheta} = \omega_{by} s_\gamma + \omega_{bz} c_\gamma \end{cases} \tag{2.104}$$

2.4.3 Equations of Attitude Dynamics

In guidance law design, inputs are the overloadings of the missle, while the autopilot must provide these overloadings to guidance law to successfully hit-to-kill the target.

Besides, the overloading is produced by angle of attack or sideslip angle. Herein, for convenience, we will build the equations of attitude of these two angles in the wind frame. The angular velocity in the wind frame can be separated into two parts: 1) one is yielded by wind frame relatively to body frame; 2) the other is yielded by body frame relatively to inertial frame and projected into the wind frame. That is,

$$\boldsymbol{\omega}_v = (\boldsymbol{\omega}_b^v)_v + (\boldsymbol{\omega}_g^b)_v \tag{2.105}$$

where

$$\begin{aligned}(\boldsymbol{\omega}_g^b)_v &= \left(T_v^b\right)^T \begin{bmatrix} \omega_{bx} \\ \omega_{by} \\ \omega_{bz} \end{bmatrix} \\ &= \begin{bmatrix} \omega_{bx}c_\alpha c_\beta - \omega_{by}s_\alpha c_\beta + \omega_{bz}s_\beta \\ \omega_{bx}s_\alpha + \omega_{by}c_\alpha \\ -\omega_{bx}c_\alpha s_\beta + \omega_{by}s_\alpha s_\beta + \omega_{bz}c_\beta \end{bmatrix}\end{aligned} \tag{2.106}$$

and

$$\begin{aligned}(\boldsymbol{\omega}_b^v)_v &= \begin{bmatrix} 0 \\ -\dot{\beta} \\ 0 \end{bmatrix} + \begin{bmatrix} c_{-\beta} & 0 & -s_{-\beta} \\ 0 & 1 & 0 \\ s_{-\beta} & 0 & c_{-\beta} \end{bmatrix} \begin{bmatrix} 0 \\ 0 \\ -\dot{\alpha} \end{bmatrix} \\ &= \begin{bmatrix} \dot{\alpha}s_\beta \\ -\dot{\beta} \\ -\dot{\alpha}c_\beta \end{bmatrix}\end{aligned} \tag{2.107}$$

Then, we import Eq. (2.73) to express the acceleration of wind coordinate system relative to inertial coordinate system:

$$\frac{d\mathbf{V}}{dt} = \left(\frac{\delta \mathbf{V}}{\delta t} + \boldsymbol{\omega}_v \times \mathbf{V}\right) \tag{2.108}$$

where

$$\frac{\delta \mathbf{V}}{\delta t} = \begin{bmatrix} \dot{V} \\ 0 \\ 0 \end{bmatrix} \tag{2.109}$$

and

$$\begin{aligned}\boldsymbol{\omega}_v \times \mathbf{V} &= (\boldsymbol{\omega}_g^b)_v \times \mathbf{V} + (\boldsymbol{\omega}_b^v)_v \times \mathbf{V} \\ &= \begin{vmatrix} \mathbf{i_{vx}} & \mathbf{j_{vy}} & \mathbf{k_{vz}} \\ \omega_{g_{vx}}^b & \omega_{g_{vy}}^b & \omega_{g_{vz}}^b \\ V & 0 & 0 \end{vmatrix} + \begin{vmatrix} \mathbf{i_{vx}} & \mathbf{j_{vy}} & \mathbf{k_{vz}} \\ \omega_{b\,vx}^v & \omega_{b\,vy}^v & \omega_{b\,vz}^v \\ V & 0 & 0 \end{vmatrix} \\ &= \begin{bmatrix} 0 \\ (-\omega_{bx}c_\alpha s_\beta + \omega_{by}s_\alpha s_\beta + \omega_{bz}c_\beta)V \\ -(\omega_{bx}s_\alpha + \omega_{by}c_\alpha)V \end{bmatrix} + \begin{bmatrix} 0 \\ -\dot{\alpha}c_\beta V \\ \dot{\beta}V \end{bmatrix}\end{aligned} \tag{2.110}$$

Substituting Eqs. (2.109) and (2.110) into Eq. (2.108) and multiplying m in each term of Eq. (2.108), we get

$$\begin{cases} F_{vx} = m\dot{V} \\ F_{vy} = mV\left(-\omega_{bx}c_\alpha s_\beta + \omega_{by}s_\alpha s_\beta + \omega_{bz}c_\beta - \dot{\alpha}c_\beta\right) \\ F_{vz} = mV\left(\omega_{bx}s_\alpha + \omega_{by}c_\alpha + \dot{\beta}\right) \end{cases} \tag{2.111}$$

where F_{vx}, F_{vy}, F_{vz} are the components of net external force with respect to the wind frame, and we have presented the net external force is yielded by four parts. Now, we will analyze there force one by one as follows:

I) TVC

Using Eq. (2.69) to project into the wind frame, we obtain

$$\begin{aligned} \begin{bmatrix} F_{pvx} \\ F_{pvy} \\ F_{pvz} \end{bmatrix} &= \left(T_v^b\right)^T \begin{bmatrix} F_p \\ 0 \\ 0 \end{bmatrix} \\ &= \begin{bmatrix} F_p c_\alpha c_\beta \\ F_p s_\alpha \\ -F_p c_\alpha s_\beta \end{bmatrix} \end{aligned} \tag{2.112}$$

II) Aerodynamic force

The components of the aerodynamic force are below:

$$\begin{bmatrix} F_{avx} \\ F_{avy} \\ F_{avx} \end{bmatrix} = \begin{bmatrix} -X \\ Y \\ Z \end{bmatrix} \tag{2.113}$$

III) Lateral thrust force

Using Eq. (2.69) to project into wind frame, we have

$$\begin{aligned} \begin{bmatrix} F_{tvx} \\ F_{tvy} \\ F_{tvz} \end{bmatrix} &= \left(T_v^b\right)^T \begin{bmatrix} 0 \\ F_{tby} \\ F_{tbz} \end{bmatrix} \\ &= \begin{bmatrix} -F_{tby}s_\alpha c_\beta + F_{tbz}s_\beta \\ F_{tby}c_\alpha \\ F_{tby}c_\alpha s_\beta + F_{tbz}c_\beta \end{bmatrix} \end{aligned} \tag{2.114}$$

IV) Gravity force

Using Eqs. (2.72) and (2.69), we get

$$\begin{aligned} \begin{bmatrix} mg_{vx} \\ mg_{vy} \\ mg_{vz} \end{bmatrix} &= \left(T_v^b\right)^T \left(T_g^b\right) \begin{bmatrix} 0 \\ -mg \\ 0 \end{bmatrix} \\ &= \begin{bmatrix} mg_{bx}c_\alpha c_\beta - mg_{by}s_\alpha c_\beta + mg_{bz}s_\beta \\ mg_{bx}s_\alpha + mg_{by}c_\alpha \\ -mg_{bx}c_\alpha s_\beta + mg_{by}s_\alpha c_\beta + mg_{bz}c_\beta \end{bmatrix} \end{aligned} \tag{2.115}$$

where

$$\begin{bmatrix} mg_{bx} \\ mg_{by} \\ mg_{bz} \end{bmatrix} = \begin{bmatrix} -mgs_{\vartheta} \\ -mgc_{\vartheta}c_{\gamma} \\ mgc_{\vartheta}s_{\gamma} \end{bmatrix} \tag{2.116}$$

Substituting Eqs. (2.112)-(2.115) into Eq. (2.111), the first equation $\dot{V}$ is the same as Eq. (2.90). Thus, the attitude equations are

$$\begin{cases} \dot{\alpha} = \omega_{bz} - \dfrac{s_{\beta}}{c_{\beta}}(\omega_{bx}c_{\alpha} - \omega_{by}s_{\alpha}) - \dfrac{1}{mVc_{\beta}}(F_{pvy} + F_{avy} + F_{tvy} + mg_{vy}) \\ \dot{\beta} = \omega_{bx}s_{\alpha} + \omega_{by}c_{\alpha} + \dfrac{1}{mV}(F_{pvz} + F_{avz} + F_{tvz} + mg_{vz}) \end{cases} \tag{2.117}$$

2.4.4 Model of Tail Fins

The X-tail is located in the bottom of the missile, which is based on the Patriot Advanced Capability-3 (PAC-3) or MIM-104F missile [13]. From the end to the head of the missile, the signs of the first fin deflection δ_1 is on the top-left corner, and the others abide by the direction of clockwise are δ_2, δ_3, δ_4, respectively. Besides, the relationship between fin deflections and total equivalent fin deflections of aileron deflection angle, rudder deflection angle, and elevator deflection angle is analyzed below, and Fig. 2.11 shows the X-tail physical characteristics [50].

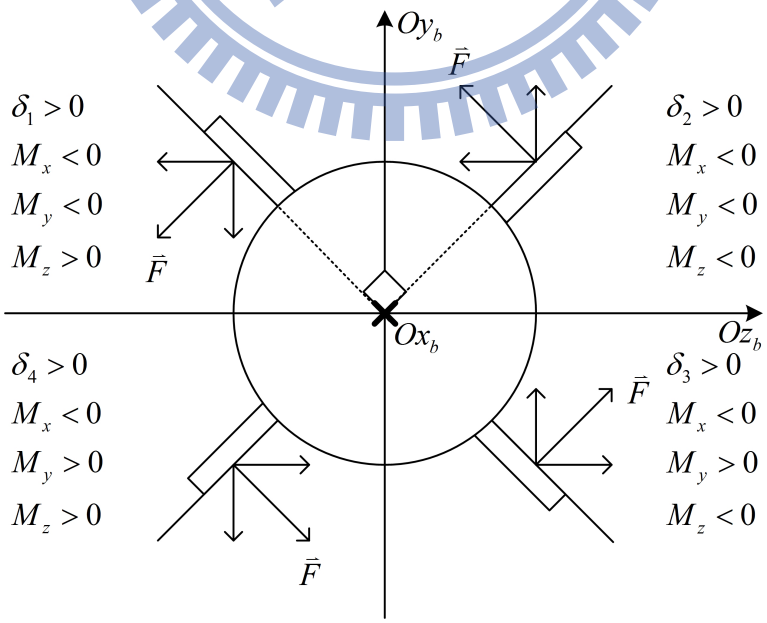

Fig. 2.11. Force analysis of X-tail

$$\delta_x = \delta_1 + \delta_2 + \delta_3 + \delta_4 \tag{2.118}$$

$$\delta_y = \frac{\sqrt{2}}{2}(\delta_1 + \delta_2 - \delta_3 - \delta_4) \tag{2.119}$$

$$\delta_z = \frac{\sqrt{2}}{2}(-\delta_1 + \delta_2 + \delta_3 - \delta_4) \tag{2.120}$$

The matrix form is

$$\begin{aligned}\begin{bmatrix} \delta_x \\ \delta_y \\ \delta_z \end{bmatrix} &= \frac{1}{2}\begin{bmatrix} 2 & 2 & 2 & 2 \\ \sqrt{2} & \sqrt{2} & -\sqrt{2} & -\sqrt{2} \\ -\sqrt{2} & \sqrt{2} & \sqrt{2} & -\sqrt{2} \end{bmatrix}\begin{bmatrix} \delta_1 \\ \delta_2 \\ \delta_3 \\ \delta_4 \end{bmatrix} \\ &= T(\delta)\begin{bmatrix} \delta_1 \\ \delta_2 \\ \delta_3 \\ \delta_4 \end{bmatrix}\end{aligned} \tag{2.121}$$

2.4.5 Reaction-Jet Control System (RCS)

This technology has been successfully implemented in PAC-3 since the Iraq War in 2003. This system, installed in front of the center of gravity of the missile or between the center of gravity and the top of the missile, yields lateral thrust changing the missile's attitude immediately for additional auxiliary thrust mounted [51]. It is contented 180 impulse attitude control motors (IACMs), arraying in 10 circles (each one composed of 18 IACMs), staggered distributing along the O_{xb}-axis equably. Note that the IACM is disposable. Define ith circle ($i = 1,\ 2, \cdots,\ 10$) for each circle from top to the center of gravity and jth IACM ($j = 1,\ 2, \cdots,\ 18$) for the number in each circle, the odd and even number circles are shown in Fig. 2.12.

In Fig. 2.12, the layout of the odd number circles presents that the first IACM is opposite direction to the O_{yb}-axis, and the number of the others follows the direction of counterclockwise, respectively. In the similar manner, the layout of the even number circles presents that the first IACM is on the left 20 degrees of the opposite direction to the O_{yb}-axis. The angle of each IACM is described below:

$$\Phi_{ij} = \begin{cases} (j-1) \times 2\pi/18 & \text{for } i \text{ is odd} \\ (j-1) \times 2\pi/18 + 2\pi/36 & \text{for } i \text{ is even} \end{cases} \tag{2.122}$$

or

$$\Phi_{ij} = \frac{2j - i^*}{18}\pi \tag{2.123}$$

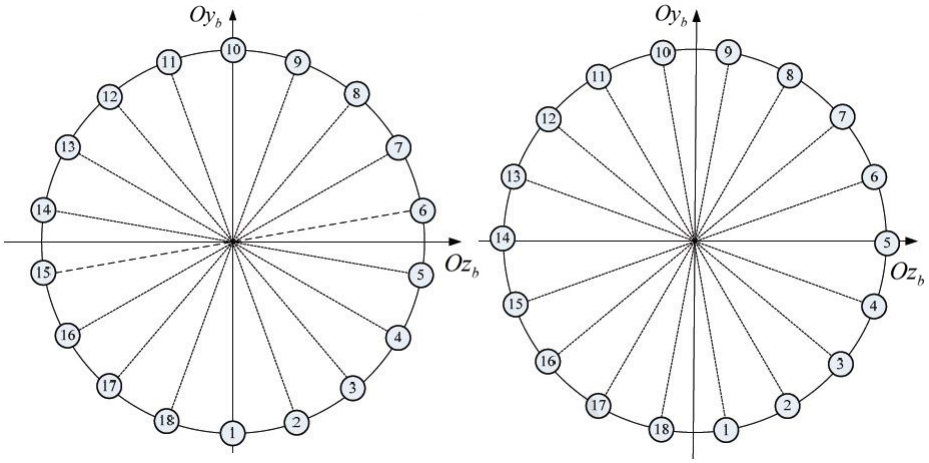

Fig. 2.12. The layout scheme of IACMs, left side for odd number and right side for even number

where $i^* = 2$ when i is odd, and $i^* = 1$ when i is even. The force and moment of each (i, j) IACM is presented as

$$\begin{cases} F_{tby}^{ij} = Kc_{\Phi_{ij}} s_{ij} \\ F_{tbz}^{ij} = -Ks_{\Phi_{ij}} s_{ij} \end{cases} \tag{2.124}$$

and

$$\begin{cases} M_{tby}^{ij} = -l_i F_{tbz}^{ij} \\ M_{tbz}^{ij} = l_i F_{tby}^{ij} \end{cases} \tag{2.125}$$

where K is the force of each IACM; l_i is the moment arm of ith circle from the center of gravity of the missile to the location of the ith circle; and s_{ij} is defined as if (i, j) IAMC is untapped or used once, $s_{ij} = 0$ and if (i, j) IAMC is opened, $s_{ij} = 1$. The total components of the lateral force and moment are

$$\begin{cases} F_{tby} = \sum_{i=1}^{10} \sum_{j=1}^{18} F_{tby}^{ij} \\ F_{tbz} = \sum_{i=1}^{10} \sum_{j=1}^{18} F_{tbz}^{ij} \end{cases} \tag{2.126}$$

and

$$\begin{cases} M_{tby} = \sum_{i=1}^{10} -l_i \sum_{j=1}^{18} F_{tbz}^{ij} \\ M_{tbz} = \sum_{i=1}^{10} l_i \sum_{j=1}^{18} F_{tby}^{ij} \end{cases} \tag{2.127}$$

CHAPTER THREE
OUTPUT TRACKING CONTROL FOR A NONLINEAR SYSTEM

Similar to system stabilizability analysis and synthesis, the task of output tracking has received considerable attention in both theoretical and practical industry applications [52]-[54]. The objective of output tracking control is to design a feedback law such that the output of a controlled plant can track a desired reference signal. To solve the tracking-control problem effectively, many methods and techniques have been presented. Those include regulator-based approach [55], inversion-based approach [56]-[58], Lyapunov-based approach [59], Takagi-Sugeno (T-S) fuzzy model-based approach [60] and sliding mode control-based (SMC) approach [61]-[63]. In this thesis, we will study the output tracking problem from a blended control viewpoint via the following three techniques: CSMC, TSMC and NTSMC schemes.

3.1 Problem Formulation

Consider a nonlinear control system as described by [62]

$$\dot{\mathbf{x}} = \mathbf{f}_o(\mathbf{x}) + G_o(\mathbf{x})\mathbf{u} \tag{3.1}$$

$$\text{and } \mathbf{y} = \mathbf{h}(\mathbf{x}) \tag{3.2}$$

where $\mathbf{x} = [x_1, \cdots, x_n]^T \in \mathbb{R}^n$, $\mathbf{u} = [u_1, \cdots, u_m]^T \in \mathbb{R}^m$, and $\mathbf{y} = [y_1, \cdots, y_v]^T \in \mathbb{R}^v$ denote the state variables, control inputs, and system outputs, respectively. The functions $\mathbf{f}_o(\mathbf{x}) \in \mathbb{R}^n$, $G_o(\mathbf{x}) = [\mathbf{g}_{o1}(\mathbf{x}), \cdots, \mathbf{g}_{om}(\mathbf{x})] \in \mathbb{R}^{n\times m}$ and $\mathbf{h}(\mathbf{x}) = [h_1(\mathbf{x}), \cdots, h_v(\mathbf{x})]^T \in \mathbb{R}^v$ are smooth functions. Our interest is to construct a control input so that the output

approaches the sliding surface and achieves the desired value. For the decoupled input-output system, the new output form is obtained from differentiating several times until it is related to the input. That is, differentiating the output y_j with respect to time, we obtain

$$\dot{y}_j = \bigtriangledown h_j \cdot \dot{\mathbf{x}} = \bigtriangledown h_j \cdot (\mathbf{f}_o + G_o \mathbf{u}) = L_{\mathbf{f}_o} h_j(\mathbf{x}) + \sum_{i=1}^{m} L_{\mathbf{g}_{oi}} h_j(\mathbf{x}) u_i \tag{3.3}$$

where $L_{\mathbf{f}_o} h_j(\mathbf{x})$ and $L_{\mathbf{g}_{oi}} h_j(\mathbf{x})$ are the Lie derivatives of h_j with respect to $\mathbf{f}_o$ and $\mathbf{g}_{oi}$ (for definition, please see e.g., [64]). If $L_{\mathbf{g}_i} h_j(\mathbf{x})$ is equal to zero for i=1,$\cdots$, m, then we have to differentiate the outputs y_j repeatedly until input appears. Assume that k_j is the smallest integer such that at least one of the inputs appears in $y_j^{(k_j)}$, then

$$y_j^{(k_j)} = L_{\mathbf{f}_o}^{k_j} h_j(\mathbf{x}) + \sum_{i=1}^{m} L_{\mathbf{g}_{oi}} L_{\mathbf{f}_o}^{k_j - 1} h_j(\mathbf{x}) u_i \tag{3.4}$$

with $L_{\mathbf{g}_{oi}} L_{\mathbf{f}_o}^{k_j - 1} h_j(\mathbf{x}) \neq 0$ for at least one i in a neighborhood of the point $\mathbf{x}_0$. k_j is exactly the number of times one has to differentiate y_j in order to have the control $\mathbf{u}$ explicitly appearing, in which $\{k_1, \cdots, k_v\}$ is called the relative degree [64] of the system. We impose the following assumption:

Assumption 3.1 The System (3.1)-(3.2) has the following three properties:

I) The distribution $\triangle := \text{span}\{\mathbf{g}_{o1}(\mathbf{x}), \cdots, \mathbf{g}_{om}(\mathbf{x})\}$ is involutive.

II) It has relative degree $\{k_1, \cdots, k_v\}$, that is, for all $\mathbf{x} \in \mathbb{R}^n$, $L_{\mathbf{g}_{oi}} L_{\mathbf{f}_o}^k h_j(\mathbf{x}) = 0$ for $1 \leq i \leq m$, $1 \leq j \leq v$ and $0 \leq k < k_j - 1$, while $L_{\mathbf{g}_{oi}} L_{\mathbf{f}_o}^k h_j(\mathbf{x}) \neq 0$ for $1 \leq i \leq m$, $1 \leq j \leq v$ and $k = k_j - 1$.

III) The control inputs $\mathbf{u}$ are divided into two parts $\mathbf{u}_1 \in \mathbb{R}^{m_1}$ and $\mathbf{u}_2 \in \mathbb{R}^{m_2}$ where $m_1 \geq v$ and $m_2 \geq v$.

Performing the above procedure for each output y_j yields

$$\begin{bmatrix} y_1^{(k_1)} \\ \vdots \\ y_v^{(k_v)} \end{bmatrix} = \mathbf{f}(\mathbf{x}) + G(\mathbf{x})\mathbf{u} \tag{3.5}$$

where

$$\mathbf{f}(\mathbf{x}) = \begin{bmatrix} L_{\mathbf{f}_o}^{k_1} h_1(\mathbf{x}) \\ \vdots \\ L_{\mathbf{f}_o}^{k_v} h_v(\mathbf{x}) \end{bmatrix}, \tag{3.6}$$

$$G(\mathbf{x}) = \begin{bmatrix} G_1(\mathbf{x}) & G_2(\mathbf{x}) \end{bmatrix}, \tag{3.7}$$

$$G_1(\mathbf{x}) = \begin{bmatrix} L_{\mathbf{g}_{o1}} L_{\mathbf{f}_o}^{k_1-1} h_1(\mathbf{x}) & \cdots & L_{\mathbf{g}_{om_1}} L_{\mathbf{f}_o}^{k_1-1} h_1(\mathbf{x}) \\ \vdots & \ddots & \vdots \\ L_{\mathbf{g}_{o1}} L_{\mathbf{f}_o}^{k_v-1} h_v(\mathbf{x}) & \cdots & L_{\mathbf{g}_{om_1}} L_{\mathbf{f}_o}^{k_v-1} h_v(\mathbf{x}) \end{bmatrix} \in \mathbb{R}^{v \times m_1}, \tag{3.8}$$

$$\text{and } G_2(\mathbf{x}) = \begin{bmatrix} L_{\mathbf{g}_{o(m_1+1)}} L_{\mathbf{f}_o}^{k_1-1} h_1(\mathbf{x}) & \cdots & L_{\mathbf{g}_{om}} L_{\mathbf{f}_o}^{k_1-1} h_1(\mathbf{x}) \\ \vdots & \ddots & \vdots \\ L_{\mathbf{g}_{o(m_1+1)}} L_{\mathbf{f}_o}^{k_v-1} h_v(\mathbf{x}) & \cdots & L_{\mathbf{g}_{om}} L_{\mathbf{f}_o}^{k_v-1} h_v(\mathbf{x}) \end{bmatrix} \in \mathbb{R}^{v \times m_2}. \tag{3.9}$$

Assumption 3.2 $\text{rank}\,(G_1(\mathbf{x})) = \text{rank}\,(G_2(\mathbf{x})) = v$

Equation (3.5) can also be rewritten as

$$\begin{bmatrix} y_1^{(k_1)} \\ \vdots \\ y_v^{(k_v)} \end{bmatrix} = \mathbf{f}(\mathbf{x}) + G_1(\mathbf{x})\mathbf{u}_1 + G_2(\mathbf{x})\mathbf{u}_2 + \mathbf{d}. \tag{3.10}$$

Note that, we have introduced $\mathbf{d}$ in Eq. (3.10) to represent possible model uncertainties, measurement noise and external disturbances. In this study, we call $\mathbf{u}_1$ the main inputs which are continuous and $\mathbf{u}_2$ (with components u_{2j} for $1 \le j \le m_2$) the auxiliary inputs which are constant during a short time period once it was triggered with the following form:

$$u_{2j} := \begin{cases} N_j K & \text{if } t \in [t_{oj}, t_{oj} + \triangle t_p] \\ 0 & \text{elsewhere} \end{cases} \tag{3.11}$$

where K denotes the minimum level of auxiliary control force; $|N_j|$ is an integer which represents the number of actuators in u_{2j} being activated; t_{oj} is the time instant that the actuator u_{2j} is triggered; and $\triangle t_p$ denotes the time duration of the constant force. Note that $\mathbf{u}_1$ suffer from the output magnitude constraints, while $\mathbf{u}_2$ only provide discrete values and the integer N_j, given by Eq. (3.11), satisfies $|N_j| \le N_u$, where N_u is a positive integer, i.e., $N_j \in \{0, \pm 1, \pm 2, \cdots, \pm N_u\}$. Besides, we assume that the output magnitude of the auxiliary inputs are much larger than those of the main inputs.

Before designing the control law, we have to check if the nonlinear system is minimum phase. The scalar $k_r = k_1 + \cdots + k_v$ is called the total relative degree of the nonlinear

system [20]. The necessary and sufficient condition for the existence of a coordinate transformation and a feedback that can linearize the system completely from the Input/Output (I/O) point of view is the total relative degree k_r being the same as the order of the system, i.e., $k_r = n$. If $k_r < n$, then, the nonlinear system can only be partially linearized. In this case, the stability of the nonlinear system given by Eqs. (3.1) and (3.2) depends not only on the I/O linearized system, but also on the stability of the internal dynamics (or zero dynamics).

According to linear algebra theory, $G_1(\mathbf{x})$ can be expressed as $G_1(\mathbf{x}) = G_{1\mathbf{v}_1}(\mathbf{x})G_{1\mathbf{u}_1}(\mathbf{x})$ where a diagonal matrix $G_{1\mathbf{v}_1}(\mathbf{x}) \in \mathbb{R}^{v\times v}$ and $G_{1\mathbf{u}_1}(\mathbf{x}) \in \mathbb{R}^{v\times m_1}$ satisfy $\text{rank}\,(G_{1\mathbf{v}_1}(\mathbf{x})) = \text{rank}\,(G_{1\mathbf{u}_1}(\mathbf{x})) = v$. Given a desired $\mathbf{v}$, the minimum norm solution of $\mathbf{u}_1$ that satisfies $\mathbf{v}_1 = G_{1\mathbf{u}_1}(\mathbf{x})\mathbf{u}_1$ is $\mathbf{u}_1 = G^T_{1\mathbf{u}_1}(\mathbf{x})\left(G_{1\mathbf{u}_1}(\mathbf{x})G^T_{1\mathbf{u}_1}(\mathbf{x})\right)^{-1}\mathbf{v}_1$, that is, $\mathbf{u}_1$ is easily constructed if $\mathbf{v}_1$ has been designed. Note that, $G_1(\mathbf{x})\mathbf{u}_1 = G_{1\mathbf{v}_1}\mathbf{v}_1$. Therefore, we may assume without lose any generality that $G_1(\mathbf{x})$ is a diagonal matrix and $G_1(\mathbf{x}) = \text{diag}[g_{11}(\mathbf{x}), \cdots, g_{1v}(\mathbf{x})]$. In the same manner, we also may assume that $G_2(\mathbf{x})$ is a diagonal matrix and $G_2(\mathbf{x}) = \text{diag}[g_{21}(\mathbf{x}), \cdots, g_{2v}(\mathbf{x})]$. Under the setting, System (3.5) can be rewritten in more simpler form as follows:

$$y_j^{(k_j)} = f_j(\mathbf{x}) + g_{1j}(\mathbf{x})u_{1j} + g_{2j}(\mathbf{x})u_{2j} + d_j \tag{3.12}$$

where $\mathbf{f}_j, g_{1j}, g_{2j} : \mathbb{R}^n \to \mathbb{R}$, and u_{1j} and u_{2j} are the jth component of $\mathbf{u}_1$ and $\mathbf{u}_2$, respectively, for $j = 1, \cdots, v$. In addition, we define the output errors to be

$$e_j(t) = y_j(t) - y_{jd}(t), \quad j = 1, \cdots, v \tag{3.13}$$

where $y_{jd}(t)$ is the desired output trajectory.

The main goal of this thesis is then to design suitable control laws which integrate the main inputs u_{1j} and auxiliary inputs u_{2j} such that the output tracking performance can be achieved, i.e., $e_j(t) \to 0$ as quickly as possible.

3.2 Design of Blended Controller

In this section, we will incorporate the main inputs (i.e., tail controllers) with auxiliary inputs (i.e., lateral thrusters), called blended control, through the CSMC, TSMC and

NTSMC schemes. The idea behind the design is as follows. First, a boundary layer (BL) of the sliding surface is determined from the region where the system states will be forced out or on this BL using the minimum level of auxiliary control inputs in one time duration or period. Inside or on the BL, only the main inputs are used to keep the system states close to the sliding surface as better as possible. When the system states are outside the BL, both main and auxiliary inputs will be activated for better convergence rate of system states to the sliding surface, compared with only considering the main inputs. The level of the auxiliary inputs will be determined from the distance between the system states and the sliding surface. Moreover, because the magnitude of the auxiliary inputs are much larger than those of the main inputs, the main inputs are used to compensate for only the deterministic dynamics, while the auxiliary inputs are responsible for disturbance rejection and reaching the sliding surface. For better understanding of the design, a block diagram for the blended control is shown in Fig. 3.1.

Under the CSMC, TSMC and NTSMC schemes, the presented blended control design

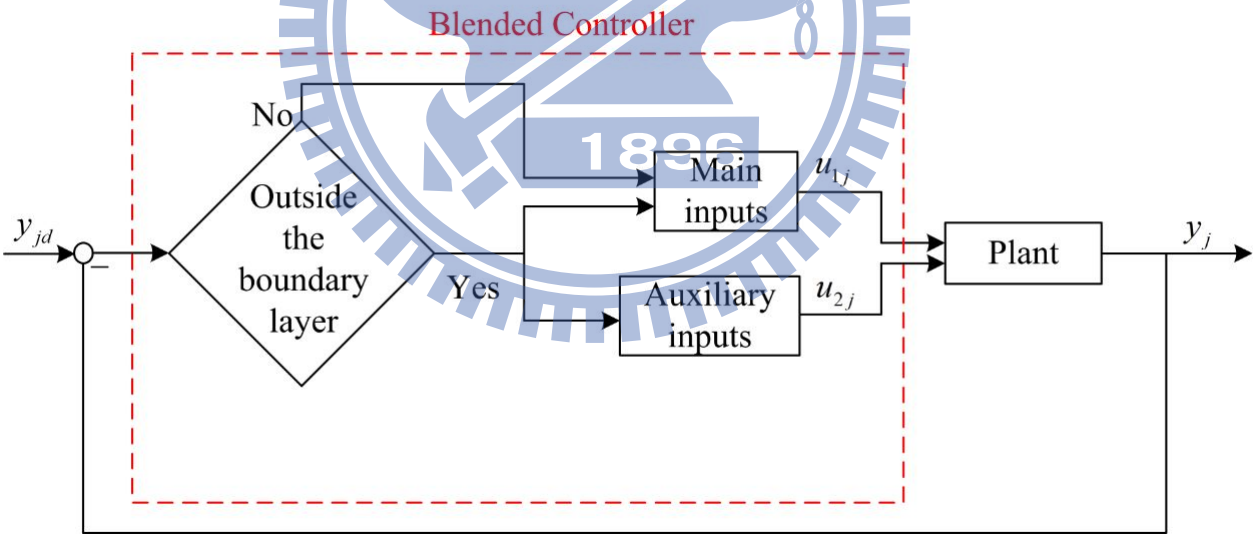

Fig. 3.1. Block diagram of blended control

include the following two features:

I) Outside the BL, the auxiliary inputs are used to account for the convergence speed of the system states to the sliding surface because they only provide constant control force, which is much larger than the main inputs, while the main inputs are employed

to compensate for deterministic dynamics and the drastic change of states produced by the activation of the auxiliary inputs for maintaining the rate of sliding variable being zero.

II) Inside or on the BL, because the auxiliary inputs are not activated so that the states variations are smooth. Therefore, only the main inputs are used for output the tracking purpose.

3.2.1 Control Design via CSMC scheme

The CSMC design consists of the following two steps: I) choose an appropriate sliding surface in terms of error states and II) construct a control law in form of

$$\mathbf{u} = \mathbf{u}^{re} + \mathbf{u}^{eq} \tag{3.14}$$

to realize the tracking performance, where $\mathbf{u}^{re}$ plays the role of making the error states reach the sliding surface in finite time, while $\mathbf{u}^{eq}$ keeps the sliding surface an invariant set and directs the output tracking errors to the origin. For the first step, we choose the sliding surface to be $s_j(t) = 0$ with

$$s_j = e_j^{(k_j-1)}(t) + a_{j(k_j-1)}e_j^{(k_j-2)}(t) + \cdots + a_{j2}\dot{e}_j(t) + a_{j1}e_j(t) \tag{3.15}$$

for $j = 1, \cdots, v$. Here, a_{jk} for $k = 1, \cdots, (k_j-1)$ are selected constants and the polynomial

$$\lambda_j^{k_j-1} + a_{j(k_j-1)}\lambda_j^{k_j-2} + \cdots + a_{j2}\lambda_j + a_{j1} \tag{3.16}$$

for $j = 1, \cdots, v$ are Hurwitz. Obviously, the output tracking performance can be achieved if the system states keep lying on the sliding surface, that is, $e_j \to 0$ as $t \to \infty$. Furthermore,

$$\begin{aligned} \dot{s}_j &= f_j(\mathbf{x}) + g_{1j}(\mathbf{x})u_{1j} + g_{2j}(\mathbf{x})u_{2j} + d_j - y_{jd}^{(k_j)} \\ &\quad + a_{j(k_j-1)}e_j^{(k_j-1)}(t) + \cdots + a_{j2}\ddot{e}_j(t) + a_{j1}\dot{e}_j(t) \end{aligned} \tag{3.17}$$

For second step, the controller design is divided into two parts: I) main inputs and II) auxiliary inputs, as described below:

I) Design of Main Inputs

The control law of each main input is designed to be the form of

$$u_{1j}^{eq} = -\frac{1}{g_{1j}(\mathbf{x})} \cdot \left[f_j(\mathbf{x}) - y_{jd}^{(k_j)}(t) + a_{j(k_j-1)} e_j^{(k_j-1)}(t) + \cdots + a_{j2}\ddot{e}_j(t) + a_{j1}\dot{e}_j(t) \right] \quad (3.18)$$

to accomplish the demand of making the sliding surface an invariant set. To guarantee the reaching condition, we assume that d_j is bounded as follows

Assumption 3.3 There exists nonnegative functions $\rho_j(\mathbf{x}, t)$, $j = 1, \cdots, v$, such that

$$|d_j| \leq \rho_j(\mathbf{x}, t) \quad (3.19)$$

Let ϵ_j be the BL width associated with s_j. Choose

$$u_{1j}^{re} = \begin{cases} -\dfrac{1}{g_{1j}(\mathbf{x})} \cdot (\rho_j + \eta_{mj}) \cdot \mathrm{sgn}(s_j) & \text{if } |s_j| \leq \epsilon_j \text{ and } u_{2j} = 0 \\ 0 & \text{otherwise} \end{cases} \quad (3.20)$$

where η_{mj} for $j = 1, \cdots, v$ are selected positive constants.

II) Design of Auxiliary Inputs

Because the auxiliary inputs involve the following two characteristics: I) being zero or nonzero constant during a time duration depending on whether or not they are triggered; II) with output magnitudes being much larger than the main inputs if they are triggered. Consequently, the control law of each auxiliary input is designed to be

$$u_{2j}^{eq} = 0 \quad (3.21)$$

$$\text{and } u_{2j}^{re} = N_j K. \quad (3.22)$$

Now, we will discuss how N_j is selected. The method is based on the sliding condition

$$\frac{d}{dt}|s_j| \leq -\eta_{rj}' \quad (3.23)$$

where η_{rj}' is a fictitious positive constant. The geometry of Condition (3.23) is shown in Fig. 3.2 below:

According to Ineq. (3.23), the system state will reach $s_j(\mathbf{x}) = 0$ within the time of

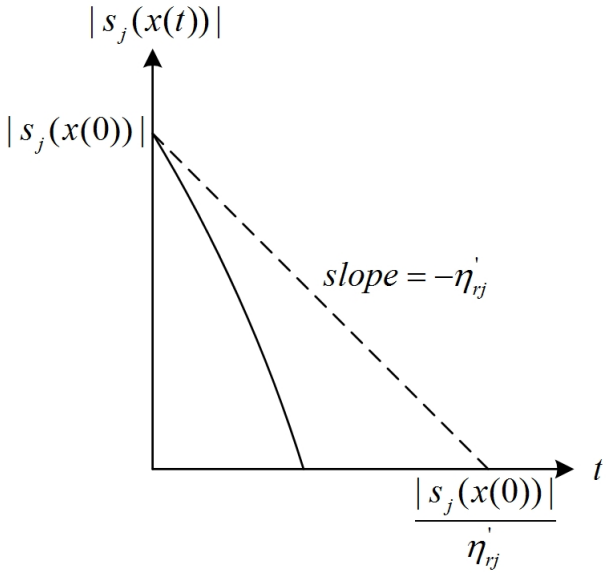

Fig. 3.2. The time response of $|s_j(\mathbf{x}(t))|$

$|s_j(\mathbf{x}(0))|/\eta_{rj}'$. When $\triangle t_p$ is given, the minimum η_{rj}' that makes the system state reaching the manifold $s_j(\mathbf{x}) = 0$ within $\triangle t_p$ is

$$\eta_{rj}' = \frac{|0 - s_j(\mathbf{x}(t))|}{\triangle t_p}. \tag{3.24}$$

We choose

$$u_{2j}^{re'} = -\frac{1}{g_{2j}} \cdot \left(\rho_{ju} + \eta_{rj}'\right) \cdot \mathrm{sgn}(s_j) \tag{3.25}$$

where $u_{2j}^{re'}$ is the fictitious control input of u_{2j}^{re} and ρ_{ju} is the upper bound of ρ_j. Then,

$$\begin{aligned} s_j(t)\dot{s}_j(t) &= -s_j(t)\left(\rho_{ju} + \eta_{rj}'\right) \cdot \mathrm{sgn}(s_j) + s_j(t) \cdot d_j \\ &\leq -\left(\rho_{ju} + \eta_{rj}'\right)|s_j| + \rho_{ju}|s_j| \\ &\leq -\eta_{rj}'|s_j| \end{aligned} \tag{3.26}$$

Inequality (3.26) accounts for the sliding variable s_j will converge in finite time. However, in fact, $u_{2j}^{re'}$ must accord with the form of N_jK. One method to determine N_j is such that the value N_jK as close $u_{2j}^{re'}$ as possible, that is, we round off $\left(u_{2j}^{re'}/K\right)$ to determine the

constant integer N_j. In more detail, Eq. (3.25) is replaced by Eq. (3.22) described below

$$\begin{aligned} u_{2j}^{re} &= \text{round}\left(u_{2j}^{re'}/K\right)K \\ &= \text{round}\left(-\frac{\left(\rho_{ju}+\eta_{rj}^{'}\right)/g_{2j}}{K}\cdot\text{sgn}(s_j)\right)K \\ &= -\text{round}\left(\frac{\left(\rho_{ju}+\eta_{rj}^{'}\right)/g_{2j}}{K}\right)\text{sgn}(s_j)\cdot K \\ &= -N_j^{'}\cdot\text{sgn}(s_j)\cdot K \\ &= N_j K \end{aligned} \tag{3.27}$$

where

$$N_j^{'} = \begin{cases} \text{round}\left(\dfrac{\left(\rho_{ju}+\eta_{rj}^{'}\right)/g_{2j}}{K}\right) & \\ & \text{if } \left|\text{round}\left(\dfrac{\left(\rho_{ju}+\eta_{rj}^{'}\right)/g_{2j}}{K}\right)\right| < N_u \\ N_u\text{sgn}(N_j^{'}) & \text{otherwise} \end{cases} \tag{3.28}$$

$$\text{and } N_j = -N_j^{'}\cdot\text{sgn}(s_j). \tag{3.29}$$

Note that the function round$(\cdot)$ is defined to round off a scalar. Then, the virtual convergence speed is approximate to be:

$$\eta_{rj} = N_j^{'}Kg_{2j} - \rho_{ju}. \tag{3.30}$$

Although the actual reaching time $|s_j(\mathbf{x}(0))|/\eta_{rj}$ can not exactly coincide with the expected reaching time $|s_j(\mathbf{x}(0))|/\eta_{rj}^{'}$, that is, this will cause inaccuracy of the reaching time which is at most in $\triangle t_p$, s_j can still converge according to the next paragraph.

Herein, we verify whether the sliding variable will converge. When s_j is outside the BL, from (3.17), we have

$$\begin{aligned} s_j(t)\dot{s}_j(t) &= s_j(t)NKg_{2j} + s_j(t)\cdot d_j \\ &\le -N_j^{'}Kg_{2j}|s_j| + \rho_{ju}|s_j| \\ &\le -(\rho_{ju}+\eta_{rj})|s_j| + \rho_{ju}|s_j| \\ &\le -\eta_{rj}|s_j| \end{aligned} \tag{3.31}$$

Clearly, the system states will approach the sliding surface with a convergence speed at least η_{rj} for j=1, $\cdots$, v in a finite time [20] whenever the system states are outside the BL. In contrast, when s_j is inside or on the BL, from (3.17), we get

$$\begin{aligned} s_j(t)\dot{s}_j(t) &= -(\rho_j + \eta_{mj})s_j(t)\text{sgn}(s_j) + s_j(t) \cdot d_j \\ &\leq -(\rho_j + \eta_{mj})|s_j| + \rho_j|s_j| \\ &\leq -\eta_{mj}|s_j| \end{aligned} \tag{3.32}$$

Similarly, the system states will reach the sliding surface in a finite time $t_{rj} = |s_j(\mathbf{x}(t_{aj}))|/\eta_{mj}$ for j=1, $\cdots$, v [20] where t_{aj} is the time when any auxiliary input is not activated. According to above analysis, it implies that we can select bigger η_{rj} advisably outside the BL to make s_j approach $s_j = 0$ faster and it still satisfies the sliding condition after s_j is inside the BL.

In addition, according to Eq. (3.28), the minimum nonzero integer of $\left|N_j^{'}\right|$ is 1, that is, it implies that

$$\left|\frac{\left(\rho_{ju} + \eta_{rj}^{'}\right)}{g_{2j}}\right| = \frac{K}{2}. \tag{3.33}$$

From Eqs. (3.24) and (3.33), the BL can be derived as follows

$$\left|\frac{\left(\rho_{ju} + \eta_{rj}^{'}\right)}{g_{2j}}\right| = \frac{K}{2}$$

$$\Rightarrow \quad \frac{\left(\rho_{ju} + \eta_{rj}^{'}\right)}{|g_{2j}|} = \frac{K}{2}$$

$$\Rightarrow \quad \frac{(\rho_{ju} + \epsilon_j/\triangle t_p)}{|g_{2j}|} = \frac{K}{2}$$

$$\Rightarrow \quad \epsilon_j = \triangle t_p \left(\frac{K\,|g_{2j}|}{2} - \rho_{ju}\right). \tag{3.34}$$

Hence, we have the next result:

Theorem 3.1 Suppose that System (3.1)-(3.2) is minimum phase and satisfies Assumption 3.1 and 3.2 having input-output relation (3.12) with relative degree $(k_1, \cdots, k_v)$ and

$k_j \geq 1$. Then, the output tracking performance $y_j \to y_{jd}$ for j=1,$\cdots$, v can be accomplished by the CSMC blended controller (3.18), (3.20)-(3.22), and (3.29) if the designed forces fulfill the physical constraints for each control channel and $\rho_j(\mathbf{x}, t)$ satisfies Assumption 3.3.

In this design idea, the features of the blended controller include:

I) Outside the BL, in order to achieve the output tracking performance as soon as possible, the auxiliary inputs provide large constant force to let the sliding variable approach the sliding surface as quickly as possible, while the main inputs compensate the deterministic dynamics and drastic change of states produced by auxiliary inputs.

II) Inside or on the BL, since the auxiliary inputs are not activated and the states variation will be smaller than those outside the BL, u_{1j} has more chance to avoid saturation. Thus, we only use u_{1j} to keep the system states close the sliding surface as better as possible.

3.2.2 Control Design via TSMC scheme

This scheme can deal with that each output of System (3.1)-(3.2) has relative degree more or equal to 2. The TSMC design consists of the following two steps: I) choosing an appropriate sliding surface in terms of error states and II) constructing a control law in form of Eq. (3.14). First, we choose sliding surface presented as

$$s_{j1} = \dot{s}_{j0} + b_{j1} s_{j0}^{q_{j1}/p_{j1}} \tag{3.35}$$

$$s_{j2} = \dot{s}_{j1} + b_{j2} s_{j1}^{q_{j2}/p_{j2}} \tag{3.36}$$

$$\vdots$$

$$s_{jk} = \dot{s}_{j(k-1)} + b_{jk} s_{j(k-1)}^{q_{jk}/p_{jk}} \tag{3.37}$$

for j=1,$\cdots$, v and k=1,$\cdots$, (k_j-1), where $s_{j0}=e_j$, $s_{jk}=s_j$, $b_{jk}>0$, $p_{jk}>q_{jk}$ and p_{jk}, q_{jk} are positive odd integers. Taking time derivative on s_{jk}, we have

$$\begin{aligned}\dot{s}_{j(k_j-1)} &= \frac{d^{(k_j)}}{dt^{(k_j)}}s_{j0}+\sum_{k=0}^{k_j-2}b_{j(k+1)}\frac{d^{(k_j-1-k)}}{dt^{(k_j-1-k)}}s_{jk}^{q_{i(k+1)}/p_{i(k+1)}}\\ &= f_j(\mathbf{x})+g_{1j}(\mathbf{x})u_{1j}+g_{2j}(\mathbf{x})u_{2j}+d_j-y_{jd}^{k_j}\\ &\quad+\sum_{k=0}^{k_j-2}b_{j(k+1)}\frac{d^{(k_j-1-k)}}{dt^{(k_j-1-k)}}s_{jk}^{q_{j(k+1)}/p_{i(k+1)}} \qquad (3.38)\end{aligned}$$

For second step, the controller design is divided into two parts: I) main inputs and II) auxiliary inputs.

I) Design of Main Inputs

We design

$$u_{1j}^{eq} = -\frac{1}{g_{1j}(\mathbf{x})}\cdot\left[f_j(\mathbf{x})-y_{jd}^{k_j}+d_j+\sum_{k=0}^{k_j-2}b_{j(k+1)}\frac{d^{(k_j-1-k)}}{dt^{(k_j-1-k)}}s_{jk}^{q_{j(k+1)}/p_{i(k+1)}}\right] \qquad (3.39)$$

and

$$u_{1j}^{re}=\begin{cases}\dfrac{1}{g_{1j}(\mathbf{x})}\cdot(\rho_j+\eta_{mj})\cdot\mathrm{sgn}(s_j) & \text{if } |s_j|\le\epsilon_j \text{ and } u_{2j}=0\\ 0 & \text{otherwise}\end{cases} \qquad (3.40)$$

where η_{mj} is selected positive constants.

II) Design of Auxiliary Inputs

Because the auxiliary inputs involve the following two characteristics: I) being zero or nonzero constant during a time duration depending on whether or not they are triggered; II) with output magnitudes being much larger than the main inputs if they are triggered. Consequently, the control law of each auxiliary input is designed to be

$$u_{2j}^{eq} = 0 \qquad (3.41)$$

$$\text{and } u_{2j}^{re} = N_jK. \qquad (3.42)$$

Now, we will discuss how N_j is selected. The method is based on the sliding condition

$$\frac{d}{dt}|s_j| \le -\eta_{rj}^{'} \qquad (3.43)$$

where $\eta_{rj}^{'}$ is a fictitious positive constant. According to Condition (3.43), the system state will reach $s_j(\mathbf{x}) = 0$ within the time of $|s_j(\mathbf{x}(0))|/\eta_{rj}^{'}$. When $\triangle t_p$ is given, the minimum $\eta_{rj}^{'}$ that makes the system state reaching the manifold $s_j(\mathbf{x}) = 0$ within $\triangle t_p$ is

$$\eta_{rj}^{'} = \frac{|0 - s_j(\mathbf{x}(t))|}{\triangle t_p}. \tag{3.44}$$

We choose

$$u_{2j}^{re^{'}} = -\frac{1}{g_{2j}} \cdot \left(\rho_{ju} + \eta_{rj}^{'}\right) \cdot \mathrm{sgn}(s_j) \tag{3.45}$$

where $u_{2j}^{re^{'}}$ is the fictitious control input of u_{2j}^{re} and ρ_{ju} is the upper bound of ρ_j. Then,

$$\begin{aligned} s_j(t)\dot{s}_j(t) &= -s_j(t)\left(\rho_{ju} + \eta_{rj}^{'}\right) \cdot \mathrm{sgn}(s_j) + s_j(t) \cdot d_j \\ &\leq -\left(\rho_{ju} + \eta_{rj}^{'}\right)|s_j| + \rho_{ju}|s_j| \\ &\leq -\eta_{rj}^{'}|s_j| \end{aligned} \tag{3.46}$$

Inequality (3.46) accounts for the sliding variable s_j will converge in finite time. However, in fact, $u_{2j}^{re^{'}}$ must accord with the form of $N_j K$. One method to determine N_j is such that the value $N_j K$ as close $u_{2j}^{re^{'}}$ as possible, that is, we round off $\left(u_{2j}^{re^{'}}/K\right)$ to determine the constant integer N_j. In more detail, Eq. (3.45) is replaced by Eq. (3.42) described below

$$\begin{aligned} u_{2j}^{re} &= \mathrm{round}\left(u_{2j}^{re^{'}}/K\right) K \\ &= \mathrm{round}\left(-\frac{\left(\rho_{ju} + \eta_{rj}^{'}\right)/g_{2j}}{K} \cdot \mathrm{sgn}(s_j)\right) K \\ &= -\mathrm{round}\left(\frac{\left(\rho_{ju} + \eta_{rj}^{'}\right)/g_{2j}}{K}\right) \mathrm{sgn}(s_j) \cdot K \\ &= -N_j^{'} \cdot \mathrm{sgn}(s_j) \cdot K \\ &= N_j K \end{aligned} \tag{3.47}$$

where

$$N_j^{'} = \begin{cases} \mathrm{round}\left(\dfrac{\left(\rho_{ju} + \eta_{rj}^{'}\right)/g_{2j}}{K}\right) & \\ & \text{if } \left|\mathrm{round}\left(\dfrac{\left(\rho_{ju} + \eta_{rj}^{'}\right)/g_{2j}}{K}\right)\right| < N_u \\ N_u \mathrm{sgn}(N_j^{'}) & \\ & \text{otherwise} \end{cases} \tag{3.48}$$

$$\text{and } N_j = -N_j^{'} \cdot \mathrm{sgn}(s_j). \tag{3.49}$$

Then, the virtual convergence speed is approximate to be:

$$\eta_{rj} = N_j^{'} K g_{2j} - \rho_{ju}. \tag{3.50}$$

Although the actual reaching time $|s_j(\mathbf{x}(0))|/\eta_{rj}$ can not exactly coincide with the expected reaching time $|s_j(\mathbf{x}(0))|/\eta_{rj}^{'}$, that is, this will cause inaccuracy of the reaching time which is at most in $\triangle t_p$, s_j can still converge according to the next paragraph.

Herein, we verify whether the sliding variable will converge. When s_j is outside the BL, from (3.38), we have

$$\begin{aligned} s_j(t)\dot{s}_j(t) &= s_j(t)NKg_{2j} + s_j(t)\cdot d_j \\ &\leq -N_j^{'} K g_{2j}|s_j| + \rho_{ju}|s_j| \\ &\leq -(\rho_{ju}+\eta_{rj})|s_j| + \rho_{ju}|s_j| \\ &\leq -\eta_{rj}|s_j| \end{aligned} \tag{3.51}$$

Clearly, the system states will approach the sliding surface with a convergence speed at least η_{rj} for j=1, $\cdots$, v in a finite time [20] whenever the system states are outside the BL. In contrast, when s_j is inside or on the BL, from (3.17), we get

$$\begin{aligned} s_j(t)\dot{s}_j(t) &= -(\rho_j+\eta_{mj})s_j(t)\mathrm{sgn}(s_j) + s_j(t)\cdot d_j \\ &\leq -(\rho_j+\eta_{mj})|s_j| + \rho_j|s_j| \\ &\leq -\eta_{mj}|s_j| \end{aligned} \tag{3.52}$$

Similarly, the system states will reach the sliding surface in a finite time $t_{rj} = |s_j(\mathbf{x}(t_{aj}))|/\eta_{mj}$ for j=1, $\cdots$, v [20] where t_{aj} is the time when any auxiliary input is not activated. According to above analysis, it implies that we can select bigger η_{rj} advisably outside the selected boundary to make s_j approach $s_j = 0$ faster and it still satisfies the sliding condition after s_j is inside or on the BL.

Moreover, according to Eq. (3.48), the minimum nonzero integer of $\left|N_j^{'}\right|$ is 1, that is, it implies that

$$\left|\frac{\left(\rho_{ju}+\eta_{rj}^{'}\right)}{g_{2j}}\right| = \frac{K}{2}. \tag{3.53}$$

From Eqs. (3.44) and (3.53), the BL can be derived as follows

$$\left|\frac{\left(\rho_{ju}+\eta_{rj}^{'}\right)}{g_{2j}}\right| = \frac{K}{2}$$

$$\Rightarrow \quad \frac{\left(\rho_{ju}+\eta_{rj}^{'}\right)}{|g_{2j}|} = \frac{K}{2}$$

$$\Rightarrow \quad \frac{\left(\rho_{ju}+\epsilon_j/\triangle t_p\right)}{|g_{2j}|} = \frac{K}{2}$$

$$\Rightarrow \quad \epsilon_j = \triangle t_p\left(\frac{K\,|g_{2j}|}{2}-\rho_{ju}\right). \tag{3.54}$$

Thus, we have the next result:

Theorem 3.2 Suppose that System (3.1)-(3.2) is minimum phase and satisfies Assumption 3.1 and 3.2 having input-output relation (3.12) with relative degree $(k_1,\cdots,\ k_v)$ with $k_j \geq 2$. Then, the output tracking performance $y_j \to y_{jd}$ for j=1,$\cdots$, v can be accomplished by the TSMC blended controller (3.39), (3.40)-(3.42), and (3.49) if the control forces fulfill the physical constraints for each control channel and $\rho_j(\mathbf{x},t)$ satisfies Assumption 3.3.

In this design idea, the features of the blended controller include:

I) Outside the BL, in order to achieve the output tracking performance as soon as possible, the auxiliary inputs provide large constant force to let the sliding variable approach the sliding surface as quickly as possible, while the main inputs compensate the deterministic dynamics and drastic change of states produced by auxiliary inputs.

II) Inside or on the BL, since the auxiliary inputs are not activated and the states variation will be smaller than those outside the BL, u_{1j} has more chance to avoid saturation. Thus, we only use u_{1j} to keep the system states close the sliding surface as better as possible.

Nevertheless, this method of TSMC scheme confronts the singularity problem for the controller. In other words, this problem occurs in Eq. (3.39) when $\dot{s}_{jk} \neq 0$ but $s_{jk} = 0$.

3.2.3 Control Design via NTSMC scheme

Finally, we introduce another controller design via NTSMC scheme to avoid the singularity phenomenon yielding from TSMC scheme. However, this scheme only can deal with that each output of System (3.1)-(3.2) has relative degree 2. Choose sliding surface presented as

$$s_{j1} = \frac{1}{c_{j1}}\dot{s}_{j0}^{p_{j1}/q_{j1}} + s_{j0} \tag{3.55}$$

where $s_{j0} = e_j$, $s_{j1} = s_j$, $c_{j1} = b_{j1}^{-q_{j1}/p_{j1}}$, and p_{j1}, q_{j1} are positive odd integers under the constraint $1 < (p_{j1}/q_{j1}) < 2$. Taking time derivative on s_{j1}, we have

$$\dot{s}_{j1} = \dot{s}_{j0} + \frac{1}{c_{j1}}\left(\frac{p_{j1}}{q_{j1}}\right)\dot{s}_{j0}^{\frac{p_{j1}}{q_{j1}}-1}\ddot{s}_{j0} \tag{3.56}$$

The controller design is divided into two parts: I) main inputs and II) auxiliary inputs.

I) Design of Main Inputs

We choose

$$u_{1j}^{eq} = -\frac{1}{g_{1j}(\mathbf{x})}\cdot\left[f_j(\mathbf{x}) - y_{jd}^2 + d_j + c_{j1}\frac{q_{j1}}{p_{j1}}\dot{s}_{j0}^{2-\frac{p_{j1}}{q_{j1}}}\right] \tag{3.57}$$

and

$$u_{1j}^{re} = \begin{cases} -\dfrac{1}{g_{1j}(\mathbf{x})}\cdot(\rho_j + \eta_{mj})\cdot\mathrm{sgn}(s_j) & \text{if } |s_j| \le \epsilon_j \text{ and } u_{2j} = 0 \\ 0 & \text{otherwise} \end{cases} \tag{3.58}$$

where η_{mj} is selected positive constants.

II) Design of Auxiliary Inputs

Because the auxiliary inputs involve the following two characteristics: I) being zero or nonzero constant during a time duration depending on whether or not they are triggered; II) with output magnitudes being much larger than the main inputs if they are triggered. Consequently, the control law of each auxiliary input is designed to be

$$u_{2j}^{eq} = 0 \tag{3.59}$$

$$\text{and } u_{2j}^{re} = N_j K. \tag{3.60}$$

Now, we will discuss how N_j is selected. The method is based on the sliding condition

$$\frac{d}{dt}|s_j| \leq -\frac{1}{c_{j1}}\frac{p_{j1}}{q_{j1}}\dot{s}_{j0}^{\frac{p_{j1}}{q_{j1}}-1}\eta_{rj}^{'} \tag{3.61}$$

where $\eta_{rj}^{'}$ is a fictitious positive constant. Making $s_j(x(t))$ achieve the sliding surface at least within $\triangle t_p$ and $\dot{s}_{j0}$ is constant in this time duration as the time duration is in a short time, then we obtain

$$\eta_{rj}^{'} = c_{j1}\left(\frac{q_{j1}}{p_{j1}}\right)\frac{1}{\dot{s}_{j0}^{(p_{j1}-q_{j1})/q_{j1}}(t_{oj})}\frac{|0-s_{j1}(x(t))|}{\triangle t_p} \tag{3.62}$$

where t_{oj} is the time instant when we decide to activate the jth auxiliary input. Although Eq. (3.62) is undefined as $\dot{s}_{j0}=0$, in this case we will adopt allowable maximum value of u_{2j} under such situation. In addition, at $\dot{s}_{j0}=0$ there is an advantage for choosing maximum u_{2j} since $\ddot{s}_{j0} \leq -\eta_{rj}$ and $\ddot{s}_{j0} \geq \eta_{rj}$ for both $s_{j1}>0$ and $s_{j1}<0$, respectively (discussed in Eq. (2.61) of Section 2.3). That is to say that if $\dot{s}_{j0}=0$, choosing maximum $\eta_{rj}^{'}$ can make $\dot{s}_{j0}$ leave $\dot{s}_{j0}=0$ fastest. Then, we choose

$$u_{2j}^{re^{'}} = -\frac{1}{g_{2j}}\cdot\left(\rho_{ju}+\eta_{rj}^{'}\right)\cdot \mathrm{sgn}(s_j) \tag{3.63}$$

where $u_{2j}^{re^{'}}$ is the fictitious control input of u_{2j}^{re} and ρ_{ju} is the upper bound of ρ_j. Then,

$$\begin{aligned} s_j(t)\dot{s}_j(t) &= \frac{1}{c_{j1}}\left(\frac{p_{j1}}{q_{j1}}\right)\dot{s}_{j0}^{\frac{p_{j1}}{q_{j1}}-1}\left[-(\rho_{ju}+\eta_{rj}^{'})s_{j1}\mathrm{sgn}(s_{j1})+s_{j1}\cdot d_j\right] \\ &\leq -\frac{1}{c_{j1}}\left(\frac{p_{j1}}{q_{j1}}\right)\dot{s}_{j0}^{\frac{p_{j1}}{q_{j1}}-1}\left[\left(\rho_{ju}+\eta_{rj}^{'}\right)|s_j|+\rho_{ju}|s_j|\right] \\ &\leq -\frac{1}{c_{j1}}\left(\frac{p_{j1}}{q_{j1}}\right)\dot{s}_{j0}^{\frac{p_{j1}}{q_{j1}}-1}\eta_{rj}^{'}|s_j| \end{aligned} \tag{3.64}$$

Inequality (3.64) accounts for the sliding variable s_j will converge in finite time. However, in fact, $u_{2j}^{re^{'}}$ must accord with the form of N_jK. One method to determine N_j is such that the value N_jK as close $u_{2j}^{re^{'}}$ as possible, that is, we round off $\left(u_{2j}^{re^{'}}/K\right)$ to determine the

constant integer N_j. In more detail, Eq. (3.63) is replaced by Eq. (3.60) described below

$$\begin{aligned} u_{2j}^{re} &= \text{round}\left(u_{2j}^{re'}/K\right)K \\ &= \text{round}\left(-\frac{\left(\rho_{ju}+\eta_{rj}^{'}\right)/g_{2j}}{K}\cdot\text{sgn}(s_j)\right)K \\ &= -\text{round}\left(\frac{\left(\rho_{ju}+\eta_{rj}^{'}\right)/g_{2j}}{K}\right)\text{sgn}(s_j)\cdot K \\ &= -N_j^{'}\cdot\text{sgn}(s_j)\cdot K \\ &= N_j K \end{aligned} \tag{3.65}$$

where

$$N_j^{'} = \begin{cases} \text{round}\left(\dfrac{\left(\rho_{ju}+\eta_{rj}^{'}\right)/g_{2j}}{K}\right) & \\ & \text{if } \left|\text{round}\left(\dfrac{\left(\rho_{ju}+\eta_{rj}^{'}\right)/g_{2j}}{K}\right)\right| < N_u \\ N_u\text{sgn}(N_j^{'}) & \text{otherwise} \end{cases} \tag{3.66}$$

$$\text{and } N_j = -N_j^{'}\cdot\text{sgn}(s_j). \tag{3.67}$$

Then, the virtual convergence speed is approximate to be:

$$\eta_{rj} = N_j^{'}Kg_{2j} - \rho_{ju}. \tag{3.68}$$

Although the actual reaching time can not exactly coincide with the expected reaching time, that is, this will cause inaccuracy of the reaching time which is at most in $\triangle t_p$, s_j can still converge according to the next paragraph.

Herein, we verify whether the sliding variable will converge. When s_j is outside the BL, from (3.38), we have

$$\begin{aligned} s_{j1}\dot{s}_{j1} &= \frac{1}{c_{j1}}\left(\frac{p_{j1}}{q_{j1}}\right)\dot{s}_{j0}^{\frac{p_{j1}}{q_{j1}}-1}\left[-(\rho_{ju}+\eta_{rj})s_{j1}\text{sgn}(s_{j1})+s_{j1}\cdot d_j\right] \\ &\le \frac{1}{c_{j1}}\left(\frac{p_{j1}}{q_{j1}}\right)\dot{s}_{j0}^{\frac{p_{j1}}{q_{j1}}-1}\left[-(\rho_{ju}+\eta_{rj})|s_{j1}|+\rho_{ju}|s_{j1}|\right] \\ &\le -\frac{1}{c_{j1}}\left(\frac{p_{j1}}{q_{j1}}\right)\dot{s}_{j0}^{\frac{p_{j1}}{q_{j1}}-1}\eta_{rj}|s_{j1}| \end{aligned} \tag{3.69}$$

It was shown by [45] that the system states will approach the BL in finite time. In contrast, when s_j is inside or on the BL, from (3.17), we get

$$\begin{aligned} s_{j1}\dot{s}_{j1} &= \frac{1}{c_{j1}}\left(\frac{p_{j1}}{q_{j1}}\right)\dot{s}_{j0}^{\frac{p_{j1}}{q_{j1}}-1}\left[-(\rho_j+\eta_{mj})s_{j1}\mathrm{sgn}(s_{j1})+s_{j1}\cdot d_j\right] \\ &\leq \frac{1}{c_{j1}}\left(\frac{p_{j1}}{q_{j1}}\right)\dot{s}_{j0}^{\frac{p_{j1}}{q_{j1}}-1}\left[-(\rho_j+\eta_{mj})|s_{j1}|+\rho_j|s_{j1}|\right] \\ &\leq -\frac{1}{c_{j1}}\left(\frac{p_{j1}}{q_{j1}}\right)\dot{s}_{j0}^{\frac{p_{j1}}{q_{j1}}-1}\eta_{mj}|s_{j1}| \end{aligned} \tag{3.70}$$

Similarly, it was shown by [45] that the system states will reach the sliding surface in finite time.

Besides, according to Eq. (3.66), the minimum nonzero integer of $\left|N_j^{'}\right|$ is 1, that is, it implies that

$$\left|\frac{\left(\rho_{ju}+\eta_{rj}^{'}\right)}{g_{2j}}\right| = \frac{K}{2}. \tag{3.71}$$

From Eqs. (3.62) and (3.71), the BL can be derived as follows

$$\left|\frac{\left(\rho_{ju}+\eta_{rj}^{'}\right)}{g_{2j}}\right| = \frac{K}{2}$$

$$\Rightarrow \quad \frac{\left(\rho_{ju}+\eta_{rj}^{'}\right)}{|g_{2j}|} = \frac{K}{2}$$

$$\Rightarrow \quad \frac{\left[\rho_{ju}+(c_{j1}q_{j1}\epsilon_j)/\left(p_{j1}\triangle t_p\dot{s}_{j0}^{(p_{j1}-q_{j1})/q_{j1}}(t_{oj})\right)\right]}{|g_{2j}|} = \frac{K}{2}$$

$$\Rightarrow \quad \epsilon_j = \frac{p_{j1}\dot{s}_{j0}^{(p_{j1}-q_{j1})/q_{j1}}(t_{oj})\triangle t_p}{c_{j1}q_{j1}}\left(\frac{K\,|g_{2j}|}{2}-\rho_{ju}\right). \tag{3.72}$$

Therefore, we have the next result:

Theorem 3.3 Suppose that System (3.1)-(3.2) is minimum phase and satisfies Assumption 3.1 and 3.2 having input-output relation (3.12) with relative degree $(k_1,\cdots,\ k_v)$ and $k_j=2$. Then, the output tracking performance $y_j \to y_{jd}$ for j=1,$\cdots$, v can be accomplished by the NTSMC blended controller (3.57), (3.58)-(3.60), and (3.67) if the control forces fulfill the physical constraints for each control channel and $\rho_j(\mathbf{x},t)$ satisfies Assumption 3.3.

In this design idea, the features of the blended controller include:

I) Outside the BL, in order to achieve the output tracking performance as soon as possible, the auxiliary inputs provide large constant force to let the sliding variable approach the sliding surface as quickly as possible, while the main inputs compensate the deterministic dynamics and drastic change of states produced by auxiliary inputs.

II) Inside or on the BL, since the auxiliary inputs are not activated and the states variation will be smaller than those outside the BL, u_{1j} has more chance to avoid saturation. Thus, we only use u_{1j} to keep the system states close the sliding surface as better as possible.

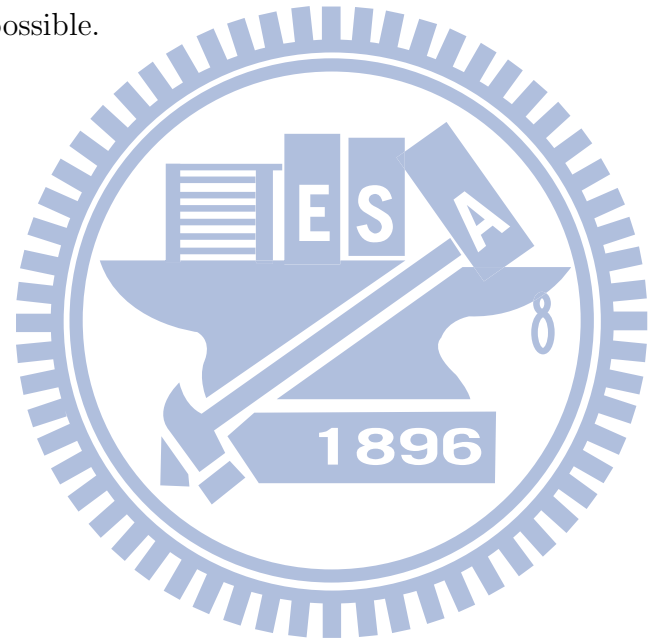

CHAPTER FOUR
APPLICATION TO MISSILE SYSTEM

In this chapter we will employ the controllers presented in Chapter 3 to control of ATBM. For simplicity, we only consider the control of dynamics in longitudinal (pitch) plane. This model may provide a common basis for developing and understanding new approaches to the missile controller problem.

4.1 Model Description

In this section, the model considered consists of the longitudinal (pitch plane) force and moment equations representative of a generic missile travelling at Mach 3 at an altitude of 20,000 (ft) and with aerodynamic coefficients represented as third order polynomials in angle of attack. The nonlinear nominal dynamic equations of the missile airframe are given in [65], [66] as follows:

$$\dot{\alpha} = \left(\frac{f_{rd}qqS}{mV}\right)\cos\left(\alpha/f_{rd}\right)\left[\phi_z(\alpha) + b_z\delta_z\right] + \omega_{bz} + \frac{\cos(\alpha/f_{rd})}{mV}F_{tbyc} \tag{4.1}$$

$$\dot{\omega}_{bz} = \left(\frac{f_{rd}qSd}{I_{zz}}\right)\left[\phi_m(\alpha) + b_m\delta_z\right] - \frac{l}{I_{zz}}F_{tbyc} \tag{4.2}$$

where the notations given in Eq. (4.1)-(4.2) can be found in nomenclature. The tail control of aerodynamic force parts are continuous, while lateral thrust control is constant during a short time period once it was triggered. The aerodynamic coefficients are approximated by [65]:

$$\phi_z(\alpha) = 0.000103\alpha^3 - 0.00945\alpha|\alpha| - 0.170\alpha \tag{4.3}$$

$$b_z = -0.034 \tag{4.4}$$

$$\phi_m(\alpha) = 0.000215\alpha^3 - 0.0195\alpha|\alpha| - 0.051\alpha \tag{4.5}$$

$$b_m = -0.206 \tag{4.6}$$

These approximations are valid for α in the range of ± 20 degrees. Besides, we adopt the following assumptions from [67] I) Ignore the total number of available IACM, but $N_u = 5$ in one time duration; II) the moment arm of the IACM is fixed ahead of the missile center of gravity; and III) an IACM can provide $K = 2500$ (lbf) sustaining $\triangle t_p = 0.02$ (sec). The output of tail actuator has time delay, which is modeled by a linear first-order system with time constant τ_t for the elevator given by

$$\dot{\delta_z} = -\frac{1}{\tau_t}\delta_z + \frac{1}{\tau_t}\delta_{zc} \tag{4.7}$$

The deflection limit of the tail fin is assumed to be ± 50 (deg) and the time constant $\tau_t = 0.005$ (sec). As the missile speed is large, the last term in the right-hand-side of Eq. (4.1) is omitted [19], that is, the maximum magnitude of $|F_{tbyc}| = 12500$ (lbf) for $N_u = 5$ accounts for $(\cos(\alpha/f_{rd})F_{tbyc})/(mV) \to 0$ for $m = 450$ (lbs) and $V = 3109.3$ (ft/sec). Actually, the moment of lateral thrust force is the main to influence the attitude of the missile. Equations (4.1), (4.2) and (4.7) can be rewritten as the following standard state-space form by defining $\mathbf{x} = [\alpha, \omega_{z_b}, \delta_z]^T$, $u_{11} = \delta_{zc}$, and $u_{21} = F_{tbyc}$:

$$\dot{\mathbf{x}} = \mathbf{f}_0(\mathbf{x}) + G_0 \begin{bmatrix} u_{11} \\ u_{21} \end{bmatrix} \tag{4.8}$$

where

$$\mathbf{f}_0(\mathbf{x}) = \begin{bmatrix} \left(\frac{f_{rd}qgS}{mV}\right)\cos\left(x_1/f_{rd}\right)\left[\phi_z(x_1) + b_z x_3\right] + x_2 \\ \left(\frac{f_{rd}qSd}{I_{zz}}\right)\left[\phi_m(x_1) + b_m x_3\right] \\ -\frac{1}{\tau_t}\delta_z \end{bmatrix} \tag{4.9}$$

and

$$G_0 = \begin{bmatrix} 0 & 0 \\ 0 & -\frac{l}{I_{zz}} \\ \frac{1}{\tau_t} & 0 \end{bmatrix} \tag{4.10}$$

Define

$$y = h(\mathbf{x}) = x_1 \tag{4.11}$$

The main goal is to track desired angle of attack x_{1d}, i.e., $x_1 \to x_{1d}$. According to Eq. (3.12), we have

$$y_1^{(2)} = f_1(\mathbf{x}) + g_{11}(\mathbf{x})u_{11} + g_{21}(\mathbf{x})u_{21} + d_1 \tag{4.12}$$

where $d_1 = 0$ and the parameters $f_1(\mathbf{x})$, $g_{11}(\mathbf{x})$ and $g_{21}(\mathbf{x})$ are given as below:

$$\begin{aligned} f_1 &= \left(\frac{f_{rd}gqS}{mV}\right)^2 \cos\left(\frac{x_1}{f_{rd}}\right)\left(0.000103x_1^3 - 0.00945x_1^2 - 0.170x_1 - 0.034x_3\right) \\ &\cdot\left\{0.000103\left[-\sin(\frac{x_1}{f_{rd}})\frac{x_1^3}{f_{rd}} + 3\cos(\frac{x_1}{f_{rd}})x_1^2\right]\right. \\ &\quad -0.00945\left[-\sin(\frac{x_1}{f_{rd}})\frac{x_1^2}{f_{rd}} + 2\cos(\frac{x_1}{f_{rd}})x_1\right] \\ &\quad -0.170\left[-\sin(\frac{x_1}{f_{rd}})\frac{x_1}{f_{rd}} + 2\cos(\frac{x_1}{f_{rd}})\right] \\ &\quad \left.-0.034\left[-\sin(\frac{x_1}{f_{rd}})\frac{x_3}{f_{rd}}\right]\right\} \\ &- \left(\frac{f_{rd}gqS}{mV}\right)\cos(\frac{x_1}{f_{rd}})\frac{x_3}{\tau_t} \\ &+ \left(\frac{f_{rd}qSd}{I_{zz}}\right)\left(0.000215x_1^3 - 0.0195x_1^2 + 0.051x_1 - 0.206x_3\right), \end{aligned} \tag{4.13}$$

$$g_{11}(\mathbf{x}) = -0.034\left(\frac{f_{rd}gqS}{mV\tau_t}\cos\left(x_1/f_{rd}\right)\right), \tag{4.14}$$

$$\text{and } g_{21}(\mathbf{x}) = -\frac{l}{I_{zz}} \tag{4.15}$$

Clearly, $g_{11}(\mathbf{x})$ and $g_{21}(\mathbf{x})$ are nonzero. Besides, because System (4.8)-(4.11) has relative degree 2, we have to check the stability of the zero-dynamics. Herein, assuming only the tail works in the steady state, i.e. $u_{21} = 0$. In order to determine the stability of the internal, we have to choose a coordinate transformation to transform the system dynamics into the so-called normal form. To this end, we choose

$$\mu_1 = y_1 = x_1 \tag{4.16}$$

$$\text{and } \mu_2 = \dot{y}_1 = \left(\frac{f_{rd}gqS}{mV}\right)\cos\left(x_1/f_{rd}\right)\left[\phi_z(x_1) + b_z x_3\right] + x_2. \tag{4.17}$$

We have to determine a third function $\psi(\mathbf{x})$ such that $\mathbf{z} = [\mu_1\ \mu_2\ \psi]^T$ qualifies a coordinate transformation and satisfies

$$L_{G_{01}}\psi = \frac{\partial\psi}{\partial x_3}\frac{1}{\tau_t} = 0 \tag{4.18}$$

where G_{01} is 1st column of G_0 given by Eq. (4.10). A trivial candidate of $\psi(\mathbf{x})$ is selected below

$$\psi = x_2 \tag{4.19}$$

because the Jacobian matrix of $\mathbf{z}$ is

$$\frac{\partial \mathbf{z}}{\partial \mathbf{x}} = \begin{bmatrix} 1 & 0 & 0 \\ \dfrac{\partial \mu_2}{\partial x_1} & 1 & -0.034\left(\dfrac{f_{rd} g q S}{mV}\right)\cos\left(x_1/f_{rd}\right) \\ \dfrac{\partial \psi}{\partial x_1} & 1 & 0 \end{bmatrix} \tag{4.20}$$

which is nonsingular for any constrained $\mathbf{x}$. This means the state transformation is a local diffeomorphism. Thus, the internal dynamics is represented by the equation

$$\dot{\psi} = \left(\frac{f_{rd} q S d b_m}{I_{zz} b_z}\right)\left[(\mu_2 - \psi)\frac{1}{\left(\dfrac{f_{rd} g q S}{mV}\right)\cos\left(\mu_1/f_{rd}\right)} - \phi_z(\mu_1)\right] \tag{4.21}$$

The associated zero-dynamics is obtained by letting $\mu_1 = 0$ and $\mu_2 = 0$ as

$$\dot{\psi} = -\frac{f_{rd} q S d b_m f_{rd} g q S}{I_{zz} b_z m V}\psi \tag{4.22}$$

which is clearly exponentially stable. Thus, System (4.8)-(4.11) is minimum phase.

After that, the control objective is to design the proper controller to achieving the output tracking performance. Define error $e_1 = x_1 - x_{1d}$ where x_{1d} is desired angle of attack. We now recall the overall controllers from Chapter 4 as follows:

A) Blended controller via CSMC scheme

Sliding surface:

$$s_1 = \dot{e}_1 + a_{11} e_1 \tag{4.23}$$

Tail:

$$u_{11} = \begin{cases} -\dfrac{1}{g_{11}}\left[f_1(\mathbf{x}) - \ddot{\alpha}_d + a_{11}\dot{e}_1\right] \\ \qquad\qquad \text{if } |s_1| \le \epsilon_1 \text{ and } u_{21} \neq 0 \\ -\dfrac{1}{g_{11}}\left[f_1(\mathbf{x}) - \ddot{\alpha}_d + a_{11}\dot{e}_1 + (\rho_1 + \eta_{m1})\cdot \mathrm{sgn}(s_1)\right] \\ \qquad\qquad \text{otherwise} \end{cases} \tag{4.24}$$

where $\epsilon_1 = (|g_{21}|\, K \triangle t_p)/2$.

Lateral Thrust:

$$u_{21} = N_1 K \tag{4.25}$$

where

$$N_1 = -N_1' \mathrm{sgn}(s_1)$$

$$N_1' = \begin{cases} \mathrm{round}\left(\dfrac{(\rho_{1u} + \eta_{r1}')/g_{21}}{K}\right) \\ \qquad \text{if } \left|\mathrm{round}\left(\dfrac{(\rho_{1u} + \eta_{r1}')/g_{21}}{K}\right)\right| < N_u \\ N_u \mathrm{sgn}(N_1') \\ \qquad \text{otherwise} \end{cases} \tag{4.26}$$

$$\eta_{r1}' = \frac{|s_1(x(t))|}{\triangle t_p}$$

B) Blended controller via TSMC scheme

Sliding surface:

$$s_1 = \dot{e}_1 + b_{11} e_1^{q_{11}/p_{11}} \tag{4.27}$$

Tail:

$$u_{11} = \begin{cases} -\dfrac{1}{g_{11}}\left[f_1(\mathbf{x}) - \ddot{\alpha}_d + b_{11}\left(\dfrac{q_{11}}{p_{11}}\right) e_1^{(q_{11}-p_{11})/p_{11}} \dot{e}_1\right] \\ \qquad \text{if } |s_1| \le \epsilon_1 \text{ and } u_{21} \neq 0 \\ -\dfrac{1}{g_{11}}\left[f_1(\mathbf{x}) - \ddot{\alpha}_d + b_{11}\left(\dfrac{q_{11}}{p_{11}}\right) e_1^{(q_{11}-p_{11})/p_{11}} \dot{e}_1 + (\rho_1 + \eta_{m1}) \cdot \mathrm{sgn}(s_1)\right] \\ \qquad \text{otherwise} \end{cases} \tag{4.28}$$

where $\epsilon_1 = (|g_{21}|\, K \triangle t_p)/2$.

Lateral Thrust:

$$u_{21} = N_1 K \tag{4.29}$$

where

$$N_1 = -N_1^{'}\text{sgn}(s_1)$$

$$N_1^{'} = \begin{cases} \text{round}\left(\dfrac{\left(\rho_{1u}+\eta_{r1}^{'}\right)/g_{21}}{K}\right) & \\ & \text{if } \left|\text{round}\left(\dfrac{\left(\rho_{1u}+\eta_{r1}^{'}\right)/g_{21}}{K}\right)\right| < N_u \\ N_u\text{sgn}(N_1^{'}) & \\ & \text{otherwise} \end{cases} \tag{4.30}$$

$$\eta_{r1}^{'} = \frac{|s_1(x(t))|}{\triangle t_p}$$

C) Blended controller via NTSMC scheme

Sliding surface:

$$s_1 = e_1 + \frac{1}{c_{11}}\dot{e}_1^{p_{11}/q_{11}} \tag{4.31}$$

Tail:

$$u_{11} = \begin{cases} -\dfrac{1}{g_{11}}\left[f(\mathbf{x}) - \ddot{\alpha}_d + c_{11}\left(\dfrac{q_{11}}{p_{11}}\right)\dot{e}^{2-\frac{p_{11}}{q_{11}}}\right] & \\ & \text{if } |s_1| \le \epsilon_1 \text{ and } u_{21} \neq 0 \\ -\dfrac{1}{g_{11}}\left[f(\mathbf{x}) - \ddot{\alpha}_d + c_{11}\left(\dfrac{q_{11}}{p_{11}}\right)\dot{e}^{2-\frac{p_{11}}{q_{11}}} + (\rho_1+\eta_{m1})\,\text{sgn}(s_1)\right] & \\ & \text{otherwise} \end{cases} \tag{4.32}$$

where $\epsilon_1 = \left(p_{11}\dot{e}_1^{(p_{11}-q_{11})/q_{11}}(t_{o1}) \triangle t_p\right)/(2c_{11}q_{11})$.

Lateral Thrust:

$$u_{21} = N_1 K \tag{4.33}$$

where

$$N_1 = -N_1' \text{sgn}(s_1)$$

$$N_1' = \begin{cases} \text{round}\left(\dfrac{\left(\rho_{1u} + \eta_{r1}'\right)/g_{21}}{K}\right) & \\ & \text{if } \left|\text{round}\left(\dfrac{\left(\rho_{1u} + \eta_{r1}'\right)/g_{21}}{K}\right)\right| < N_u \\ N_u \text{sgn}(N_1') & \\ & \text{otherwise} \end{cases} \tag{4.34}$$

$$\eta_{r1}' = c_{11}\left(\frac{q_{11}}{p_{11}}\right)\frac{1}{\dot{s}_{10}^{(p_{11}-q_{11})/q_{11}}(t_{o1})}\frac{|s_1(x(t))|}{\triangle t_p}$$

4.2 Simulation Results

In this section, we will verify whether or not the RCS is helpful for the angle-of-attack control of the missile system from simulation viewpoint. In simulations, the physical and geometric parameters are given by [65], [66] $I_z = 182.5$ (slug $\cdot$ ft^2), $m = 450$ (lbs), $V = 3109.3$ (ft/sec), $S = 0.44$ (ft^2), $d = 0.75$ (ft), $q = 6132.8$ (lbs/ft^2), and $l = 2$ (ft). The parameters of the controllers are given as $a_{11} = 20$, $b_{11} = 20$, $q_{11} = 5$, $p_{11} = 7$, and $c_{11} = b_{11}^{p_{11}/q_{11}}$. The initial states are set to be zeros and the desired angle of attack is selected as $\alpha_d = 20$ (degree). Moreover, to alleviate the phenomenon of chattering produced by sign function, we replace $\text{sgn}(s_1)$ by saturation function defined

$$\text{sat}(s_1, \epsilon) := \begin{cases} \text{sgn}(s_1) & \text{if } |s_1| > \epsilon \\ \dfrac{s_1}{\epsilon} & \text{if } |s_1| \le \epsilon \end{cases} \tag{4.35}$$

where ϵ is chosen to be 0.01. Besides,

$$\eta_{m1} = \begin{cases} 165 & \text{if } |s_1| \le \epsilon \\ 1000 & \text{if } |s_1| > \epsilon \end{cases}. \tag{4.36}$$

The criterion for the tracking performance being successful is defined as the tracking error $|e_1| \le 0.01$.

Numerical results for nominal system ($d_1 = 0$) to perform our tracking task are summarized in Tables 4.1-4.2 and Figs. 4.1-4.36 in which blue lines and magenta lines denote the responding curve for blended control and tail control, respectively. Among these, we use the following twelve control schemes: the first six contain the blended control and

the tail control using sign-type CSMC, TSMC and NTSMC designs labeled SICSMCB, SICSMCT, SITSMCB, SITSMCT, SINTSMCB and SINTSMCT, respectively, while the others are the blended control and the tail control based on saturation-type CSMC, TSMC and NTSMC designs labeled SACSMCB, SACSMCT, SATSMCB, SATSMCT, SANTSMCB and SANTSMCT, respectively.

The simulations in the case of using sign-type SMC designs involve in Figs. 4.1-4.15. Among these, Figs. 4.1, 4.6 and 4.11 show the time evolution of output tracking error $\alpha - \alpha_d$. Figs. 4.2, 4.7 and 4.12 display the time evolution of the three system states. Figs. 4.3, 4.8 and 4.13 exhibit the time evolution of the sliding variables. Figs. 4.4, 4.9 and 4.14 behave the time evolution of commanded tail inputs. Finally, Figs. 4.5, 4.10 and 4.15 account for how many IACMs the RCS provides. Table 4.1 summarizes the time for successfully achieving output tracking performance ($|e_1| \leq 0.01$) using sign-type SMC tail and blended controllers. It is observed from Table 4.1 that the blended controllers consume less time than tail controllers for successfully achieving the desired output. Indeed, the blended design saves approximately 0.2598 (sec), 0.0786 (sec) and 0.0951 (sec) for CSMC, TSMC and NTSMC schemes, respectively. It is seen form Fig. 4.3 that the responding curve of SICSMCB has a small change at $t = 0.04$ (sec) and a peak at $t = 0.06$ (sec), which are resulted from different number of IACMs being activated as can also be seen from Fig. 4.5. After 0.06 (sec), because the system states has entered the boundary layer ϵ_1, the lateral thrust is not triggered and only the tail is used for output tracking task. The same scenario can also be found from Figs. 4.8, 4.10 for SITSMCB and Figs. 4.13, 4.15 for SINTSMCB. According to Eq. (2.46), the convergence time is calculated to be 0.3137 (sec) and 0.2293 (sec) for SITSMCB and SINTSMCB, after reaching the sliding surface, predicted by TSMC and NTSMC theory, respectively. However, the convergence time found from simulation is approximate 0.3312 (sec) and 0.2769 (sec) for SITSMCB and SINTSMCB, respectively, which is a little bit larger than predicted value. This might result from occurrence of chatter on sliding surface in Figs. 4.17 and 4.18 which leads to not only the chattering inputs (shown in Figs. 4.9 and 4.14) but also the imprecision of the output error (observed in Figs. 4.20 and 4.21). This chattering phenomenon results from the computer simulation whose step size can not divide into infinitesimally small.

In addition, besides TSMC and NTSMC schemes, CSMC scheme has the same chattering phenomenon shown in Figs. 4.4, 4.16 and 4.19. In a practical realization, the fact that the switching frequency is finite implies that the trajectories of the system generally not lie on the switching surface. In fact, they lie within a neighboring region of the surface and this non-ideal characteristic provokes the manifestation of a physical phenomenon [68]. There are three disadvantages of these sign-type SMC schemes during the physical implementation. First, it is unavoidable that the switching of the control take place at a very high frequency but the physical system may not tolerate such behavior at the input. Second, energy is wasted when the system is near the sliding surface. Third, it can yield resonance, excite unmodeled dynamics or even damage to mechanisms [20].

To alleviate the chattering behavior, the saturation-type SMC designs have been introduced in [69]. Numerical simulations using saturation-type SMC schemes rather than sign-type SMC schemes are given in Figs. 4.22-4.36. Among these, Figs. 4.22, 4.27 and 4.32 show the time evolution of output tracking error $\alpha - \alpha_d$. Figs. 4.23, 4.28 and 4.33 display the time evolution of the three system states. Figs. 4.24, 4.29 and 4.34 exhibit the time evolution of the sliding variables. Figs. 4.25, 4.30 and 4.35 behave the time evolution of commanded tail inputs. Finally, Figs. 4.26, 4.31 and 4.36 account for how many IACMs the RCS provides. It is observed from Figs. 4.22, 4.27 and 4.32 the output tracking performance are achieved by both tail controllers and blended controllers; however, the convergence times of the output errors by blended controllers via the three saturation-type SMC schemes are found to be faster than those by tail controllers. Table 4.2 displays the time for successfully achieving output tracking performance ($|e_1| \leq 0.01$) using saturation-type SMC tail and blended controllers. Indeed, the blended design saves approximately 0.2593 (sec), 0.0785 (sec) and 0.0951 (sec) for CSMC, TSMC and NTSMC schemes, respectively. The remaining two states are found to reach their steady state after the desired output is achieved. It is seen from Fig. 4.24 that the responding curve of SACSMCB has a small change at $t = 0.04$ (sec) and a peak at $t = 0.06$ (sec), which resulted from different number of IACMs be activated as can also be seen from Fig. 4.26. Besides, Fig. 4.25 shows that the responding curve of SACSMCB experiences two jumps. The 1st jump corresponding to the system states have entered the region where the RCS

does not activate, while the 2nd jump associated with the system states have entered the boundary layer of the saturation function where the control gain is changed by Eq. 4.36 from 1000 to 165, which can also be identified in Figs. 4.24 and 4.26. The same scenario can also be found from Figs. 4.29, 4.30, 4.31 for SITSMCB and Figs. 4.34, 4.30, 4.36 for SINTSMCB. After the system states has entered the boundary layer of saturation function, all the sliding variables using saturation-type SMC design remain inside the boundary layer. These agree with the results of Chapter 4. From these simulations, it can be concluded that the proposed blended controllers can achieve desired output faster than the tail controllers.

Although the TSMC can theoretically improve CSMC from asymptotical convergence to finite time convergence and NTSMC can avoid singularity problem of TSMC, they all suffer from the chattering problem by using sign-type SMC design due to the computer simulation. The chattering problem will make the sliding variables not lie on the sliding manifold. This means that both TSMC and NTSMC can not achieve finite time convergence and accuracy tracking performances in practical applications. On the other hand, although replacing the sign-type SMC design by saturation-type SMC design will evoke imprecision of output tracking task, it can avoid the chattering problem resulting in damaging to mechanisms. Therefore, no matter what sign-type or saturation-type functions are used in CSMC, TSMC and NTSMC schemes, the finite time convergence can not achieve in practical applications.

In this example, because the distance between the selected initial states and the sliding surface of TSMC and NTSMC are smaller than that of CSMC, both the blended controllers and tail controllers via TSMC and NTSMC schemes consume less time than CSMC for tracking performance. Besides, the number of required IACMs for blended controllers via both TSMC and NTSMC schemes are less than that of CSMC scheme. However, the above two results depend on the locations of the initial states, that is, if the initial states are closer to the sliding surface the convergence time for output tracking task via the three SMC schemes mentioned previously generally is faster and moreover, the required number of IACMs for blended controller via the aforementioned three SMC schemes will be fewer.

In summary, the performance of tracking accuracy and convergence time by using blended controllers via CSMC, TSMC and NTSMC are superior to those by using the tail controllers only no matter what CSMC, TSMC or NTSMC are used. This accounts for that the novel missiles prefer to adopt tails and RSC instead of tails only.

Table 4.1. Time for successfully achieving output tracking performance ($|e_1| \leq 0.01$) using sign-type SMC tail and blended controllers

	Tail Controller	Blended Controller
SMC Scheme	0.66650	0.40670
TSMC Scheme	0.45440	0.37580
NTSMC Scheme	0.47150	0.37640

Table 4.2. Time for successfully achieving output tracking performance ($|e_1| \leq 0.01$) using saturation-type SMC tail and blended controllers

	Tail Controller	Blended Controller
SMC Scheme	0.66715	0.40790
TSMC Scheme	0.45470	0.37620
NTSMC Scheme	0.47160	0.37650

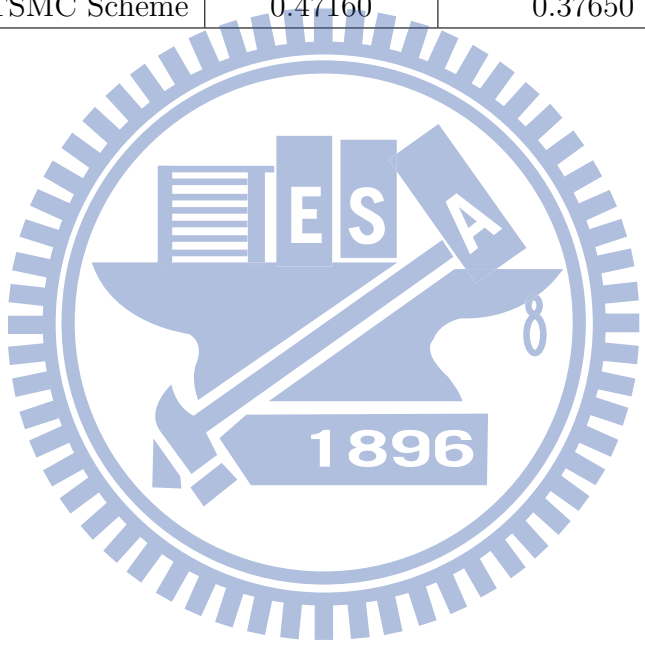

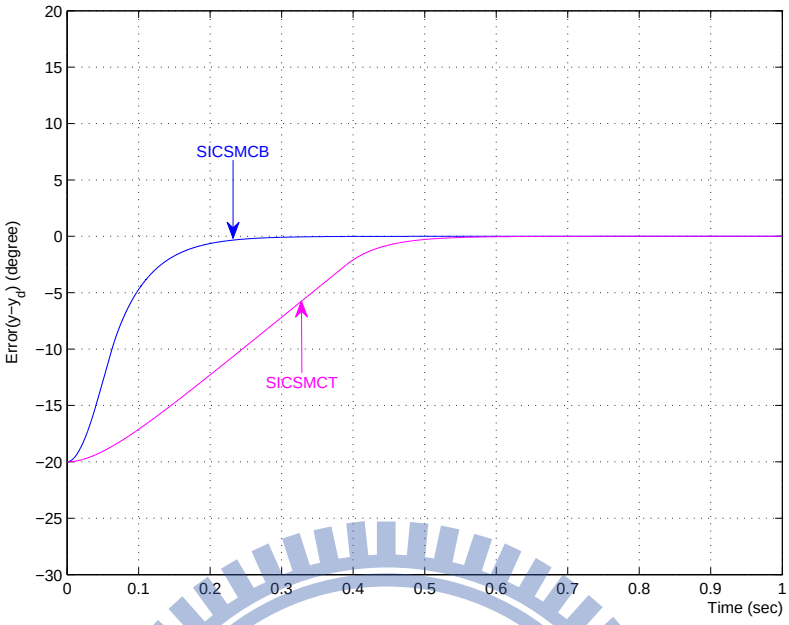

Fig. 4.1. Time evolution of error $e_1 = \alpha - \alpha_d$ by sign-type SMC scheme

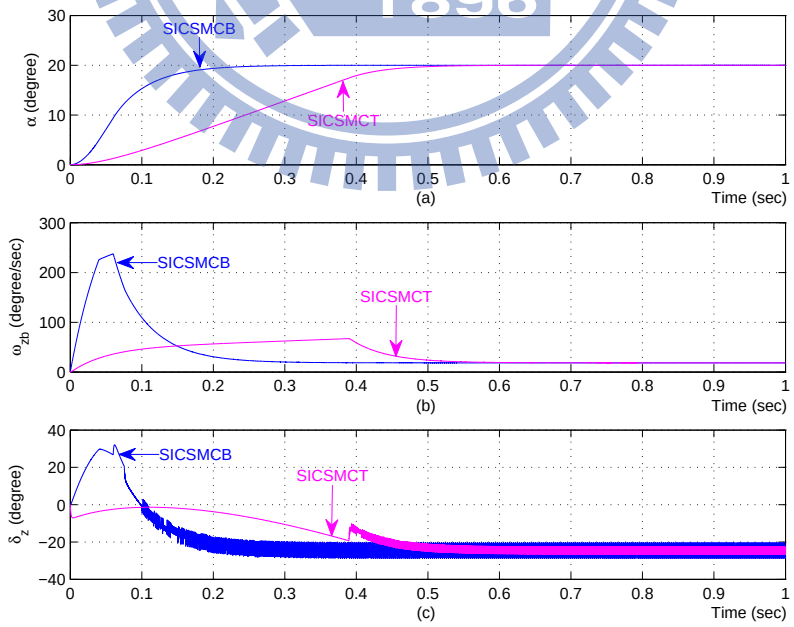

Fig. 4.2. Time evolution of (a)α (b)ω_{zb} (c)δ_z by sugn-type SMC scheme

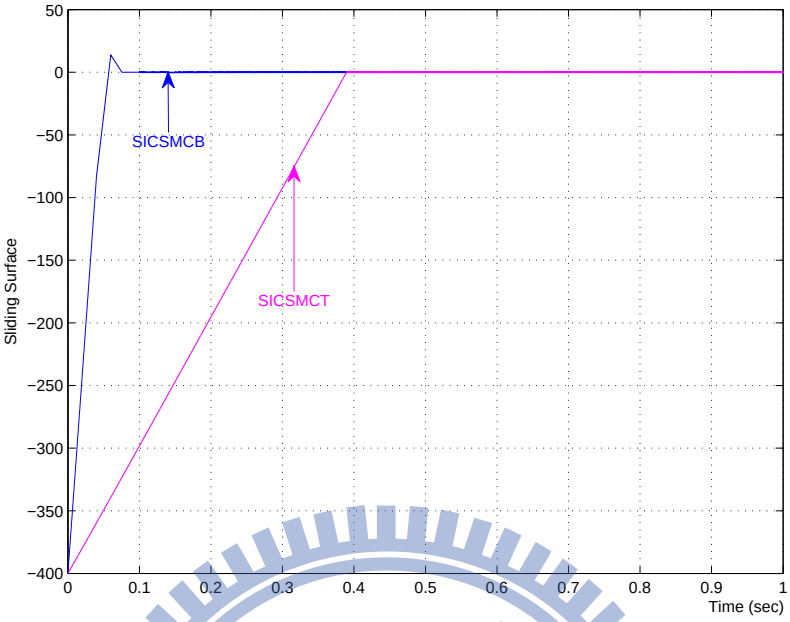

Fig. 4.3. Time evolution of the sliding variables by sign-type SMC scheme

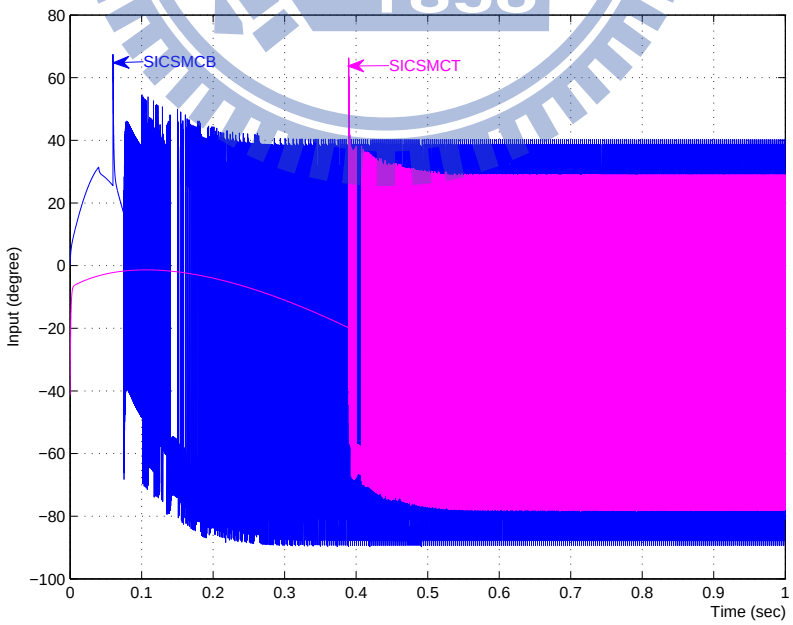

Fig. 4.4. Time evolution of δ_{zc} by sign-type SMC scheme

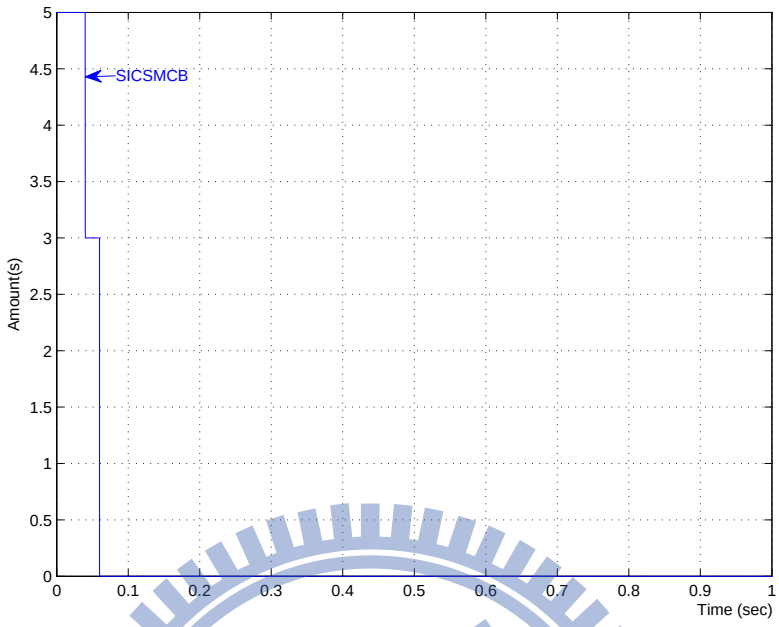

Fig. 4.5. Time evolution of the number of the consumed IACMs by sign-type SMC scheme

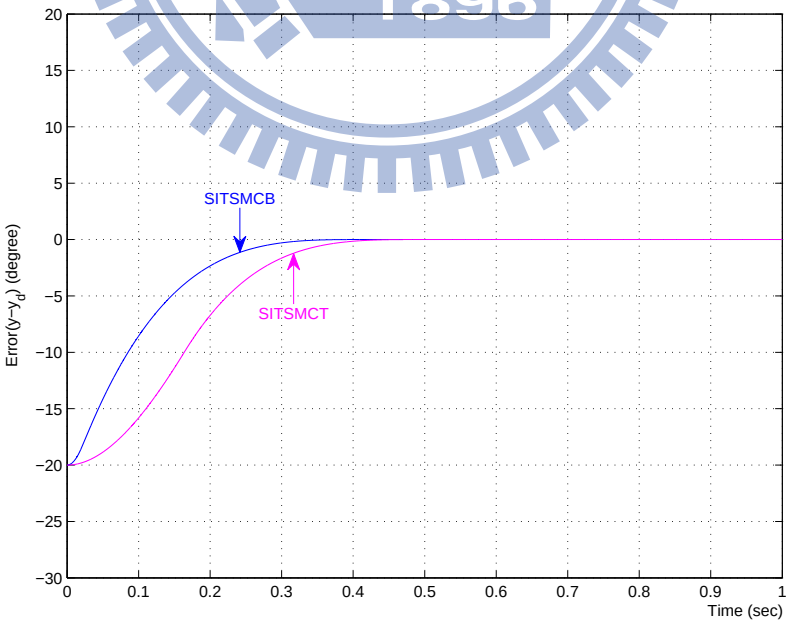

Fig. 4.6. Time evolution of error $e_1 = \alpha - \alpha_d$ by sign-type TSMC scheme

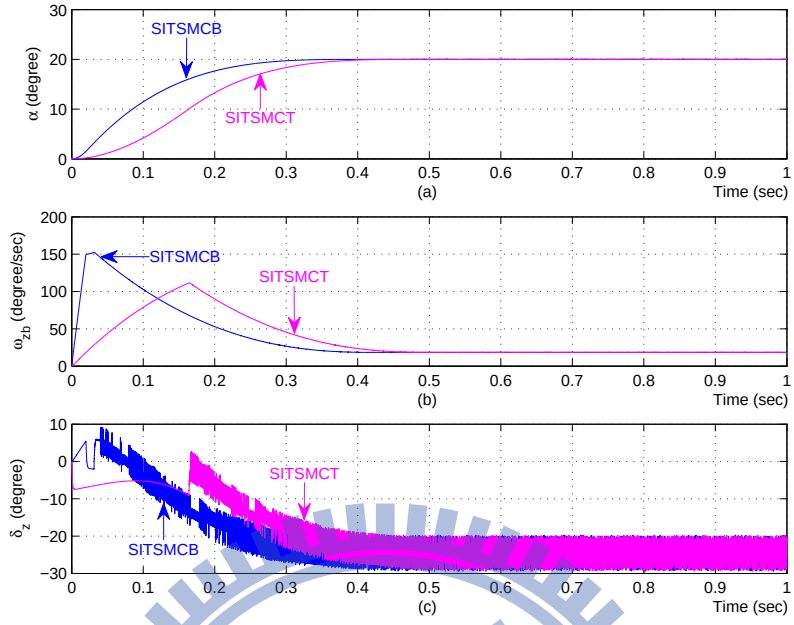

Fig. 4.7. Time evolution of (a)α (b)ω_{zb} (c)δ_z by sign-type TSMC scheme

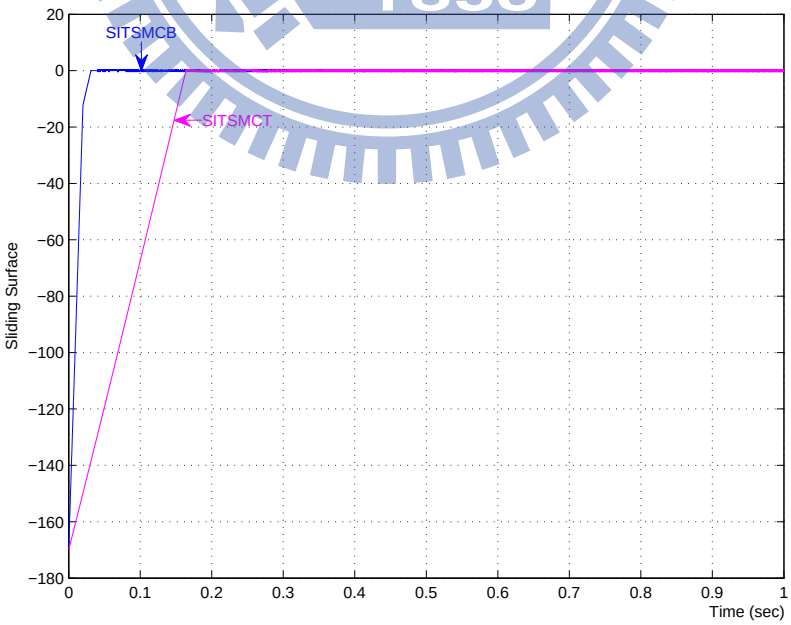

Fig. 4.8. Time evolution of the sliding variables by sign-type TSMC scheme

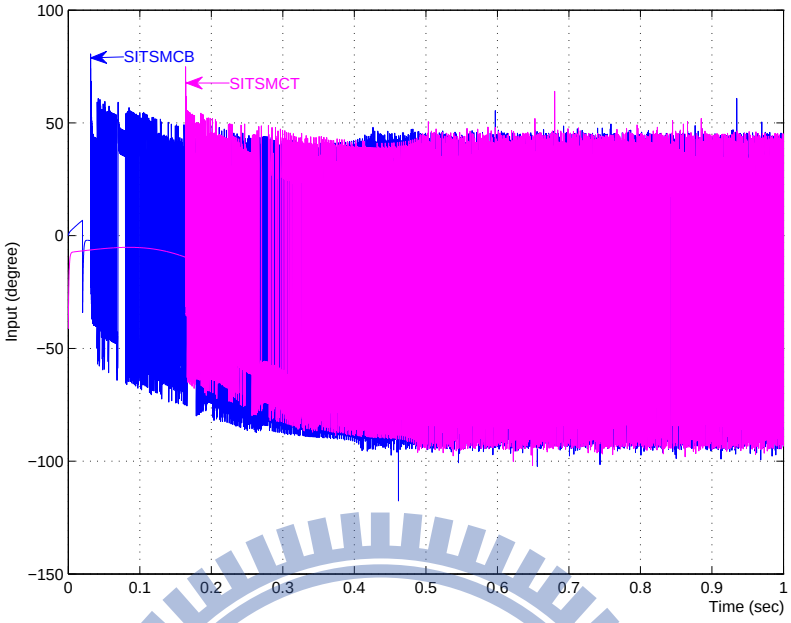

Fig. 4.9. Time evolution of δ_{zc} by sign-type TSMC scheme

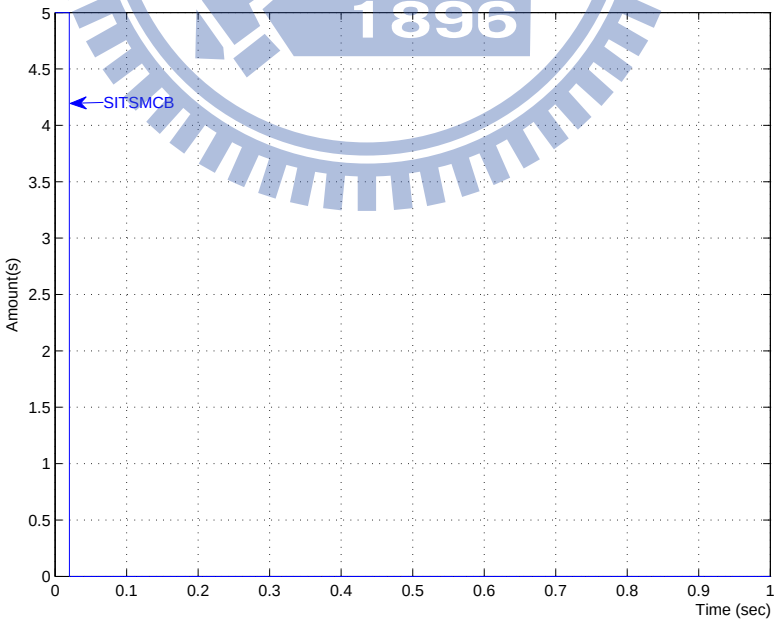

Fig. 4.10. Time evolution of the number of the consumed IACMs by sign-type TSMC scheme

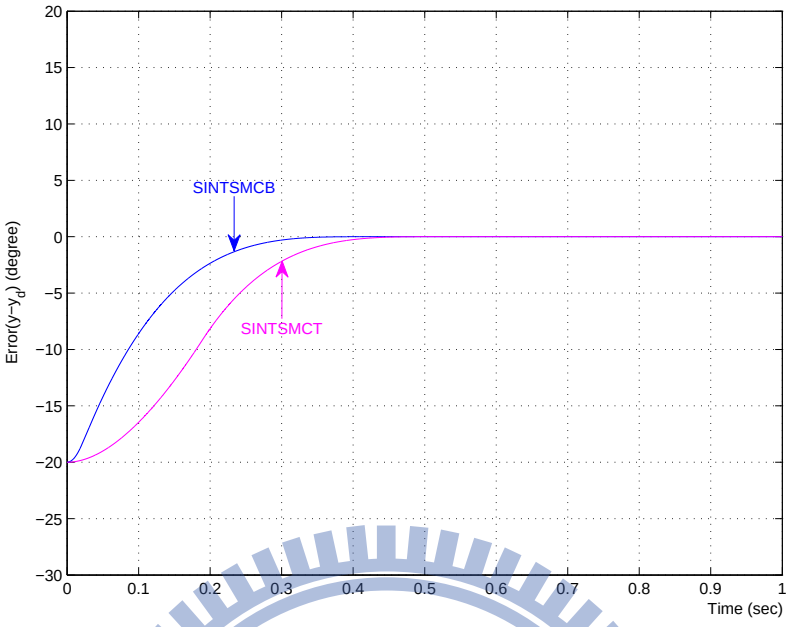

Fig. 4.11. Time evolution of error $e_1 = \alpha - \alpha_d$ by sign-type NTSMC scheme

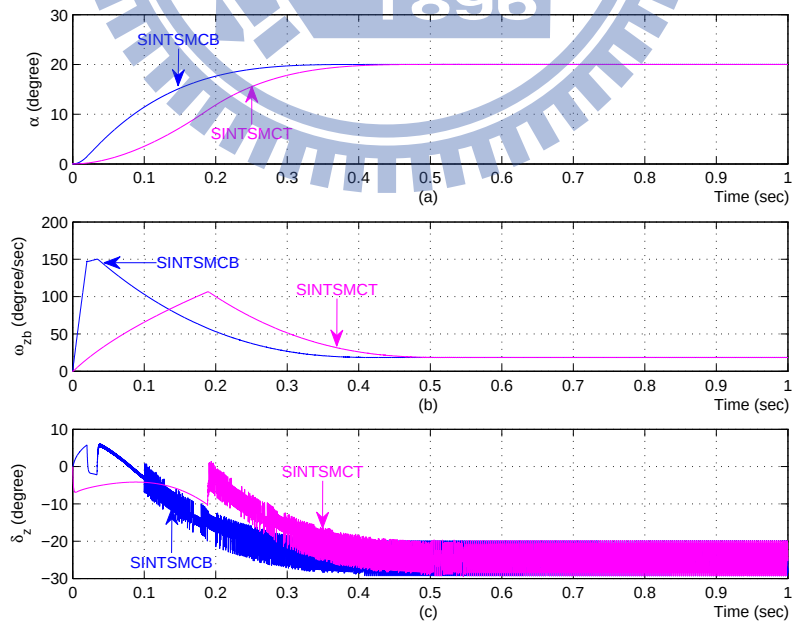

Fig. 4.12. Time evolution of (a)α (b)ω_{zb} (c)δ_z by sign-type NTSMC scheme

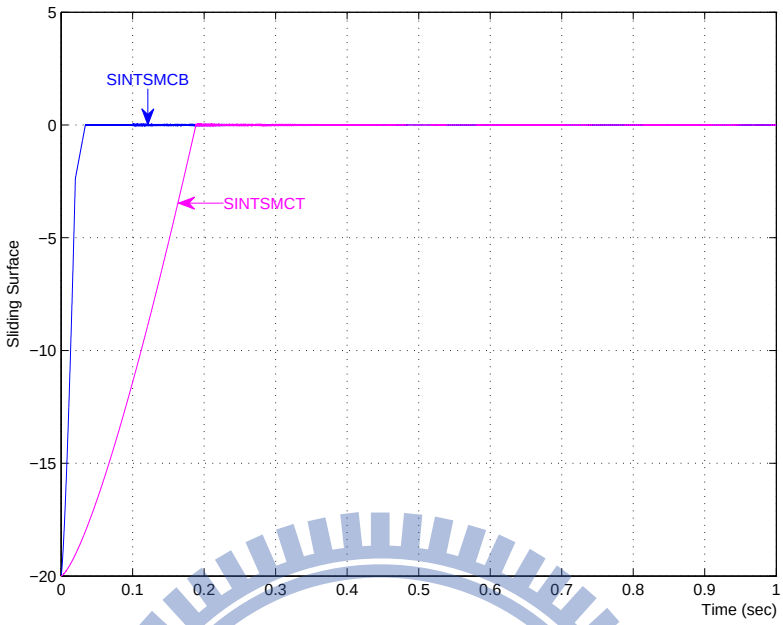

Fig. 4.13. Time evolution of the sliding variables by sign-type NTSMC scheme

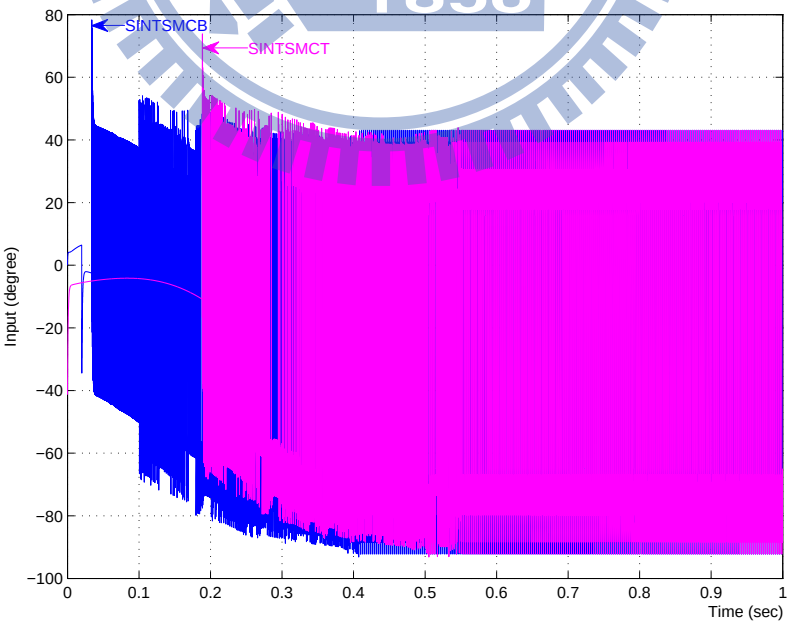

Fig. 4.14. Time evolution of δ_{zc} by sign-type NTSMC scheme

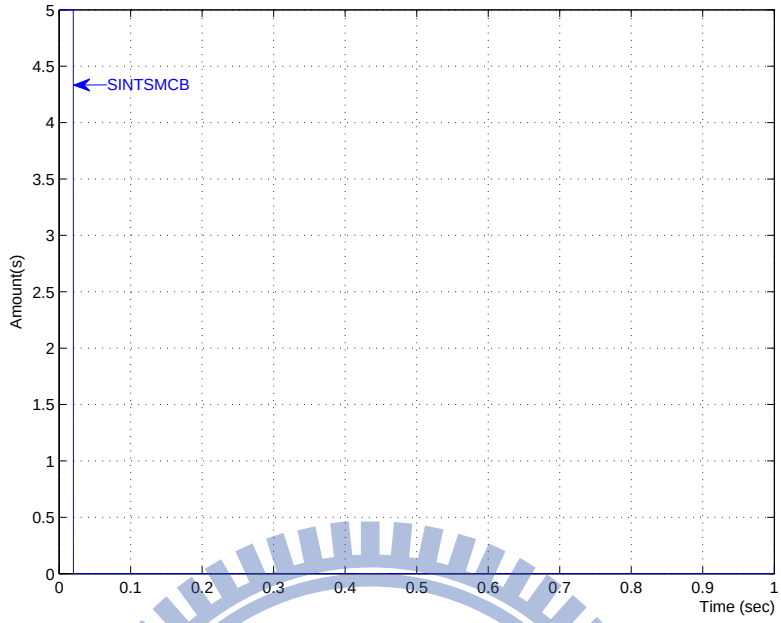

Fig. 4.15. Time evolution of the number of the consumed IACMs by sign-type NTSMC scheme

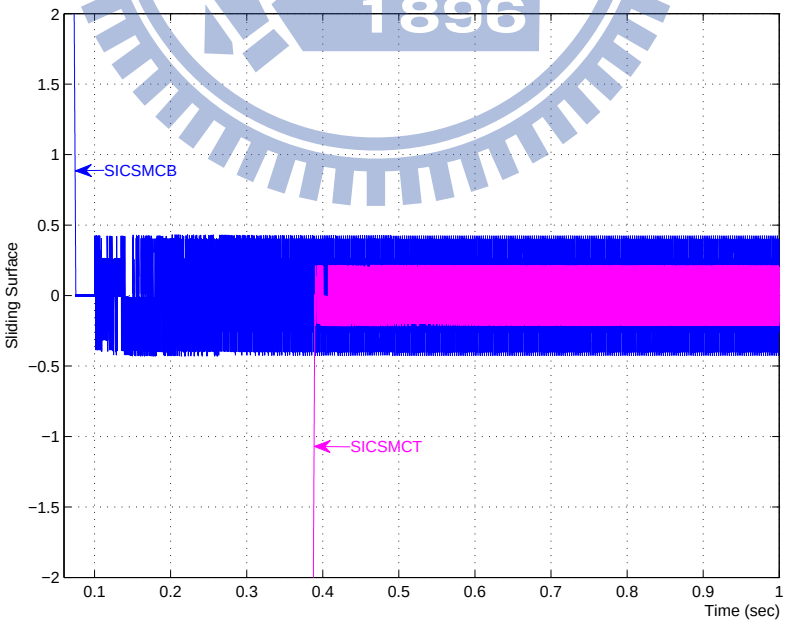

Fig. 4.16. Time evolution of the sliding variables in magnified scale by sign-type SMC scheme

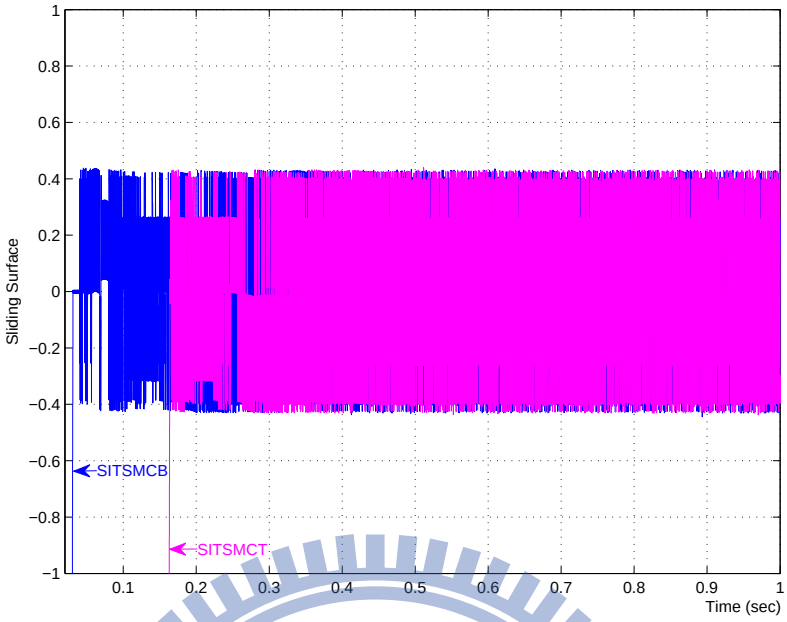

Fig. 4.17. Time evolution of the sliding variables in magnified scale by sign-type TSMC scheme

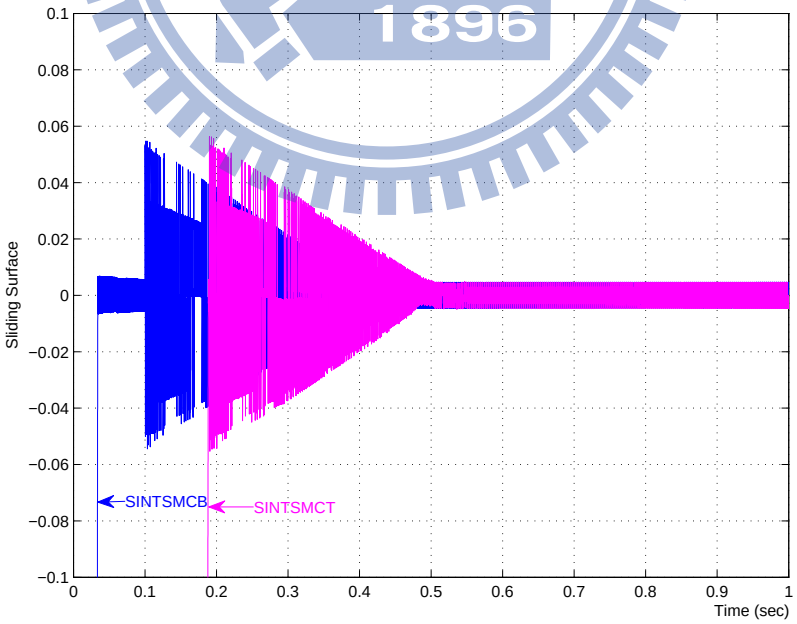

Fig. 4.18. Time evolution of the sliding variables in magnified scale by sign-type NTSMC scheme

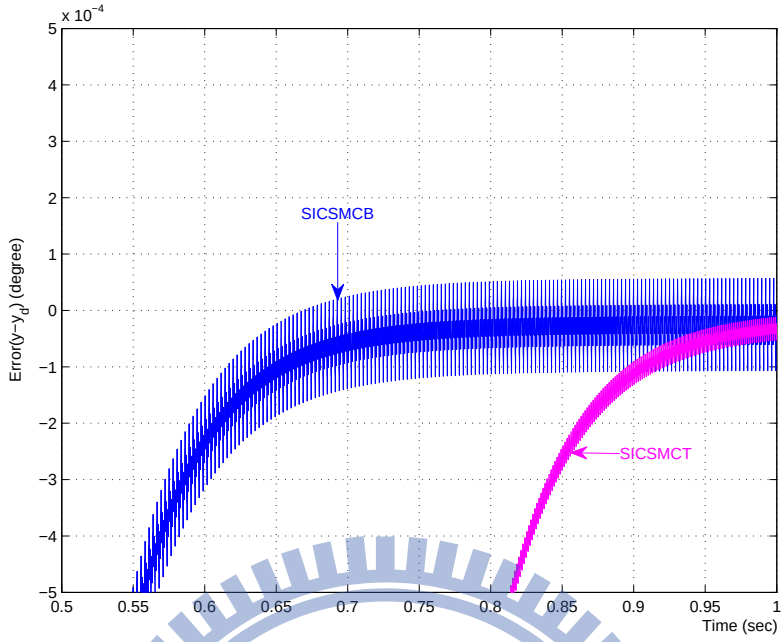

Fig. 4.19. Time evolution of error $e_1 = \alpha - \alpha_d$ in magnified scale by sign-type SMC scheme

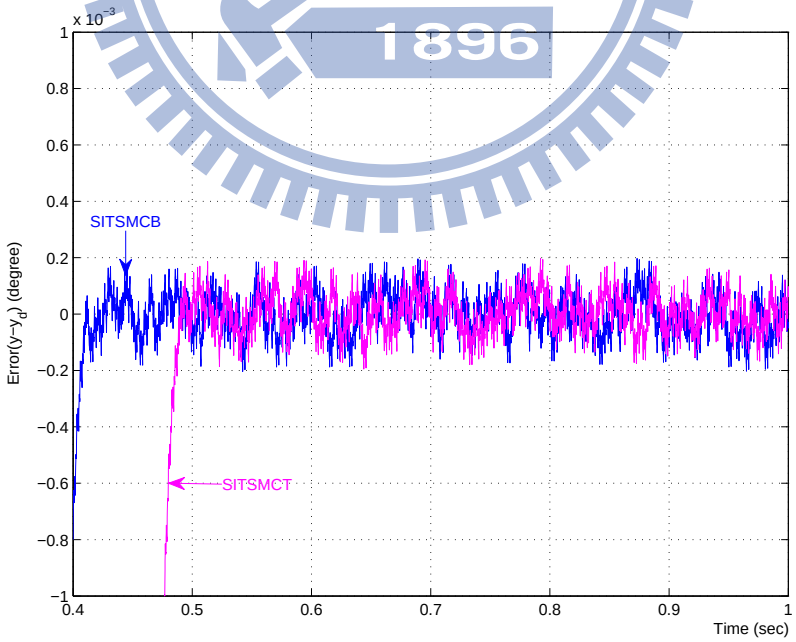

Fig. 4.20. Time evolution of error $e_1 = \alpha - \alpha_d$ in magnified scale by sign-type TSMC scheme

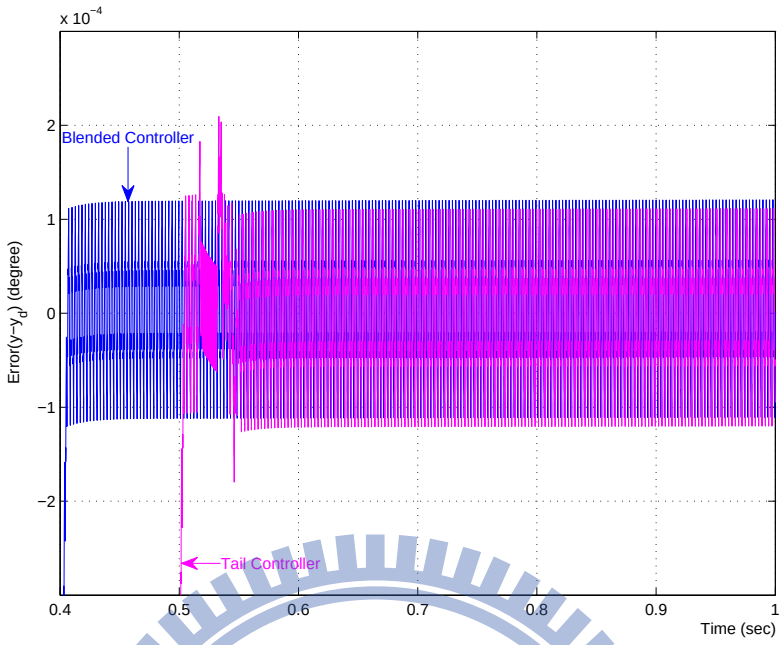

Fig. 4.21. Time evolution of error $e_1 = \alpha - \alpha_d$ in magnified scale by sign-type NTSMC scheme

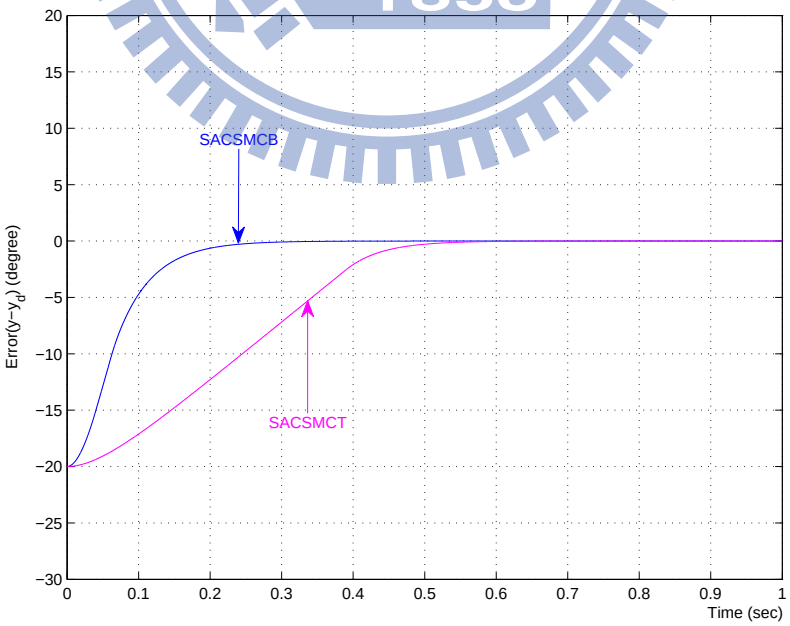

Fig. 4.22. Time evolution of error $e_1 = \alpha - \alpha_d$ by saturation-type SMC scheme

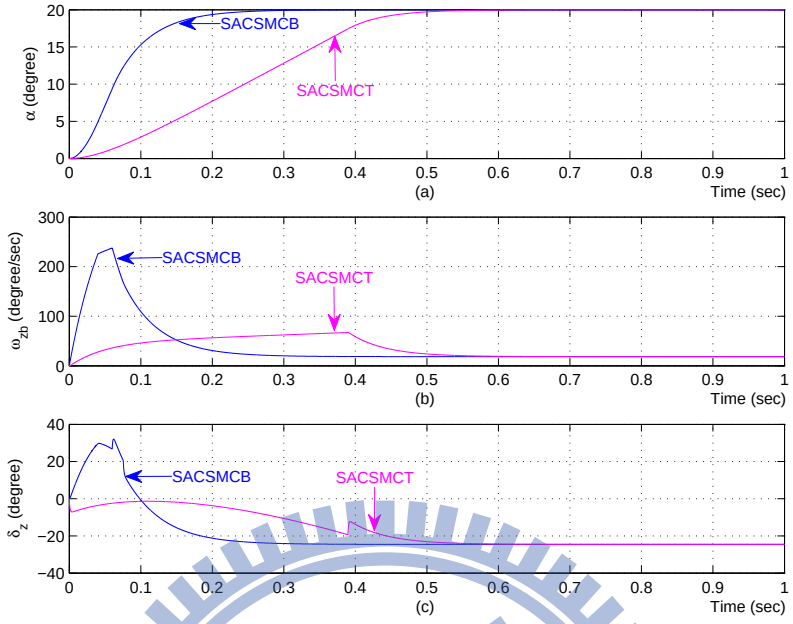

Fig. 4.23. Time evolution of (a)α (b)ω_{zb} (c)δ_z by saturation-type SMC scheme

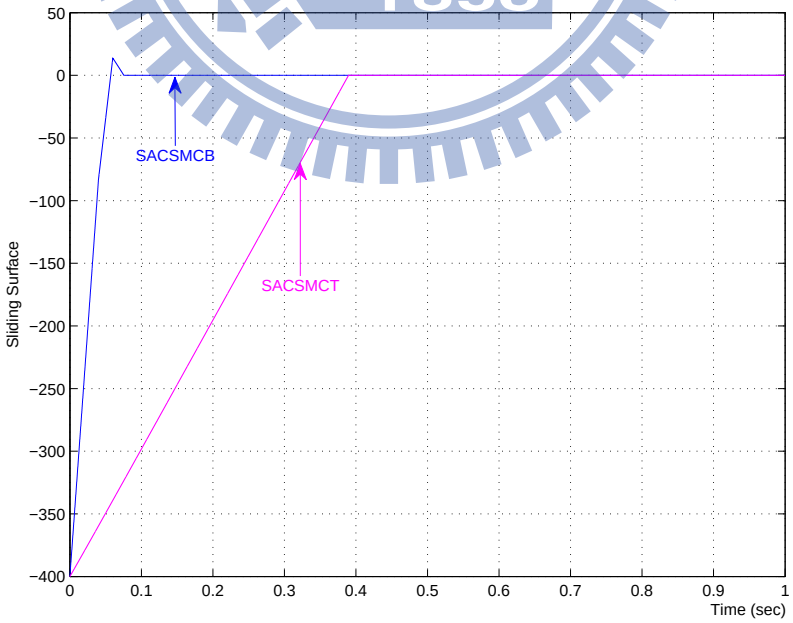

Fig. 4.24. Time evolution of the sliding variables by saturation-type SMC scheme

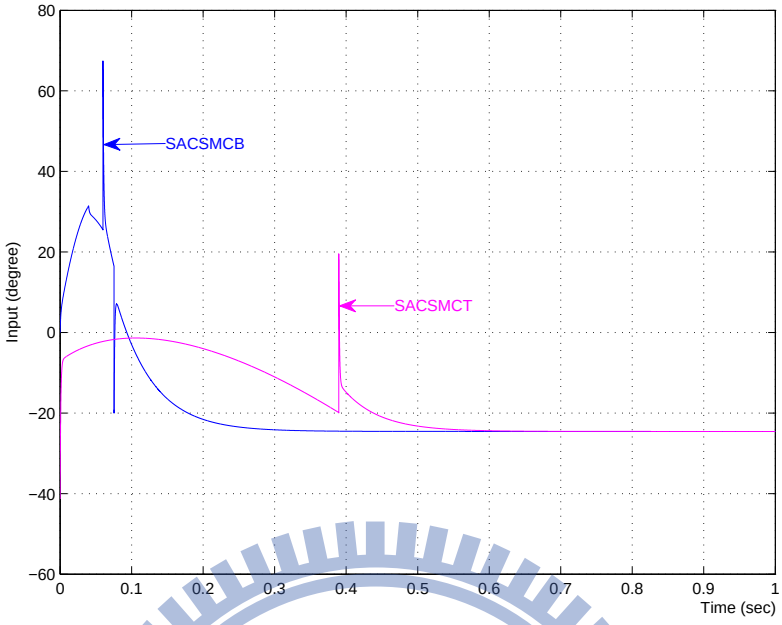

Fig. 4.25. Time evolution of δ_{zc} by saturation-type SMC scheme

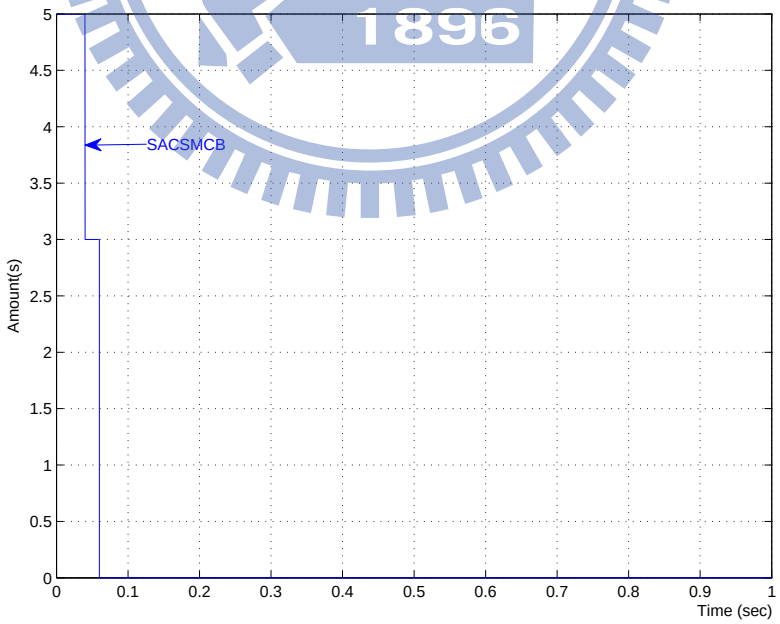

Fig. 4.26. Time evolution of the number of the consumed IACMs by saturation-type SMC scheme

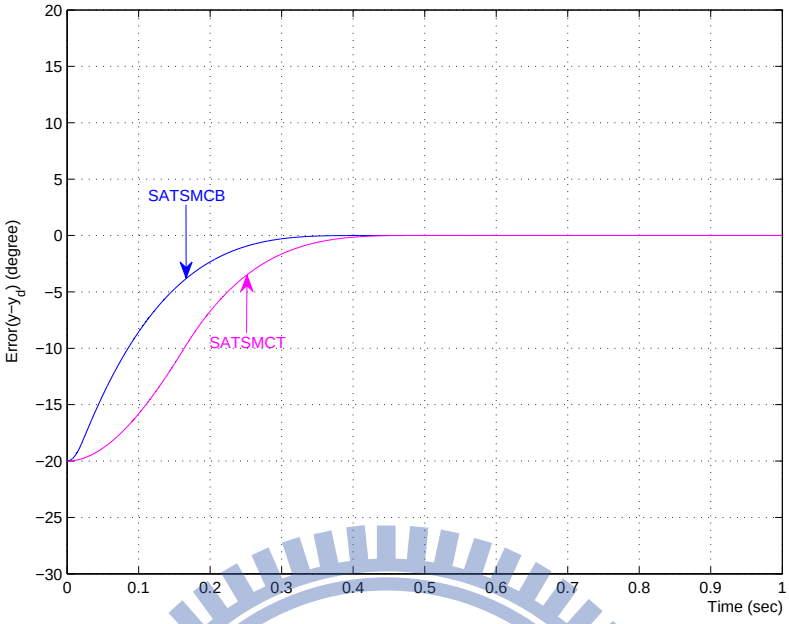

Fig. 4.27. Time evolution of error $e_1 = \alpha - \alpha_d$ by saturation-type TSMC scheme

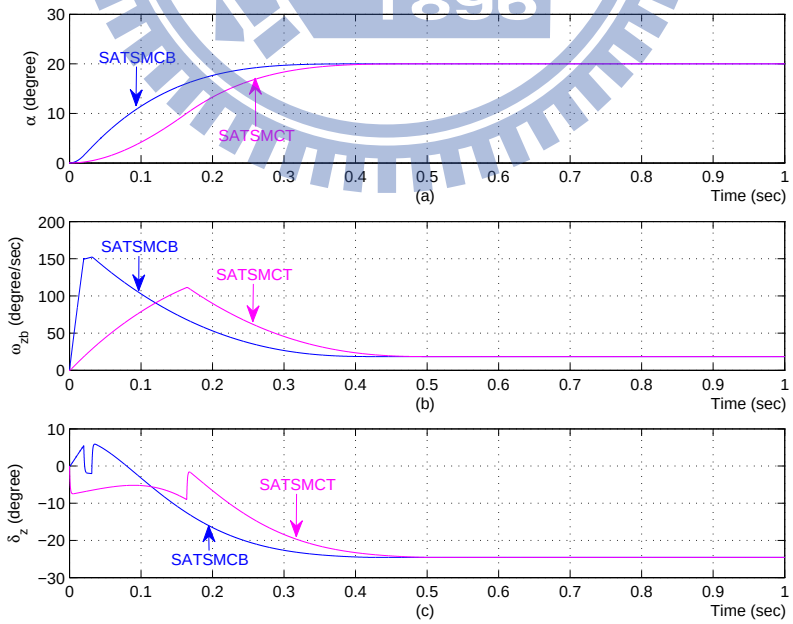

Fig. 4.28. Time evolution of (a)α (b)ω_{zb} (c)δ_z by saturation-type TSMC scheme

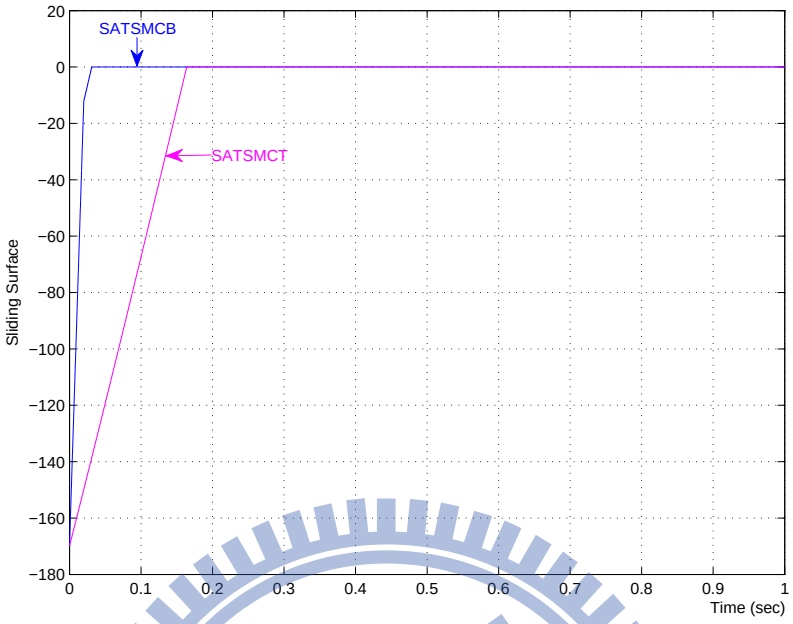

Fig. 4.29. Time evolution of the sliding variables by saturation-type TSMC scheme

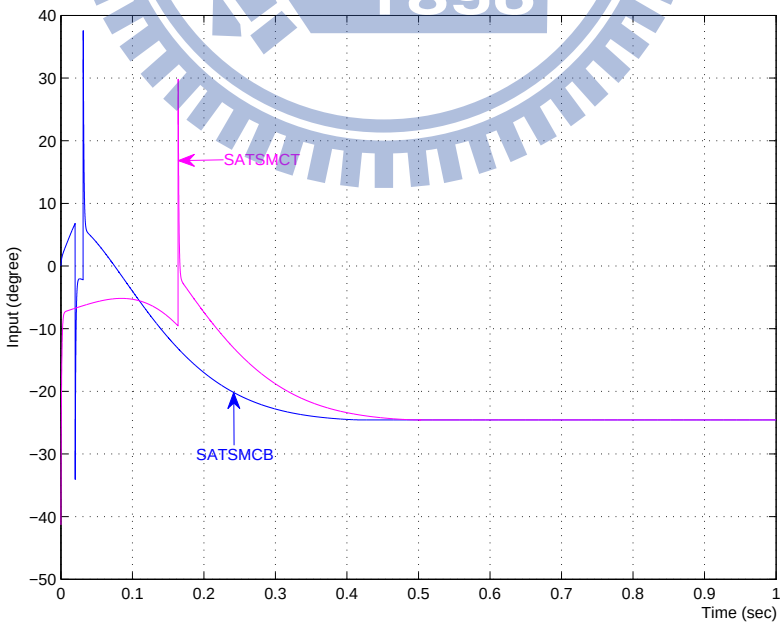

Fig. 4.30. Time evolution of δ_{zc} by saturation-type TSMC scheme

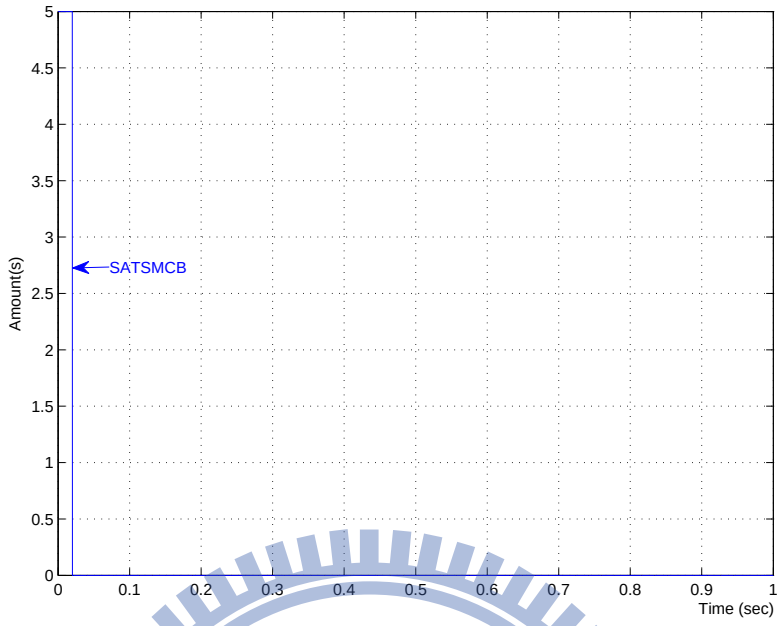

Fig. 4.31. Time evolution of the number of the consumed IACMs by saturation-type TSMC scheme

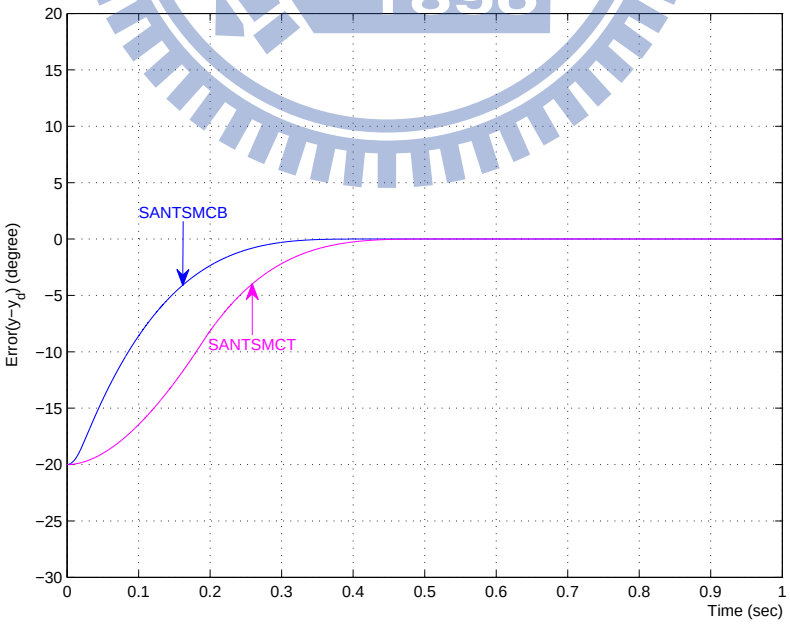

Fig. 4.32. Time evolution of error $e_1 = \alpha - \alpha_d$ by saturation-type NTSMC scheme

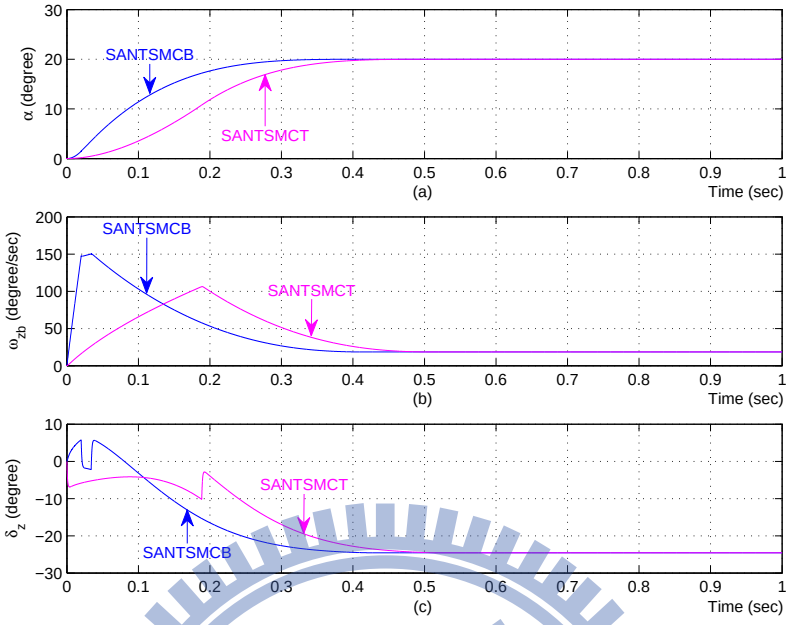

Fig. 4.33. Time evolution of (a)α (b)ω_{zb} (c)δ_z by saturation-type NTSMC scheme

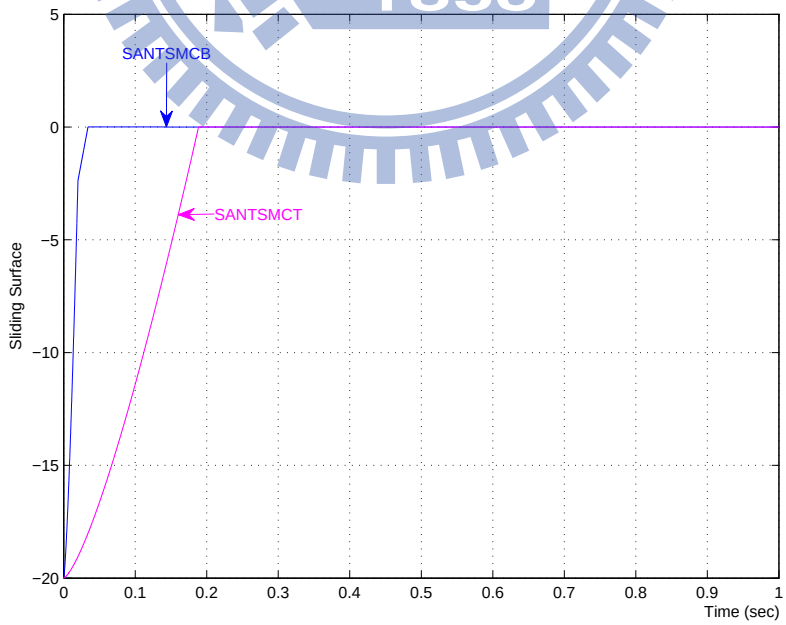

Fig. 4.34. Time evolution of the sliding variables by saturation-type NTSMC scheme

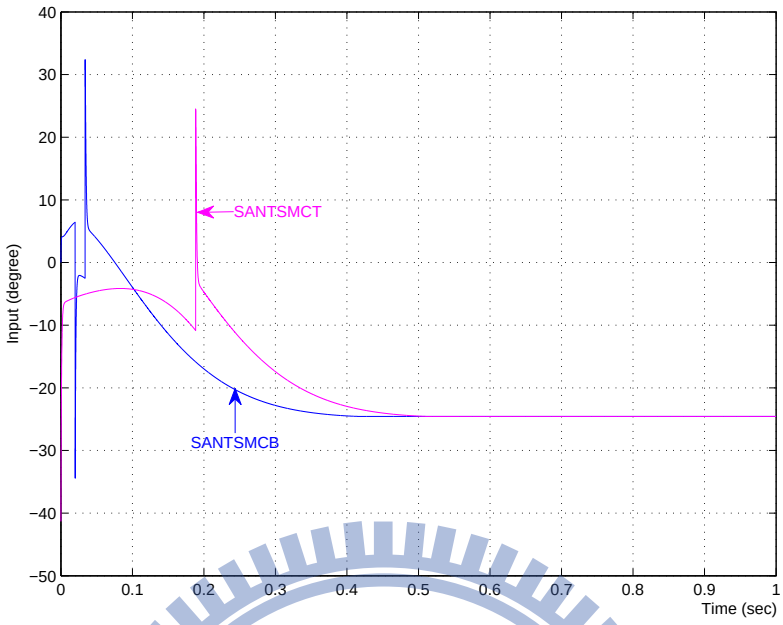

Fig. 4.35. Time evolution of δ_{zc} by saturation-type NTSMC scheme

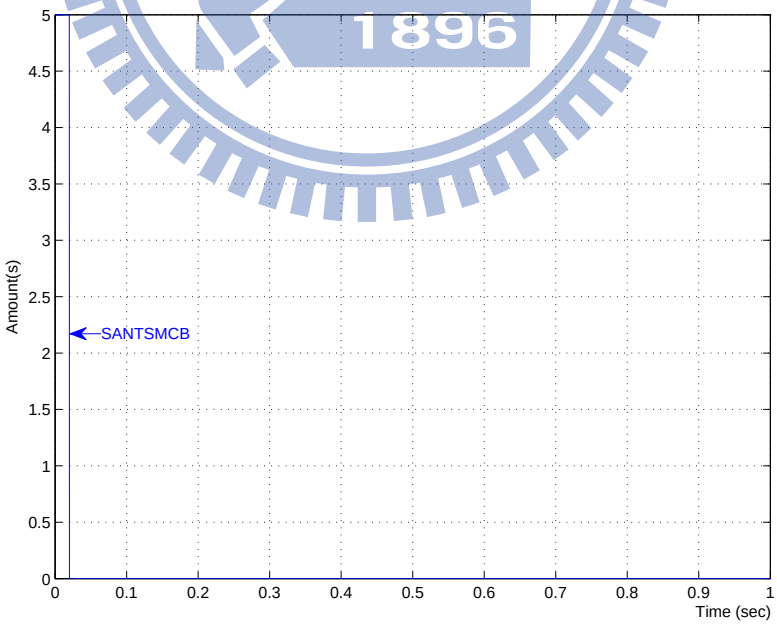

Fig. 4.36. Time evolution of the number of the consumed IACMs by saturation-type NTSMC scheme

CHAPTER FIVE
CONCLUSIONS AND
SUGGESTIONS FOR FURTHER RESEARCH

5.1 Conclusions

In this thesis, at first, in Chapter 3, we have introduced a six degrees of freedom mathematical model of PAC-3 and then the model of the X-tail and the RCS were also constructed. In Chapter 4, we have studied the missile attitude tracking problem using blended controllers via three SMC techniques: I) CSMC, II) TSMC, and III) NTSMC schemes. A characteristic of the CSMC is that the convergence of the system states to the equilibrium points is usually asymptotical due to the asymptotical convergence of the linear switching manifolds that are commonly chosen. Thus, the TSMC was developed. Compared with the linear hyperplane based sliding mode, TSMC offers finite time convergence and better static tracking precision. But the TSMC design methods have a singularity problem. Base on the TSMC, the NTSMC have been presented to avoid the singularity for the TSMC. However, in practical realization, the three sign-type SMC schemes, found in this thesis, suffer from the chattering problem which might result in the following three undesired phenomena: I) high frequency switching of the control, II) waste of energy and III) excited unmodelled dynamics. This problem might cause that the predicted convergence time in TSMC and NTSMC theories are no longer available because the sliding variable can not lie on the sliding surface and then lead to the imprecision of output tracking task. Therefore, the features of finite time convergence and accurate convergence by TSMC and NTSMC schemes are no longer valid. In order to eliminate the chattering problem in practice, these sign-type SMC designs are replaced by saturation-type SMC designs. The numerical results have shown that the tracking preci-

sion by saturation-type SMC designs still satisfies the criterion for tracking performance being successful.

The simulation results have also demonstrated that the blended control can performs faster for tracking task than the tail control, decrease the required number of IACMs and furthermore, improve the tracking performance. The above results sufficiently account for the features of the blended control and benefit the developing of the ATBM for reducing the MD between missile and target to achieve the HTK goal.

5.2 Suggestions for Further Research

To further extend the research covered in this thesis, we note several directions:

1) study the three-dimensional missile model which may exists coupling effects resulting from the spinning missile with angular velocity ω_{xb} [48], [13] under the constraint of the states and rate of the states.

2) In order to fully utilize each IACM for the spinning missile in the three-dimensional missile model, the ignition control algorithm must be considered.

3) In real life situation, the control law must considers the influences of jet interaction effects [13],[19], [70], [71] which is the cause of incident air flowing when any IACM is triggered. We thus may introduce these influences to let the model closer to the real life situation.

4) Integrate the designed control law into the missile guidance law to verify whether the ATBM will intercept the TBM.

References

[1] L.-K. Zhu, *Research on Compound Control Technique with Direct Thrust and Aerodynamic Force for Air Defence Missile*, Ph.D, Dissertation, Graduate School of National University of Defense Technology, Hunan, 2008.

[2] J. Cirincione, "The Performance of the Patriot Missile in the Gulf War," *An Edited Draft of a Report prepared for the Government Operations Committee*, U.S. House of Representatives, Oct. 1992.

[3] 直心義 譯, "爲什麼要直接碰撞傷害," *863*先進防禦技術通訊*:A*類, 140(2):1 6, 2000.

[4] R. R. Chamberlain, "Calculation of Three-Dimensional Jet Interaction Flowfields," AIAA Paper 1990-2099, 26^{th} *AIAA Joint Propulsion Conference and Exhibit*, Jul. , 1990.

[5] R. D. Weil and K. A. Wise, "Blended Aero and Reaction Jet Missile Autopilot Design Using VSS Techniques," *Proceedings of the 30th IEEE Conference on Decision and Control*, pp. 2828-2829, Dec. 1991.

[6] M. Innocenti and A. Thukral, "Simultaneous Reaction Jet and Aerodynamic Control of Misille Systems," AIAA Paper 1993-3739, *AIAA Guidance Navigation and Control Conference*, Aug. ,1993.

[7] W. R. Chadwick, "Augmentation of High-Altitude Maneuver Performance of Tail-Controlled Missile Using Lateral Thrust," *Tech. Rep. ADA 328973, AD Report*, 1997.

[8] A. Thukral and M. Innocenti, "A Sliding Mode Missile Pitch Autopilot Synthesis for High Angle of Attack Maneuvering," *IEEE Transactions on Control Systems Technology*, Vol. 6, No. 3, 1998.

[9] H. Rui and S. Koichi, "Autopilot Design for a Missile with Reaction-Jet Using Coefficient Diagram Method," AIAA Paper 2001-4162, *AIAA Guidance, Navigation, and Control Conference and Exhibit*, Aug. 2001.

[10] S. D. Brierly and R. Longchamp, "Application of Sliding-Mode Control to Air-Air Interception Problem," *IEEE Transactions on Aerospace and Electronic Systems*, Vol. 26, No. 2, pp. 306-325, 1990.

[11] T. L. Vincent, R. G. Cottrell, and R. W. Morgan, "Minimizing Maneuver Advantage Requirements for A Hit-To-Kill Interceptor," AIAA Paper 2001-4276, *AIAA Guidance, Navigation, and Control Conference and Exhibit*, Aug. 2001.

[12] 郭建國, 周軍和周風岐, "直接力/氣動力複合控制技術分析," 航空兵器, Vol. 5, pp. 12-15, 2004.

[13] Y.-X. Yin, *Research on Guidance and Control Method of Interceptor Missile with Aerodynamics and Lateral Thrust Blended*, Ph.D, Dissertation, Harbin Institute of Technology, Harbin, 2008.

[14] F. S. Alvi, C. Shih, and A. Krothapalli, "Active Control of the Feedback Loop in High-Speed Jets," AIAA Paper 2001-16270, 39^{th} *AIAA Aerospace Sciences and Exhibit*, Jan. , 2001.

[15] K. A. Wise and D. J. Broy, "Agile Missile Dynamics and Control," *Journal of Guidance, Dynamics and Control*, Vol. 21, No.3, pp.441-449, 1998.

[16] P. K. Menon and V. R. Jragavarapu, "Adaptive Techniques for Multiple Actuator Blending," AIAA Paper 1998-4494, *AIAA Guidance Navigation and Control Conference and Exhibit*, Aug. 1998.

[17] W. K. Schroeder and K. Liu, "An Appropriate Application of Fuzzy Logic: Missile Autopilot for Dual Control Implementation," *IEEE International Symposium on Intelligent Control*, 1994.

[18] Z.-H. Wu and C.-Y. Dong, "Reaction Jet and Aerodynamics Compound Control Missile Autopilot Design Based on Adaptive Fuzzy Sliding Mode Control," *International Symposium on Instrumentation and Control Technology: Sensors, Automatic Measurement, Control, and Computer Simulation*, 6th, 2006.

[19] Y.-T. Bi, *Research on Guidance and Control For Missile With Lateral Jests And Aerodynamic Surfaces*, Ph.D, Dissertation, Harbin Institute of Technology, Harbin, 2010.

[20] J.-J. E. Slotine and W. Li, *Applied Nonlinear Control*, Prentice-Hall, Englewood Cliffs, NJ, 1991.

[21] V. I. Utkin, *Sliding Modes and Their Application in Variable Structure Systems*, 1st ed., MIR Publishers, Moscow, Russia, 1978.

[22] C. Edwards and S. K. Spurgeon, *Sliding Mode Control: Theory and Applications*, Taylor & Francis, 1998.

[23] V. I. Utkin, "Variable Structure Systems With Sliding Modes," *IEEE Transaction on Automatic Control*, Vol. 22, No.2, pp. 212-222, 1997.

[24] J. D. Bošković, S. M. Li, and R. K. Mehra, "Robust Adaptive Variable Structure Control of Spacecraft Under Control Input Saturation," *Journal of Guidance, Control, and Dynamics*, Vol. 24, No. 1, pp. 14-22, 2001.

[25] Y.-P. Chen and S.-C. Lo, "Sliding-Mode Controller Design for Spacecraft Attitude Tracking Maneuvers," *IEEE Transactions on Aerospace and Electric Systems*, Vol. 29, No. 4, pp. 1328-1333, 1993.

[26] T. A. W. Dwyer III, "Exact Nonlinear Control of Spacecraft Slewing Maneuvers with Internal Momentum Transfer," *Journal of Guidance, Control and Dynamics*, Vol. 9, No. 2, pp. 240-247, 1986.

[27] T. A. W. Dwyer III and H. Sira-Ramirez, "Variable-Structure Control of Spacecraft Attitude Maneuvers," *Journal of Guidance, Control and Dynamics*, Vol. 11, No. 3, pp. 262-270, 1988.

[28] K.-M. Koo and J.-H. Kim, "Robust Control of Robot Manipulators with Parametric Uncertainty," *IEEE Transactions on Automatic Control*, Vol. 39, No. 6, pp. 1230-1233, 1994.

[29] J.-J. E. Slotine and S. S. Sastry, "Tracking Control of Non-Linear Systems Using Sliding Surfaces, with Application to Robot Manipulators," *International Journal of Control*, Vol. 38, No. 2, pp. 465-492, 1983.

[30] J.-J. E. Slotine and W. Li, "On the Adaptive Control of Robot Manipulators," *International Journal of Robotics Research*, Vol. 6, pp. 49-57, 1987.

[31] C.-Y. Su and Y. Stepanenko, "Adaptive Sliding Mode Control of Robot Manipulators with General Sliding Manifold," *Proceedings of the 1993 IEEE/RSJ International Conference on Intelligent Robots and Systems*, pp. 1255-1259, 1993.

[32] K.-S. Yeung and Y.-P. Chen, "A New Controller Design for Robot Manipulators Using The Theory of Variable Structure Systems," *IEEE Transactions on Automatic Control*, Vol. 33, No. 2, pp. 200-206, 1988.

[33] X.-H. Yu and J.-X. Xu, *Variable Structure Systems: Towards the 21st Century*, Springer-Verlag, Vol. 274, pp. 1-32, 2002.

[34] V. I. Utkin, *Sliding Modes in Control Optimization*, Springer-Verlag, Heidelberg, 1992.

[35] V. I. Utkin, "Block Control Principle," *Automation and Remote Control*, Vol. 51, No. 5, pp. 601-609, 1990.

[36] L. Fridman, *Sliding Modes after the First Decade of the 21st Century*, Springer-Verlag, Vol. 412, pp. 3, 2012.

[37] H. K. Khalil, *Nonlinear System*, 2nd ed., Englewood Cliffs, NJ: Prentice-Hall, 1996.

[38] J. Stewart, *Calculus Early Transcendentals International Edition Edition*, 5th ed., Thomson Brooks/Cole, pp. 398-399,2003.

[39] M. Zak, "Terminal Attractors for Addressable Memory in Neural Network," *Physics Letter*, Vol. 33, No. 12, pp. 18-22, 1988.

[40] X.-H. Yu and Z.-H. Man, "Model Reference Adaptive Control Systems with Terminal Sliding Modes," *International Journal of Control*, Vol. 64, No. 6, pp. 1165-1176, 1996.

[41] X.-H. Yu and Z.-H. Man, "Multi-input Uncertain Linear Systems with Terminal Sliding-Mode Control," *Automatica*, Vol. 34, No. 3, pp. 389-392, 1998.

[42] Z.-H. Man, A. P. Paplinski, and H.-R. Wu, "A Robust MIMO Terminal Sliding Mode Control Scheme for Rigid Robotic Manipulators," *IEEE Transactions on Automatic Control*, Vol. 39, No. 12, pp. 2464-2469, 1994.

[43] X.-H. Yu, and Z.-H. Man, "Terminal Sliding Mode Control of MIMO Linear Systems," *IEEE Transactions on Circuits and Systems I: Fundamental Theory and Applications*, Vol. 44, No. 11, pp. 1065-1070, 1997.

[44] Y. Feng, X.-H. Yu, and Z.-H. Man, "Non-Singular Terminal Sliding Mode Control and Its Application for Robot Manipulators," *Proceedings of 2001 IEEE International Symposium on Circuits and Systems*, Vol. 3, pp. 545–548, Sydney, 2001.

[45] Y. Feng, X.-H. Yu, and Z.-H. Man, "Non-Singular Terminal Sliding Mode Control of Rigid Manipulators," *Automatica*, Vol. 38, No. 12, pp. 2159-2167, 2002.

[46] J. H. Blakelock, *Automatic Control of Aircraft and Missile*, 2nd ed., John Wiley and Sons, Inc., New York, 1991.

[47] G. M. Siouris, *Missile Guidance and Control Systems*, 1st ed., Springer-Verlag, Inc., New York, 2004.

[48] 錢杏芳, 林瑞雄和趙亞男, 導彈飛行力學, 1st ed., 北京理工大學出版社, 北京, 2000.

[49] P. B. Ferdinand and J. J. Russell, *Vector Mechanics for Engineers: Dynamics*, 8th ed., McGraw-Hill, New York, 2007.

[50] H.-C. Luan and J.-X. Lin, "Relationship of Maneuvering And Motion for the Submarine with X-rudder," *Ship and Ocean Engineering*, Vol. 36, No. 2, pp. 100-102, 2007.

[51] B. Xu, "Patriot Series Surface-to-Air Missile," *Surface-to-Air Weapon*, Vol. 3, pp. 19-24, 2004.

[52] Y. Karayiannidis, G. Rovithakis and Z. Doulgeri, "Force Position Tracking for a Robotic Manipulator in Compliant Contact with a Surface Using Neuro-Adaptive Control," *Automatica*, Vol. 43, No. 1, pp. 1281-1288, 2007.

[53] H. J. Uang and B. S. Chen, "Robust Adaptive Optimal Tracking Design for Uncertain Missile Systems: a Fuzzy Approach," *Fuzzy Sets and Systems*, Vol. 126, No. 1, pp. 63-87, 2002.

[54] T. Bell, "Automatic Tractor Guidance Using Carrier-Phase Differential GPS," *Computers and Electronics in Agriculture*, Vol. 25, No. 1, pp. 53-66, 2000.

[55] J. Huang, *Nonlinear Output Regulation: Theory and Applications*, Society for Industrial and Applied Mathematics, Philadelphia, 2004.

[56] S. Devasia, D. G. Chen, and B. Paden, "Nonlinear Inversion-Based Output Tracking," *IEEE Transactions on Automatic Control*, Vol. 41, No. 7, pp. 930-942, 1996.

[57] R. M. Hirschorn, "Invertibility of Nonlinear Control Systems," *SIAM Journal on Control and Optimization*, Vol. 17, No. 2, pp. 289-297, 1979.

[58] S. N. Singh, "A Modified Algorithm for Invertibility in Nonlinear Systems," *IEEE Transactions on Automatic Control*, Vol. 26, No. 2, pp. 595-598, 1981.

[59] T.-L. Liao, L.-C. Fu and C.-F. Hsu, "Output Tracking Control of Nonlinear Systems with Mismatched Uncertainties," *Systems and Control Letters*, Vol. 18, No. 1, pp. 39-47, 1992.

[60] C. Lin, W. Q.-Guo Wang, and T. H. Lee, "H_{infty} Output Tracking Control for Nonlinear Systems via T-S Fuzzy Model Approach," *IEEE Transactions on Systems, Man, and Cybernetics, Part B*, Vol. 36, No. 2, pp. 450-457, 2006.

[61] A. Adhami-Mirhosseini, M. J. Yazdanpanah, and A. Khaki-Sedigh, "Robust Tracking of a class of Perturbed Nonlinear Systems via Multivariable Nested Sliding Mode Control," *Journal of Dynamic Systems, Measurement, and Control ASME*, Vol. 134, No. 3, 2012.

[62] Y.-W. Liang, S.-D. Xu, T.-C. Chu, and C.-C. Cheng, "Reliable Output Tracking Control for a Class of Nonlinear Systems," *IEICE Transactions on Fundamentals of Electronics, Communications and Computer Sciences*, Vol. E87-A, No. 9, 2004.

[63] C.-S. Chiu, "Derivative and Integral Terminal Sliding Mode Control for a Class of MIMO Nonlinear Systems," *Automatica*, Vol. 48, No. 2, pp. 316-326, 2012.

[64] A. Isidori, *Nonlinear Control System*, 3rd ed., Springer-Verlag, London, 1995.

[65] R. A. Hull and Z. Qu, "Dynamic Robust Recursive Control Design and Its Application to a Nonlinear Missile Autopilot," *Proceeding of the American Control Conference*, Albuquerque, New Mexico, pp. 833–837, 1997.

[66] Q.-G. Li, C.-H. Jiang, and C.-Y. Zhang, "Enhanced Back-Stepping Control for Missile Autopilot Based on Nonlinear Disturbance Observer," *Electronics Optics and Control*, Vol. 14,No. 5, 2007.

[67] J. Wang, W.-C. Chen, and X.-L. Yin, "Control Policy Design for Missile Using Impulsive Attitude Control Motors," *Systems Engineering and Electronics*, Vol. 30, No. 9, 2008.

[68] S. D. Brierley and R. Longchamp, "Application of Sliding-Mode Control to Air-Air Interception Problem," *IEEE Transactions on Aerospace and Electronic Systems*, Vol. 26, No. 2, pp. 306-325, 1990.

[69] M. J. Corless and G. Leitmann, "Continuous State Feedback Guaranteeing Uniform Ultimate Boundedness for Uncertain Dynamic Systems," *IEEE Transactions on Automatic Control*, Vol. 26, No. 5, pp. 1139-1144, 1981.

[70] S. F. Gimelshein, D. A. Levin, and G. F. Karabadzhak, "Modeling of Jet Interactions in a Space Environment Using the Direct Simulation Monte Carlo Method," AIAA Paper 2003-1032, 41^{st} *AIAA Aerospace Sciences Meeting and Exhibit*, Jan., 2003.

[71] J. Ratzlaff and P. Orkwis, "A Numerical Study of 3D Turbulent Cooling Jet Interaction Over a Range of Blowing Ratios," AIAA Paper 2004-2351, 34^{th} *AIAA Fluid Dynamics Conference and Exhibit*, Jul., 2004.